STEELMAKING WITH THE ESS FURNACE: A MODEL-BASED METALLURGICAL ANALYSIS

Thabisani Nigel Phuthi

August 24, 2020

STEELMAKING WITH THE ESS FURNACE: A MODEL-BASED METALLURGICAL ANALYSIS

by

Thabisani Nigel Phuthi

Supervised by

J.H. Zietsman

submitted in partial fulfilment of the requirements for the degree

Master of Engineering

in the

Faculty of Engineering, Built Environment and Information Technology

of the

University of Pretoria

on

August 24, 2020

Dedication

To Christ, in whom I have placed my faith for guidance, strength and comfort through this journey and beyond.

Acknowledgements

I would like to thank the Glencore Chair in Pyrometallurgical Modelling at the University of Pretoria for funding and providing me with the opportunity to do this research while expanding my personal capabilities. I am also thankful to Envirosteel (Pty) Ltd, for allowing us to explore their design in a research capacity.

I am ever so grateful to my family and friends for being supportive of me through this long, difficult but worthwhile journey. Of these people, I dedicate a special thanks to my parents, whose love and support I have always cherished.

I extend my gratitude to Ex Mente Technologies for all their assistance, which I cannot begin to quantify. A special thanks to Johan, in his capacity as my research supervisor, as Managing Director of Ex Mente Technologies, as a spiritual advisor and as a friend. Thank you for supplementing my research work with software solutions, facilities and the expertise of yourself and your employees. It enabled me to do this work with greater efficiency than I would have from my own capacity. Thank you as well, for the words of wisdom and encouragement you gave when my joy was overshadowed by the struggles I was facing during this research project.

Abstract

STEELMAKING WITH THE ESS FURNACE: A MODEL-BASED METALLURGICAL ANALYSIS

by Thabisani Nigel Phuthi

Supervisor: Dr Johan H. Zietsman
Department of Materials Science and Metallurgical Engineering

Master of Engineering

This research project investigated the option of steelmaking with the ESS furnace by using computational modelling to estimate steady state decarburisation rates. It focused on understanding metallurgical phenomena that would dictate refining rates of molten pig iron with iron ore. The results obtained are aimed at designers and potential users of the furnace technology to improve their understanding of the expected steady-state process behaviour. A mass-and-energy-balance model with a decarburisation sub-model was developed to estimate feed material requirements for steady state operation.

Modelling and simulation results suggest that it may not be possible to produce steel under the conditions proposed. However, the furnace still holds potential if ideal operational conditions are understood and applied.

Modelling also gave insight into which areas areas of concern, such as bubble formation in the furnace's channel induction heaters, and necessity for a well designed refractory lining to contain heat and allow the process to operate at a stable condition under the conditions proposed.

Keywords: ESS furnace, steelmaking, metallurgical analysis, modelling, mass and energy balance, decarburisation kinetics

Contents

List of Figures

List of Tables

Part I

Introduction

Chapter 1

Background

This chapter presents a brief overview of the South African steelmaking industry at the time this project was done. The ideas behind the ESS furnace design and how it can contribute to the industry are also presented, followed by the background of this research project and how it aims at contributing to the ESS process and the steelmaking industry of South Africa.

1.1 The South African Steelmaking Industry

At the time this work was done, South Africa was the only sub-Saharan primary steel producing country (Ashman 2016). In 2015, steelmaking directly contributed more than 1.1% to South Africa's Gross Domestic Product (GDP). Its indirect contributions were seen in the top five steel consuming industries, which in total contributed 15% to the total GDP and more than 8 million jobs in South Africa (O'Flaherty 2015).

At the time this project was initiated, an increase in world production volumes had led to a global oversupply which increased producer competition in the steel market (Montiea 2015). The South African Department of Trade and Industry also listed the following challenges faced by the steel industry in 2018 (DTI-RSA 2018):

- Low economic activities and slow growth in apparent steel demand in the country.
- Rising costs of production.
- Ageing mine-to-metal processing equipment.
- Increases in raw materials, electricity, rail, logistics and export costs.
- Increased competitiveness in the sale of finished goods against that of low price imports.
- Global trends moving towards recycling, leading to lower demand for primary steel production.

Adding to the challenges was that the electricity supply was at times lower than the demand, which forced Eskom, South Africa's major power producer, to apply load-shedding even to industrial operations (Montiea 2015). Calls were made for more innovative technology which would allow production of high quality steel at lower electrical energy consumption than conventional steelmaking processes (Nel 2014).

1.2 ESS Furnace in Steelmaking

The Envirosteel smelter, in short referred to as the ESS furnace was invented and patented by Envirosteel Pty Ltd as a versatile unit for ferroalloy and ironmaking processes (Fourie and Erasmus 2016). The process combines, reverberatory, open-hearth and induction furnace technologies and one successful pilot-scale application was in limonite smelting to produce ferronickel (Fourie and Erasmus 2015). The furnace was proposed to have the capability of refining pig iron to low-carbon steel by using iron ore as an oxidant to remove carbon from the pig iron (Fourie and Erasmus 2015). The process design could possibly have lower

electrical and chemical energy requirements than existing steelmaking processes. This would be achieved by combustion of carbon monoxide produced in furnace reactions as the major heat source, rather than adding fuel and reductants to supplement energy.

At the time of this project, there was no operational commercial-scale ESS furnace, but a pilot-scale plant was being commissioned and tested at Mintek's Pyrometallurgy Division in South Africa.

1.3 Project Background

This research project was initiated in the Glencore Chair Pyrometallurgical Modelling group at the University of Pretoria, in collaboration with Envirosteel (Pty) Ltd in 2016. Since there was no operational ESS steelmaking furnace at the time, it was proposed that computational modelling and simulation would be a useful approach to investigate phenomena that would dictate successful steady-state operation of the ESS furnace when refining pig iron to low-carbon steel. Information obtained from computational investigations would help with the ongoing efforts to estimate steady-state behaviour of the furnace. Successful implementation of the knowledge would therefore assist with design and improvement of a new low-cost steelmaking alternative, which would, in turn, help in providing solutions for the challenges being faced in South Africa at the time.

1.4 Document Overview

In Part I an introduction to the research project is presented. Chapter 1 presents the background and motivation for the project. Chapter 2 defines the aims, significance and outcomes of this work from research and industrial perspectives. Chapter 3 gives a description of the ESS furnace and gives a brief history of its applications in the ferroalloy industry.

Part II presents a review of literature relevant to this work. Chapter 4 presents fundamental theory for pyrometallurgical process modelling, and similar work from literature. Chapters 5 and 6 are reviews of open hearth and induction furnace literature respectively, where the two are compared to the ESS steelmaking furnace. Chapter 7 is a review of literature describing decarburisation in steelmaking processes.

Part III explains the approach and methods used to do the project.

Part IV describes modelling of the ESS steelmaking furnace. Chapter 10 describes the model specification, following which, a system analysis and identification of key phenomena are presented in Chapters 11 and 12 respectively. Chapters 13 and 14 identify and define assumptions and simplifications made about the steelmaking process to make developing the process model a practical, but useful exercise. Chapters 15 and 16 detail the mathematical formulation and implementation of the model.

Part V includes details of the simulations done in Chapter 17 and the results obtained thereof in Chapter 18. A discussion about the ESS furnace applied to steelmaking, after going through the modelling process and obtaining results from simulations, is then presented in Chapter 19.

Part VI sums up the this document with conclusions reached about the ESS process in Chapter 20.1, recommendations for future research in Chapter 20.2 and a summary in Chapter 20.3. References to literature used in this project are provided thereafter.

Chapter 2

Research Focus

This chapter clarifies the focus and direction of this research project by stating the topic, question, problem statement, purpose and objectives set for this work. This method of defining the research focus was taken from Booth, Colomb, and Williams (2009)

2.1 Topic

The topic of this research is as follows:

Steelmaking with the ESS Furnace - A Model-based Metallurgical Analysis

2.2 Question

Can low carbon steel ($<$0.25 wt%C) be produced successfully in this reactor from the perspective of pyrometallurgical phenomena, under the conditions proposed by the inventors?

2.3 Problem Statement

There is a lack of understanding about how pyrometallurgical phenomena will influence steady-state behaviour of the ESS furnace when it is used to decarburise molten pig iron to low-carbon steel.

2.4 Purpose

The purpose of this work was to investigate metallurgical phenomena that will influence steady state refining of pig iron to steel when using the ESS furnace. By understanding these phenomena, the technology would be better designed and improved to produce steel at lower electrical energy consumptions than existing processes.

2.5 Scope

The scope of this research was limited to investigating metallurgical phenomena that would occur within the ESS furnace hearth during steady-state operation when it is used for steelmaking. Air pre-heating technology and induction heating were excluded from the study because this would have too large a scope for the research project.

2.6 Project Objectives

Objectives were set to guide modelling and simulation of a hypothetical ESS steelmaking furnace design. These are as follows:

1. Identify metallurgical phenomena in the proposed ESS process in a steelmaking application. To investigate the potential performance of the ESS furnace design, it is critical to be aware of metallurgical phenomena that occur in steelmaking processes.
2. Use the identified phenomena to develop a steady-state process model of the furnace. Computational investigations are valuable for equipment design in that they provide a relatively inexpensive method of investigation in comparison to pilot plant testing. Furthermore, a process model was the only option for analysis, because there was no fully operational steelmaking ESS furnace at the time.
3. Use the developed model to investigate the expected performance of the furnace during steady state operation with typical South African mineral resources.

Chapter 3

The ESS Furnace

This chapter describes the physical attributes of the ESS furnace to provide context for further reference in this document. The descriptions are as provided from conversations with, and literature published by the inventors of the furnace. The ESS furnace has a stationary, rectangular hearth with four vertical walls, and is covered by an arched roof as shown in Figure 3.1 (Fourie and Erasmus 2015).

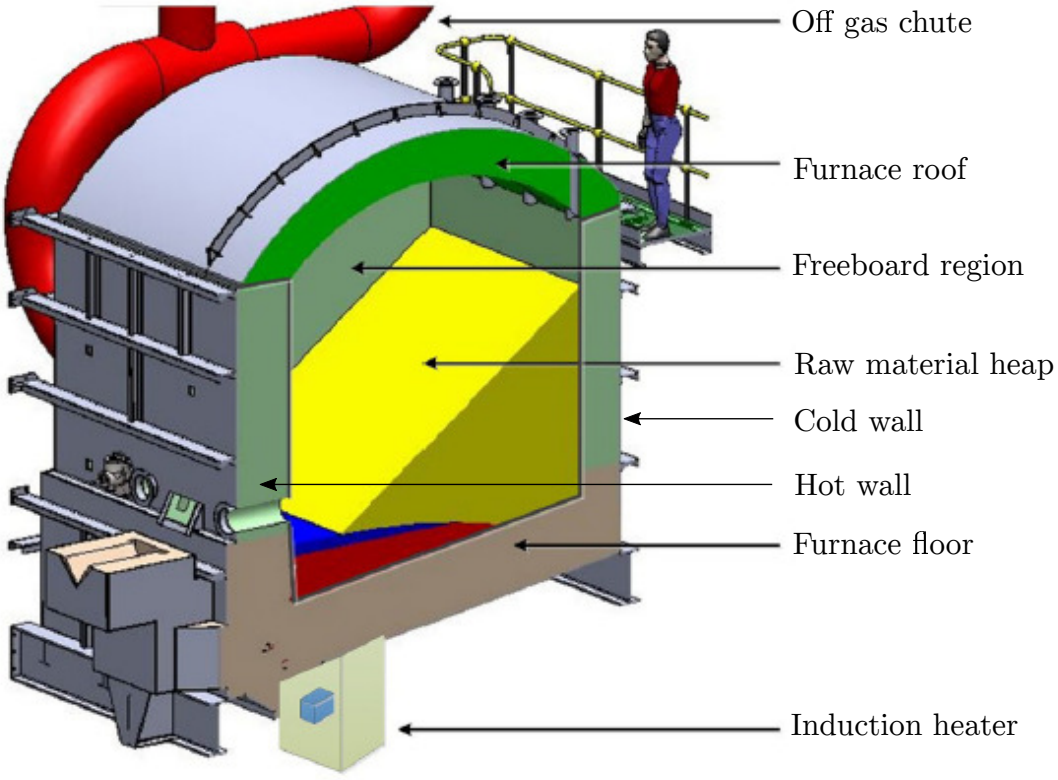

Figure 3.1: Sectioned three-dimensional view of the ESS furnace (Fourie and Erasmus 2017).

3.1 Wall Configuration

All upright walls consist of refractory material encased by a steel shell, which helps to maintain structural integrity (Fourie and Erasmus 2016). The front wall of the furnace is referred to as the "hot wall" because it is in contact with molten alloy and slag at the lowest part of the hearth (Fourie and Erasmus 2016). Figure 3.2 is a schematic representation of and end-section view of the hot wall.

Tuyeres used for feeding preheated air and pulverised coal are placed in this wall above the slag meniscus line. Inlet passages feed molten pig iron from the furnace's channel induction heaters directly into the alloy bath.

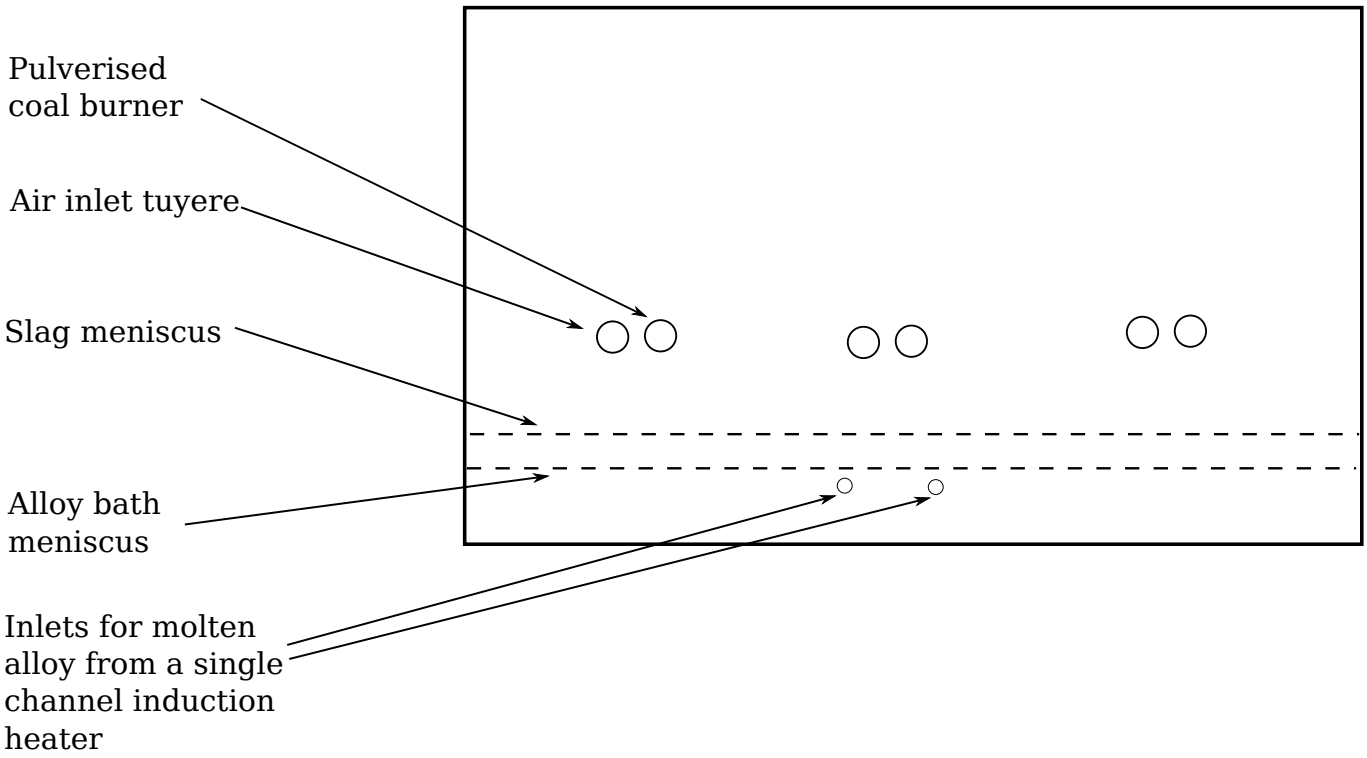

Figure 3.2: Schematic representation of the ESS steelmaking furnace hot wall configuration.

The rear wall of the furnace is referred to as the "cold wall". A heap of solid raw material rests against this wall, reducing the area exposed to radiation.

In one of the side walls a taphole is installed for removing spent slag from the furnace, and so this side wall is referred to as the "slag-tapping end wall". A schematic representation of this wall is shown in Figure 3.3. On this same wall, but below the slag taphole, an inlet passage is installed for feeding molten pig iron into the furnace's alloy bath. The pig iron may be fed from any preferred source, but the recommended configuration is where the steelmaking furnace is directly connected to an ironmaking furnace, such that molten pig iron can be continuously fed into the ESS steelmaking furnace (Fourie and Erasmus 2016). An exhaust gas outlet is installed further up this end wall, which is used to extract spent gas from the furnace.

Opposite to the slag-tapping end wall is the alloy-tapping end wall, where alloy is removed from the molten bath and into post-treatment ladles.

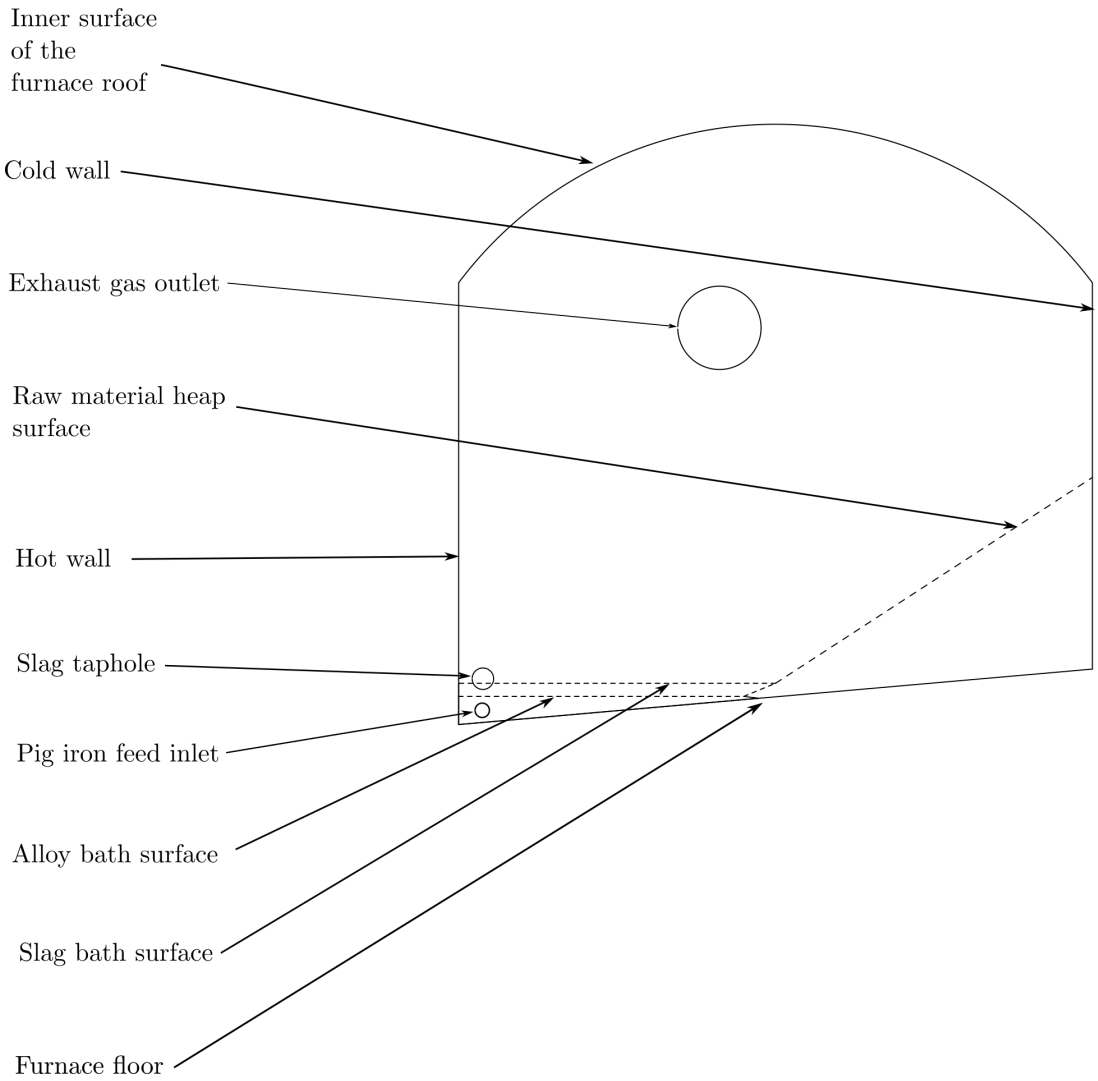

Figure 3.3: Schematic representation of the ESS steelmaking furnace slag-tapping end wall configuration.

3.2 Floor Configuration

Figure 3.4 is a schematic representation of the furnace floor as seen from above.

The floor is made of refractory material that lies on top of a steel support structure. An outlet port is installed close to the hot wall, which leads to an induction heating channel below the furnace. During steady operation, approximately half of the floor is covered by solid raw material in a heap, while the other is covered by the molten alloy bath. The furnace floor is sloped, with the lowest point located close to the hot wall as shown in Figure 3.3.

3.3 Roof Configuration

The ESS furnace is covered by an arched roof made of refractory material with an external steel casing. There are no other features of particular interest on the roof.

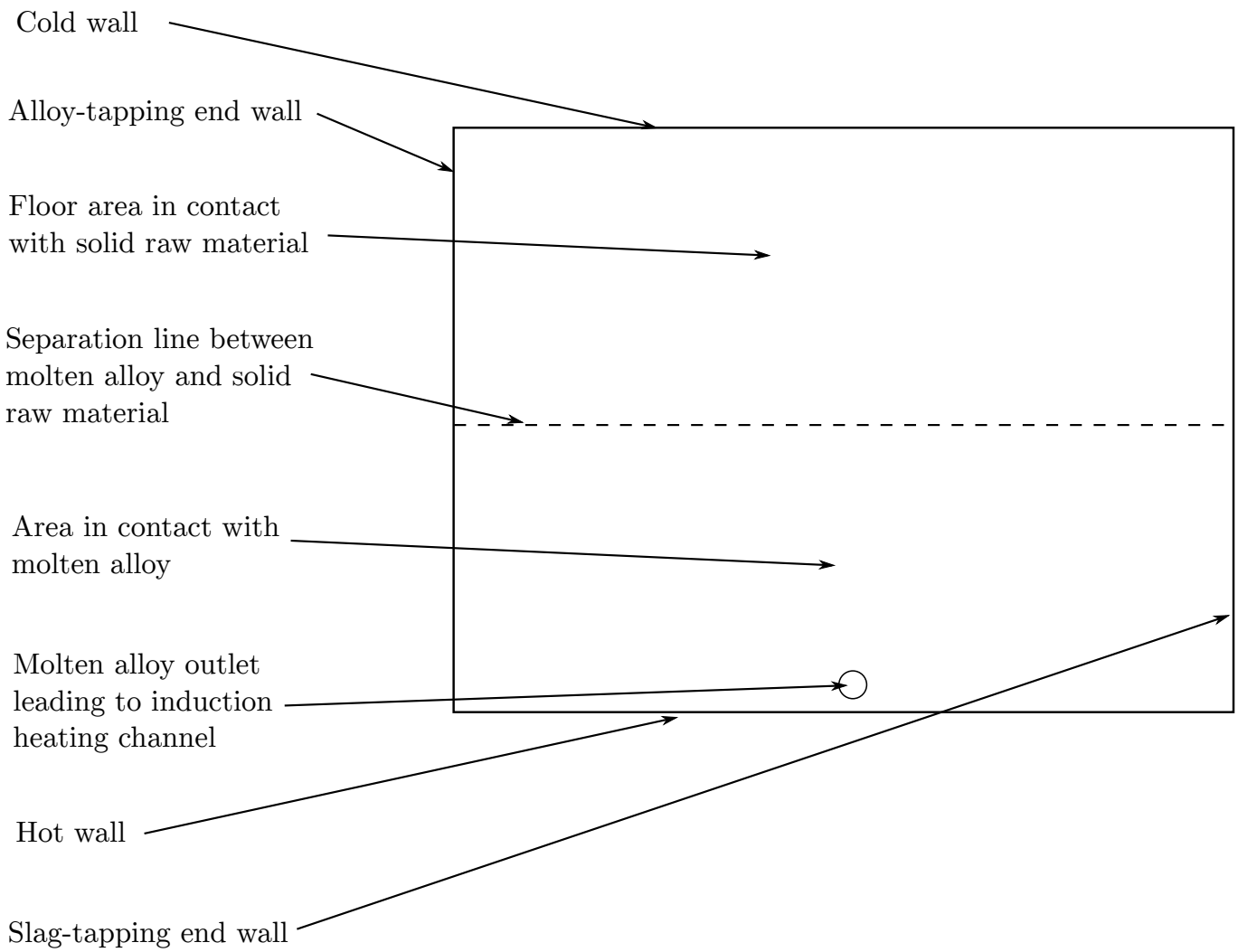

Figure 3.4: Schematic representation of the ESS steelmaking furnace configuration as seen from above.

3.4 Channel Induction Heater

A channel type induction heater that is used to regulate alloy bath temperature is installed below the ESS steelmaking furnace floor, outside of its walls. An outlet port on the furnace floor directs molten alloy through what is referred to as a down passage to the heating channel. From the heating channel, there are two up passages which lead back to the molten alloy bath of the furnace. Figure 3.5 is a schematic representation of the channels and passages of the induction heater where molten alloy will flow during steady operation.

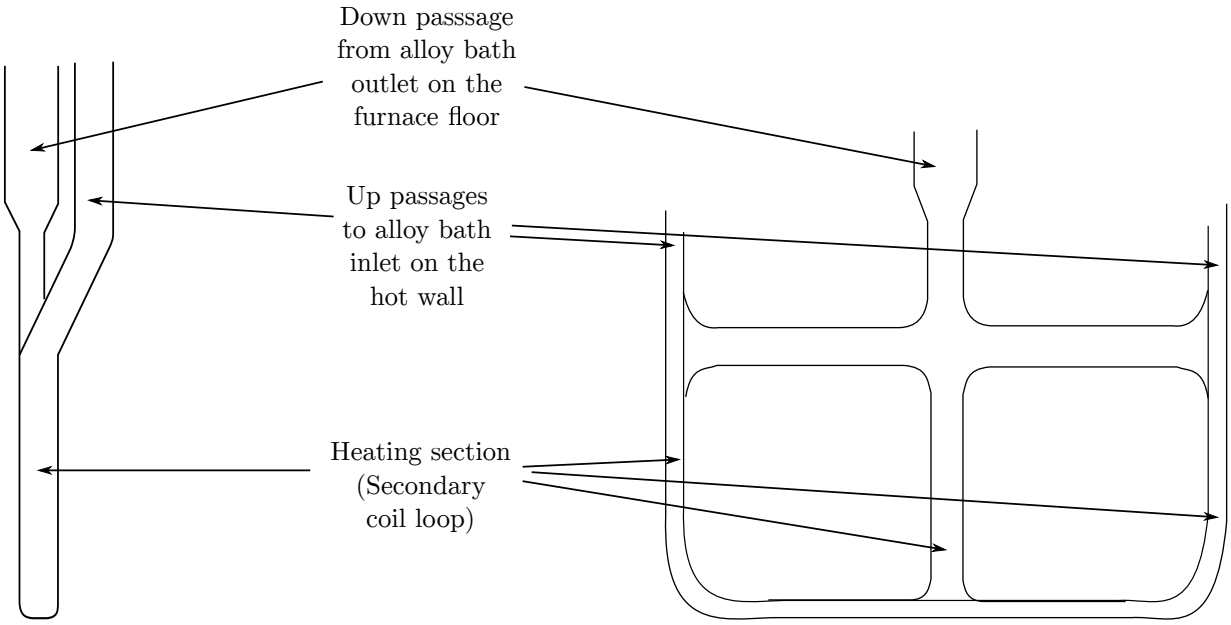

Figure 3.5: Schematic representation of the secondary coil channel configuration in the ESS steelmaking furnace's induction heater.

Chapter 4

Theoretical Background

This chapter describes theory that was fundamental to process modelling done in this research work. This included mass and energy conservation laws, thermodynamics and thermochemistry used to estimate equilibria in chemical reactions, and process kinetics to determine potential steady-state behaviour of the furnace.

4.1 Mass Conservation

The law of mass conservation states that matter in an isolated system cannot be created or destroyed. For pyrometallurgical process modelling, this law is used to place a constraint on equations when solving for the potential products of the particular process. The total mass of material, put in as an input of mass balances, must always equal the total mass of products obtained from it, regardless of what processes occur in between (Atkins and Paula 2010). This is put in effect for all pyrometallurgical mass balances models, except where nuclear reactions occur.

4.2 Thermodynamics

Thermodynamics is governed by 4 laws, of which the first and second law were applied in the model developed in this project. These are discussed in this section.

4.2.1 The Zeroeth Law

The "Zeroeth law" is so-named, because it was defined after three laws were already established and numbered, but was required as the first law in order to define absolute temperature (T) as a property, which is fundamental to the other three laws. It states that:

> *If body A is in thermal equilibrium with body B, and B is in thermal equilibrium with C, then body C is in equilibrium with A.*

This means that if some property relating to heat exchange (i.e. temperature) is measured, it will be of the same value for all three bodies A, B and C (Atkins and Paula 2010).

4.2.2 The First Law

The first law of thermodynamics provides the basis of defining the concept of the internal energy of a system. It states that:

> *The change in internal energy (U) of any system is the sum of heat (q) input to the system and work (w) done by the system*

and is described mathematically by Equation 4.1.

$$\Delta U = q_{\text{in},i} - w_{\text{out},i} \tag{4.1}$$

This is a restating of the law of conservation of energy which states that: the total energy (E) of an isolated system remains constant over time. This total energy, is that referred to as internal energy (U) of a system in the first law of thermodynamics (Atkins and Paula 2010).

The first law also became a basis for the introduction of heat capacity ($C_{\text{conditions}}$) and enthalpy (H), which are invaluable accounting tools when doing thermodynamic calculations. The heat capacities of various materials has been determined empirically at various temperatures, and has been found to be a function of temperature as well. An example of a material's heat capacity calculation under constant pressure conditions is shown in Equation 4.2, where c_n denotes coefficient number n.

$$C_P = c_0 + c_1 T + c_2 T^2 + \frac{c_3}{T} \tag{4.2}$$

The enthalpy of a substance at a given temperature is described using equation 4.3.

$$H(T) = H_{f,298.15K} + \int_{298.15K}^{T} \left(\frac{C_P}{T}\right) dT \tag{4.3}$$

The value $H_{f,298.15K}$ is an experimentally determined value known as the enthalpy of formation of a substance. It denotes the amount of energy required to produce a given substance and make its temperature 298.15 K.

Equation 4.1 is therefore described using enthalpy by Equation 4.4 and ultimately Equation 4.5 where work is replaced by the product PV, since in thermodynamics, work is the energy released by a system when its volume is changed.

$$\Delta U = \Delta H - w_{\text{out},i} \tag{4.4}$$

$$\Delta U = \Delta H - P\Delta V \tag{4.5}$$

4.2.3 The Second Law

The second law of thermodynamics introduces the concept of entropy, which is a the statistical distribution of energy states that the atoms or molecules of a system will occupy at a given temperature. The law states that:

The entropy (S) of the universe increases in the course of spontaneous change

which means that any isolated system will tend to reach some stable condition, where its particles are at the highest entropy (i.e. the most probable energy states) (Atkins and Paula 2010). The entropy of a material at a given temperature can be determined using Equation 4.6.

$$S(T) = S_{298.15K} + \int_{298.15K}^{T} \frac{C_P}{T} dT \tag{4.6}$$

Entropy also open system changes as it exchanges heat with it's surroundings, in such a way that an increase in entropy of the system is equal to the decrease in entropy of the surroundings. Mathematically this is described by Equation 4.7.

$$\Delta S_{\text{system}} = -\Delta S_{\text{surroundings}} = \frac{q}{T} \tag{4.7}$$

However, since the change in enthalpy is defined by Equation 4.5, q can be substituted with the heat component ΔH yielding Equation 4.8.

$$\Delta S_{\text{system}} = \frac{\Delta H_{\text{system}}}{T} = -\Delta S_{\text{surroundings}} \tag{4.8}$$

By definition, the entropy of the universe in the course of spontaneous change will always increase (Atkins and Paula 2010). Therefore Equation 4.9 always holds true.

$$\Delta S_{\text{universe}} = \Delta S_{\text{system}} + \Delta S_{\text{surroundings}} > 0 \tag{4.9}$$

With Equation 4.7, Equation 4.9 can be rewritten as Equation 4.10.

$$\Delta S_{\text{universe}} = \Delta S_{\text{system}} - \frac{\Delta H_{\text{system}}}{T} \tag{4.10}$$

Multiplying by $-T$ throughout, we get Equation 4.11, where the increase in entropy of the universe (i.e. the direction in which a spontaneous change in which a system will go), is expressed using the enthalpy and entropy changes of the system only. This eliminates the need to determine entropy change of the surroundings, which is a near impossible calculation. Each side of the Equation was therefore given the name Gibbs free energy (G), which is a more ideal way of calculating the preferred direction of change in a system in the event of spontaneous change.

$$-T\Delta S_{\text{universe}} = \Delta H_{\text{system}} - T\Delta S_{\text{system}} \tag{4.11}$$

Therefore, the statement of the second law can be restated to:

The Gibbs free energy of a system decreases in the course of spontaneous change

or mathematically by Equation 4.12.

$$\Delta H_{\text{system}} - T\Delta S_{\text{system}} = \Delta G < 0 \tag{4.12}$$

4.2.4 The Third Law

The third law was defined to generate a reference point for entropy, so as to show that it can be defined on an empirical scale. Thought experiments revealed that the entropy of materials tend to reach the same value as the absolute temperature (T) approaches zero. Since the entropy of a system increases with temperature (the energy state distribution tends towards higher values), it was established that the lowest entropy state is when T approaches zero (Atkins and Paula 2010). Therefore the third law states that:

The entropy of all perfectly crystalline substances is zero at an zero absolute temperature

or mathematically by Equation 4.13.

$$\lim_{T \to 0K} S = 0 \tag{4.13}$$

4.3 Thermochemistry

Thermochemistry is the study of chemical reaction equilibria, by using principles of thermodynamics. Chemical reactions are either endothermic or exothermic, which allows use of enthalpy and Gibbs free energy (ΔG) to predict the equilibrium state when reactants are brought together in a thermochemical system. This section describes theory that was applied in this research project's modelling work.

4.3.1 Thermochemical Systems

Pyrometallurgical processes are thermochemical systems, of which most are considered open, since there is continuous extraction of gas and sometimes condensed phases. To understand and model the processes, it is necessary to understand the nature of these systems in terms of the matter they contain. This section describes the nature of matter and its classification as used in thermochemistry.

4.3.1.1 System Components

System components are described as the most basic building blocks, usually designated as the elements that make up a thermochemical system (Atkins and Paula 2010). Rao (1985) defined components as the smallest number of chemical species that must be specified in order to completely define the composition of each phase involved in the equilibrium of a thermochemical system. There are rare instances where system components can be compounds, but these were not of relevance in the model in this research work. Some systems can contain electrons as system components, particularly where complex oxides such as chromite-, magnesia- or titania-spinels are present.

4.3.1.2 Phases and Constituents

A Phase is defined as a physically observable, distinct collection of matter that has uniform chemical composition and physical state (Atkins and Paula 2010). Phases are classified under either pure or mixed substances.

Pure phases are such that the are made up of only one identifiable chemical phase, such as a crystal that is made up of only NaCl. These are generally not found in nature, but are a useful way of describing phases in model calculations. For pure phases, the phase itself is the phase constituent (i.e. NaCl is the phase constituent of the pure NaCl crystal phase). The Gibbs free energy of a thermochemical system with a single phase is calculated from the enthalpy and entropy, which are both functions of C_P and absolute temperature (T).

Mixed or solution phases are such that they are made up of two or more completely miscible chemical phases, such as a NaCl that is fully dissolved in water. In this scenario, each of water (H_2O) and dissolved Na^+ and Cl^- ions are referred to as phase constituents as they are the building blocks of phases. The Gibbs free energy of a thermochemical system with only one solution phase is the sum of its phase constituents individual Gibbs free energies at T.

If there is more than one phase constituent in the system, then the total Gibbs free energy is the sum of each phase constituent's contribution. This is represented mathematically by Equation 4.14.

$$G^{ph} = \sum_{\mathrm{pc}=1}^{n_{\mathrm{pc}}} G^{pc} \tag{4.14}$$

As a reference point, the Gibbs free energy of a phase under standard conditions is given the symbol G^0 ($T = 273\,\mathrm{K}$ and $P = 1\,\mathrm{atm}$). To calculate the Gibbs free energy of a constituent at any temperature, Equation 4.15 is used, where a is an effective concentration of the component.

$$G_{pc} = G^0_{pc} + RT \ln a \tag{4.15}$$

For pure phases $a = 1$. For systems with multiple phase constituents, the factor a for all phases by calculating a quotient of product over reactant activities. If the system is at equilibrium, the quotient is called the "equilibrium constant", denoted by K.

In an example chemical reaction (Equation 4.16), K is calculated using Equation 4.17, and Equation 4.15 is transformed to Equation 4.18 which.

$$\mathrm{aA} + \mathrm{bB} \longrightarrow \mathrm{cC} + \mathrm{dD} \tag{4.16}$$

$$K = \frac{C^c \cdot B^b}{A^a \cdot B^b} \tag{4.17}$$

$$G = G^0 + RT \ln K \tag{4.18}$$

4.3.2 Phase transitions

A phase transition is the spontaneous conversion of one phase into another (Atkins and Paula 2010). This may be due to a chemical (e.g. a reaction with another phase in the thermochemical system), or physical process (e.g. Absorption of heat, resulting in change of phase from solid to liquid). Phase transitions are accompanied by a changes in internal energy of a system. Thus with the aide of thermodynamics, phase changes have an associated Gibbs free energy change (ΔG_r), as shown by Equation 4.19.

$$\Delta G_r = \sum G_{\text{products}} - \sum G_{\text{reactants}} \tag{4.19}$$

Therefore, for a spontaneous phase transition (i.e. a chemical reaction) $\Delta G_r < 0$, and a larger negative ΔG_rmeans a higher drive for spontaneous phase transition. At equilibrium $\Delta G_r$is also related to the equilibrium activity coefficient (K) and absolute temperature (T), by Equation 4.20.

$$\Delta G_r = -RT \ln K \tag{4.20}$$

Where R is the molar gas constant.

It must be noted however, that ΔG_rdoes not indicate the speed at which the transition will occur, which is the subject of process kinetics that is discussed in Section 4.4

4.3.3 Thermochemical Equilibrium

At thermochemical equilibrium, a system will have reached its most probable state, where there is no driving force for spontaneous change. Therefore, the likely products of a reaction can be estimated through minimisation of Equation 4.20 given the constraint of mass conservation, to obtain the closest possible solution to equilibrium where $\Delta G_r = 0\,\text{J mol}^{-1}$. This is the basis for thermochemical equilibrium calculations done using Software such as FactSage® and Chemapp®.

4.4 Process Kinetics

Process kinetics refers to the study of transient behaviour in pyrometallurgical processing units. It is divided mainly into chemical reaction, and transport kinetics. These are discussed briefly in this section.

4.4.1 Chemical Reaction Kinetics

Chemical reaction kinetics is the study of the speed with which reagents that are in close proximity with one another will come together and form products (Atkins and Paula 2010). The rates of chemical reactions are proportional to concentrations of reagents and products raised to a power referred to as the order of the reaction. Rates also have an Arrhenius relationship to temperature, where an increase in temperature results in an increase in the number of activated reagents, as well as an increase in the number of collisions in fluid phase solutions. In steelmaking process units, energy is added to vessels in various forms, which sufficiently raises the temperature of the burden, such that reagents in close proximity will readily react (Fruehan 1998; Fruehan and Pistorius 2014). For these reactive species to come close to each other, transport kinetics ultimately plays the major role, which are discussed in the following section.

4.4.2 Transport Kinetics

Transport kinetics was of particular interest in this research project in that the decarburisation reaction in steelmaking, was found to be dominated under most circumstances by mass transport (Chapter 7). Each phenomenon of transport kinetics is discussed briefly in the remainder of this section.

4.4.2.1 Momentum Transfer

Momentum transfer refers to the trade in momentum between moving fluids that are brought into contact. This phenomena has an influence on the other types since movement of a fluid results in increase of properties such as convective heat transfer and mass transport coefficient. Momentum transfer is of greater significance in discrete element models such as used in computational fluid dynamics. This was not the type used for the ESS steelmaking model in this research, where a lumped-parameter model was developed instead. However, it was incorporated by virtue of calculations that determined an adjusted mass transfer coefficient, as adapted from the work by (Robertson and Staples 1974).

4.4.2.2 Heat Transfer

Conduction, convection and radiation play a major role in the ESS furnace. For this research however, radiation was simplified due to complexity of calculations and time restrictions in the project. One dimensional conduction heat transfer calculations were used in the model, which can be represented mathematically by Equation 4.21.

$$q = k \cdot A \cdot \frac{\Delta T}{L} \tag{4.21}$$

Taking an electrical conductivity analogy, where the temperature gradient (ΔT) is analogous to potential difference, and q analogous to current, Equation 4.21 can be re-written as Equation 4.22.

$$q = \frac{\Delta T}{R_{\text{therm}}} \tag{4.22}$$

where R_{therm} is the thermal resistance described by Equation 4.23.

$$R_{\text{therm}} = \frac{k \cdot A}{L} \tag{4.23}$$

4.4.2.3 Mass Transfer

Mass transfer refers mainly to the diffusion of species through a medium down a concentration gradient (Poirier and Geiger 1994). The rate at which this occurs follows Fick's first law, which is described mathematically by Equation 4.24.

$$J = -D\frac{dC}{dx} \tag{4.24}$$

The equation is adapted to mass transfer, by transforming diffusivity (D) into the mass transfer coefficient (k), flux (J) into mass transfer rate ($\frac{dm}{dt}$), and incorporating the area (A) over which diffusion is occuring, to give Equation 4.25.

$$\frac{dm}{dt} = k \cdot A\frac{dC}{dx} \tag{4.25}$$

Mass transfer rates are increased in moving fluids, because they are influenced by momentum transfer, and so k is termed the mass transport coefficient under such conditions.

4.5 Flow sheet Modelling of Pyrometallurgical Processes

In pyrometallurgical processes, the most important parameters to know are concentrations of species, temperature and pressure of regions in the vessel being used, and mass-and-heat-transfer rates between respective regions. In modelling theses processes, knowledge of mass and energy flow rates is required, in order to estimate the parameters at a given time during processing.

Flow sheet based modelling was used by Pauw (1989) for a pyrometallurgical process where he modelled an Argon-Oxygen-Decarburising furnace (AOD). It is a technique that uses specific computational elements

(referred to as modules) to calculate the state of a particular system at some point in the future, given that the initial conditions and rates of change in the system's regions are known. The resulting model by Pauw (1989), was coarsely discretised, which assumes homogeneity in large regions that are assumed to have uniform characteristics. With regards to the modules, each calculates only one of the following characteristics:

- The expected state of regions in a system given certain inputs in the form of materials and energy.
- Transformation of a flow stream through material or phase separation, due to one or more physical or chemical effects.

Flow streams were separated from modules because they were considered to not have a state, but rather calculate the expected mass or energy flow from one region to another. This was achieved by integrating differential rate equations based on fluid flow, diffusion or the type of transfer expected between materials in the two regions (i.e. conduction, convection or radiation).

The flow sheet therefore, is a list of the modules, coupled to each other in such a way that it represents the flow of material and energy between certain regions of the process. For example, in the model by Pauw (1989), the flow sheet would calculate the expected flow rate of oxygen from the gas jet of the AOD, to the alloy and finally to slag or carbon oxide gas, and would give the expected concentration in each of these as a final solution in a simulation.

To further classify the modules, Pauw (1989) used the following terms:

Ideal Mixers - These are components that calculate the concentrations of species in regions, given an in- and out-flow of material streams to and from the respective regions. A major assumption in this component is that each material region is homogeneous, irrespective of the volume that it occupies. Also of note, is that no reactions happen during mixing, and so no phase changes can occur, although the temperature can be readjusted for input streams which have varying temperatures.

Distributors - These redirect certain materials from an input stream into any number of flow streams. This is done either by defining the fraction of input material, or the phases which each output stream will receive.

Mass Input and Output - These are modules that link the process to its external environment. These modules provide a way to report the solutions to simulation equations in the form of a mass balance.

Isothermal Module - These calculate the energy changes in a given region with known material inputs and temperature. Pauw (1989) referred to this module as the "phase boundary reactor". The isothermal module is different from ideal mixers in that the effect of chemical reactions is included in calculations and how this calculation is done has been discussed in Section 4.3.

Thermal Conductors - These calculate the amount of heat transferred from one region to another, given a fully defined heat conduction equation (i.e. all parameters on the right hand side are known, or can be approximated in the model).

Energy Input and Outputs - These provide a method of reporting or accounting of energy in the system, which is referred to as an energy balance.

The approach used by Pauw (1989) was also used by Zietsman (2004) in the modelling of a freeze lining in an ilmenite smelter. Other examples included various work done with thermochemical and thermodynamic equilibria (Eriksson and Rosen 1972; Eriksson 1975; Eriksson 1974; Eriksson and Hack 1983). It has also been used by Ex Mente Technologies (Pty) Ltd to develop a flow sheet modelling software for pyrometallurgical processes, called EMSIM, which was used in the current study. Other examples of EMSIM's use is in the study by Attah-Kyei et al. (2018) and Zietsman, Pretorius, and Steyn (2018).

Part II

Literature Review

Chapter 5

Open-hearth Furnace Steelmaking

The open-hearth furnace was the second commercial-scale design for mass production of steel, after the bottom-blown Bessemer process (Fruehan 1998). Variants of the open hearth process include the Siemens, the Acid open-hearth and the Siemens-Martin process (also known as the Basic open-hearth process). Although these processes are all currently obsolete, their design and metallurgical function were similar to the ESS furnace. They were therefore studied to obtain a basis for estimation of parameters, assumptions and simplifications for the ESS furnace model development presented in Part IV.

This chapter focuses on comparing the ESS to the Siemens-Martin steelmaking process. It was selected for study because is is the most similar of the known open-hearth steelmaking processes to the ESS steelmaking process concept in terms of raw materials and operation.

5.1 Process Comparison

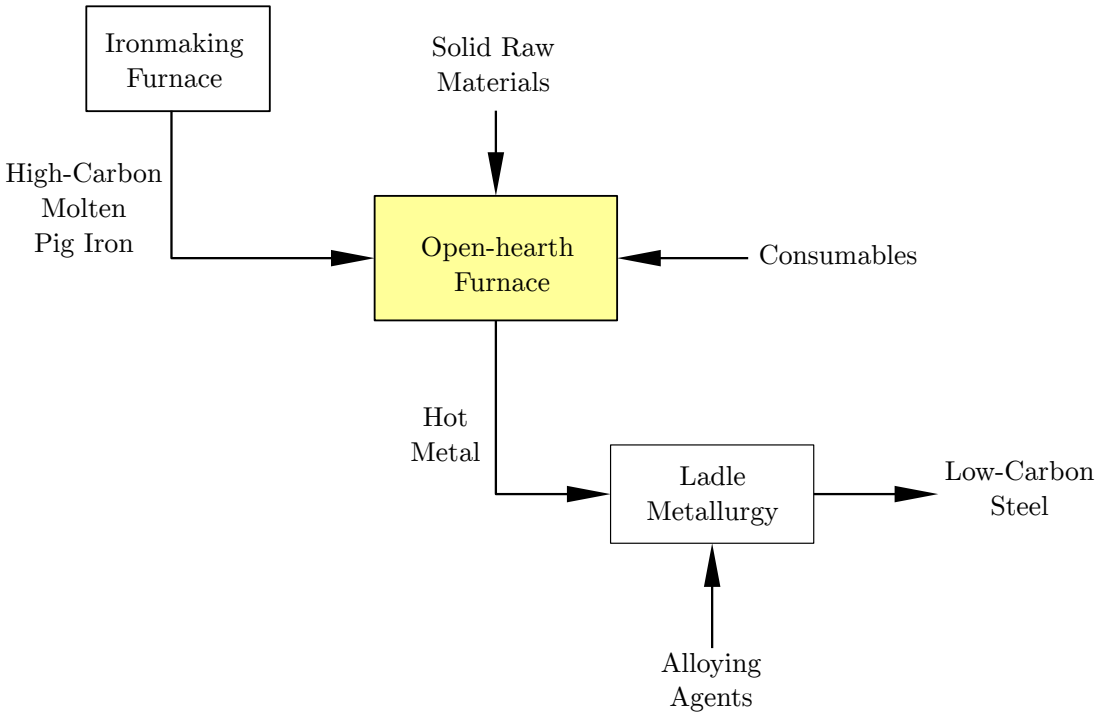

Figure 5.1: Process flow diagram of the Siemens-Martin steelmaking process.

The open-hearth furnace is used in the Siemens-Martin process as shown in Figure 5.1. This is similar to how the ESS furnace is designed for use in a steelmaking process. A major difference in operation

is that the ESS steelmaking process is continuous, where as the Siemens-Martin is a batch steelmaking process.

Molten pig iron is either produced in a separate furnace and then transferred into the open-hearth or added as solid scrap and melted directly using the heat from burning fuel. Iron ore and flux are added so that the molten pig iron is refined to a low-carbon hot metal, which is subsequently tapped into a ladle. Slag is then tapped and the furnace prepared for the next batch of pig iron. The cycle of stages from addition of raw materials to extraction of products is referred to as a "heat". Tapped steel is further adjusted at ladle stations before casting and rolling to a final steel product.

Energy is supplied by burning fuel such as natural gas and atomised heavy oils at one end of the furnace. The flame from this combustion is directed at the furnace's roof, and heat is transferred through radiation to the process material below it. Hot exhaust gas is extracted at the furnace-end opposite to where the fuel burners are situated. The exhaust is sent through checker brick heat exchangers (regenerators) that are situated below the furnace where sensible heat is recovered from the exhaust gas. The direction of gas flow through the furnace is reversible such that input checker brick heat exchangers can be either used to preheat incoming combustion air, or to extract heat from exhaust gas. This is by design, so that when the exhaust gas regenerator has reached it's maximum heat storing capacity, it is switched to an input regenerator to preheat cold combustion air.

5.2 Geometrical Comparison

Figures 5.2 (Derge 1964) and 5.3 (Sugita 2008) are schematic representations of an open-hearth furnace. The refractory lining constitutes a majority of the open-hearth furnace's construction. Materials typically used as refractory lining are as follows (Derge 1964).

1. Magnesite brick and rammed cement ($MgCO_3$)
2. Dolomite brick and rammed cement ($CaMg(CO_3)_2$)
3. Chromite rammed cement (Cr_2O_3)
4. Silica firebrick and rammed cement (SiO_2)
5. Fireclay rammed cement ($Al_2Si_2O_7 \cdot 2\,H_2O$)

More precise configurations of refractory material in the furnace is discussed in the remainder of this section. These configurations will be used as a basis for refractory material configuration in the ESS process model development discussed in Chapter 15. In the remainder of this section, geometry of individual components is discussed. The focus is on refractory materials used, since the ESS steelmaking furnace refractory configuration was not explicitly provided.

5.2.1 Front wall

The front wall of the open-hearth furnace has large mechanically operated doors, through which raw materials are charged into the furnace. The doors also provide access to the alloy bath for sampling during quality control tests. These doors are opened and closed frequently, which requires a robust, renewable refractory lining and the configuration typically used is a water-cooled steel shell, with firebrick or rammed chrome ore (Derge 1964). The ESS furnace is a closed furnace and so has no equivalent of the open-hearth furnace's front wall (Fourie and Erasmus 2016). The refractory configuration on these doors is therefore not relevant to this research.

5.2.2 Rear wall

The rear wall in earlier versions of the open-hearth furnace were vertical, whereas in later versions of the open-hearth steelmaking furnace is sloped at about 50° (Derge 1964). Materials typically used for the rear wall refractory lining were reported by Derge (1964) as the following:

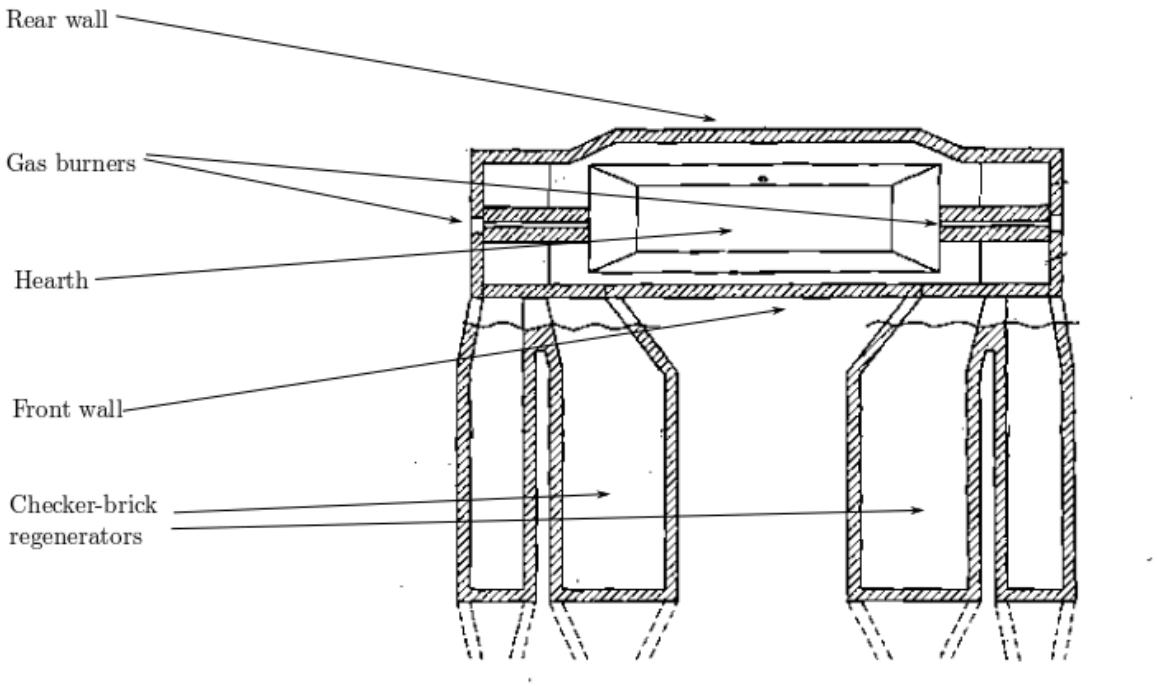

Figure 5.2: Schematic top-section view of a steelmaking open-hearth furnace (Derge 1964).

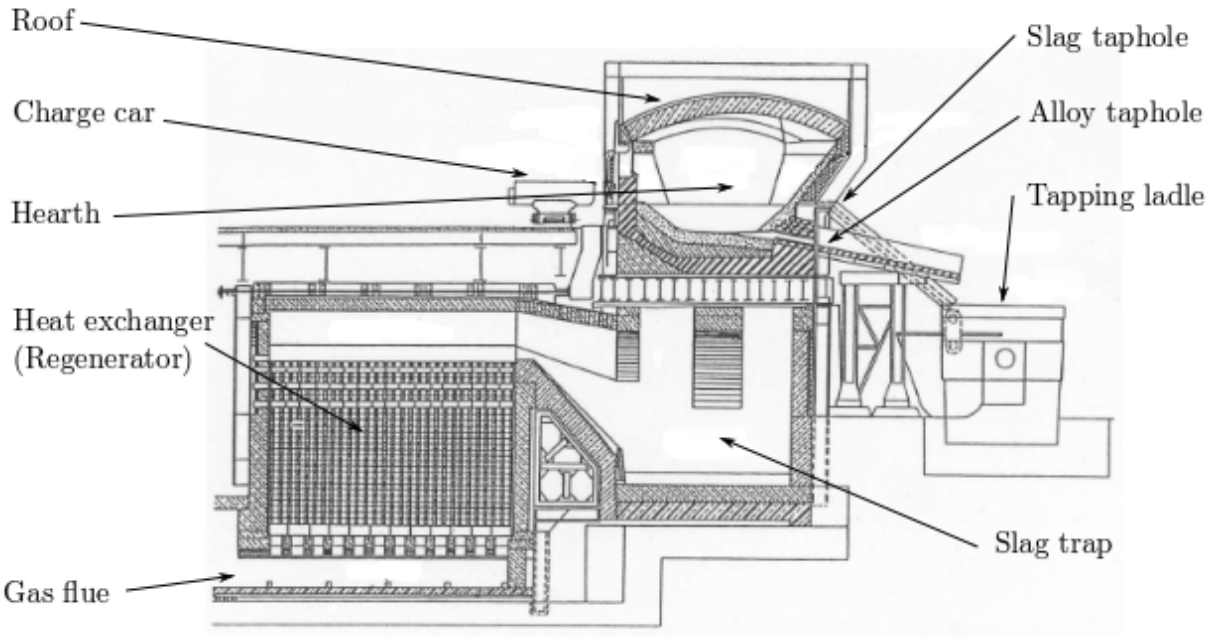

Figure 5.3: Schematic end-section view of a steelmaking open-hearth furnace (Sugita 2008).

1. A basic rammed dolomite and magnesite cement in contact with the molten bath.
2. A basic dolomite and magnesite brick on which the cement is laid.
3. A firebrick or an insulating brick made of aluminosilicate, with higher concentrations of alumina than silica which supports the basic brick.

The firebrick is supported externally by steel beams. Figure 5.4 is a schematic representation of this configuration.

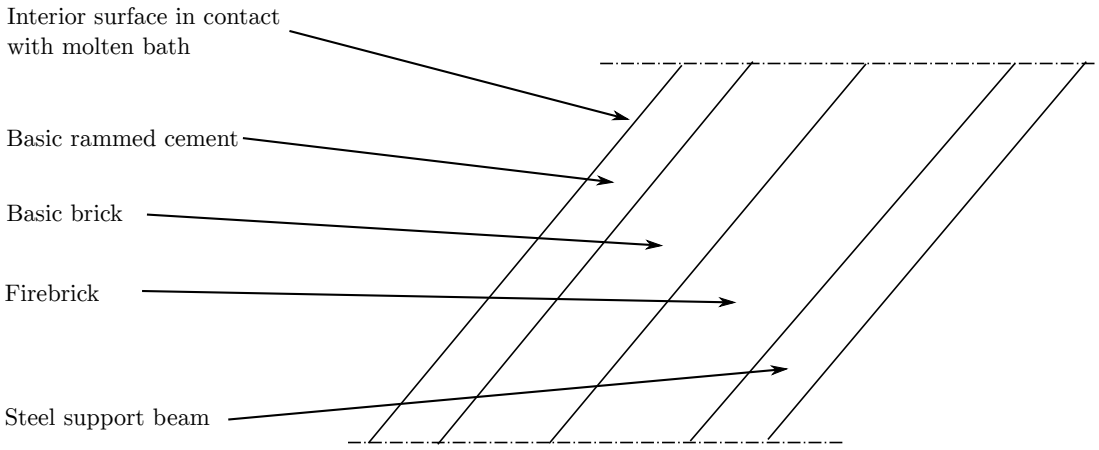

Figure 5.4: Schematic representation of rear wall refractory configuration in a steelmaking open-hearth furnace.

The rear wall of the ESS furnace is vertical and is supported by a steel casing. It is not in contact with any molten material and is therefore referred to as a "cold wall". There is a heap of solid particulate material that lies against the cold wall, which is not present in the open-hearth steelmaking furnace.

The ESS steelmaking process is a "basic" design in that there will be higher concentrations of FeO and CaO than SiO_2 and Al_2O_3 (Fourie and Erasmus 2016). There is also a high possibility of hot dust particles rising up with freeboard gas and coming into contact with the upper section of the cold wall that is not covered by the raw material heap. The ESS steelmaking furnace should therefore use a basic brick on the interior, supported by firebrick and exterior steel shell as proposed by Vert (2016).

5.2.3 End walls

The end walls of the open-hearth furnace are situated away from the hearth and are only in contact with incoming preheated air and fuel, and outgoing hot exhaust gas. This is dissimilar to the ESS furnace, which has both end walls in contact with molten slag and alloy. Investigations of refractory material for the end walls in the open-hearth were therefore excluded from this study.

5.2.4 Furnace Floor

Figure 5.5 is a schematic representation of refractory material used in a steelmaking Siemens-Martin open-hearth furnace floors.

The open-hearth has hearth with a rectangular base, which is similar to the ESS furnace. For this purpose, the refractory configuration was used in developing a floor design for the ESS steelmaking process model. It was designed primarily to achieve the following aims:

1. Hold molten alloy and slag at temperatures up to 1650 °C with minimal heat losses.
2. Survive mechanical disturbances from flow of molten alloy and slag, and directly feeding solid raw material.
3. Survive chemical attack from components in the slag during processing.

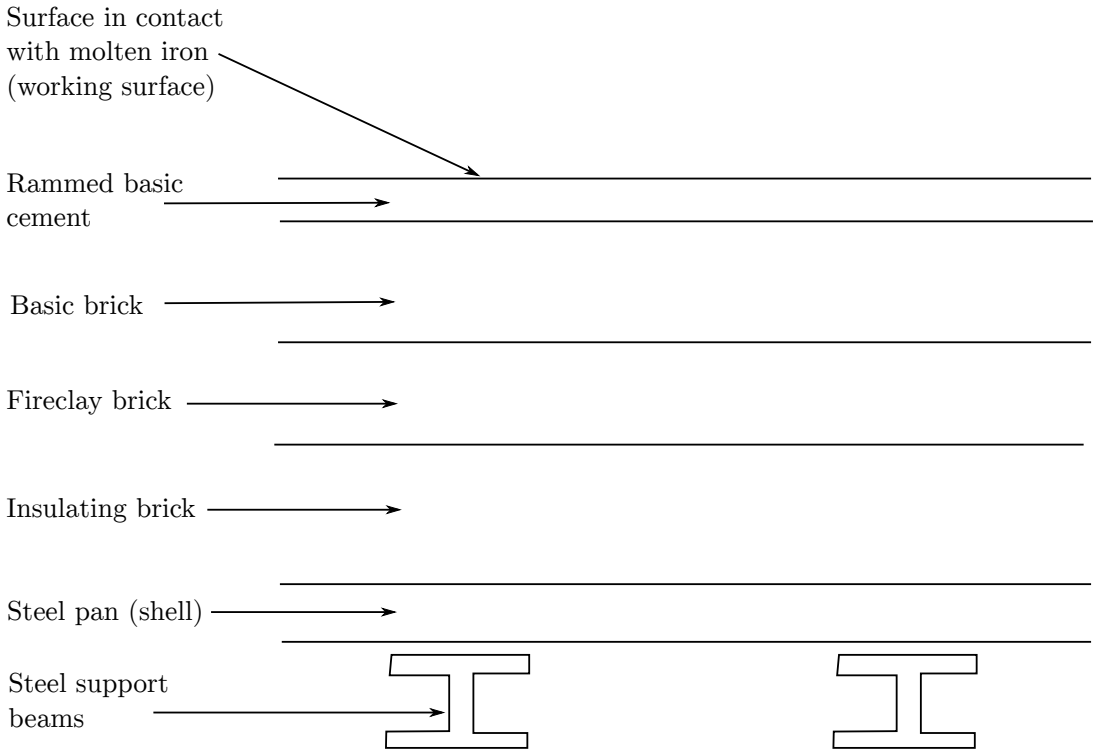

Figure 5.5: Schematic representation of the refractory materials used for a steelmaking open-hearth furnace floor (Derge 1964).

4. Provide a surface for nucleation of carbon monoxide gas bubbles necessary for decarburisation of the alloy.

5.2.5 Roof

A schematic representation of open-hearth roof design is shown in Figure 5.6 (Derge 1964).

The open-hearth has an arc-shaped roof like the ESS steelmaking furnace. The most favoured refractory material for the open-hearth steelmaking furnace roof was silica brick (Derge 1964). It has a lower thermal expansion coefficient than basic bricks and so presented less structural challenges during operation (Derge 1964). A major drawback of silica is its susceptibility to chemical attack and wear by hot basic dust containing iron-oxide and calcium-oxide particles. This refractory lining therefore had to be carefully maintained to prevent the roof from collapsing due to excessive wear (Derge 1964; Fruehan 1998).

Basic refractory bricks were also used for some open hearth furnaces, but presented major structural issues due to excessive thermal expansion of lime and dolomite. This expansion often caused spalling, which is when a layer of the brick's surface cracks and breaks off, leaving a piece that is smaller than what was initially installed (Derge 1964; Sugita 2008; Vert 2016). This can cause excessive heat losses from the furnace, as well as loss of structural integrity.

Fireclay bricks have since been developed that have superior resistance to spalling and chemical wear than those designed for use in the open-hearth. This was mainly in response to the more chemically and physically demanding steelmaking processes, such as Electric Arc Furnace (EAF), and Argon-Oxygen Decarburising vessel steelmaking (AOD) (Sugita 2008; Vert 2016).

For the ESS furnace, average temperatures of the roof are expected to be lower than those in the open-hearth steelmaking furnace (Fourie and Erasmus 2016; Fourie and Erasmus 2017). Gas and dust flow however, is expected to be higher in the ESS steelmaking furnace freeboard, due to the introduction of combustion gas above the slag layer (Fourie and Erasmus 2016; Fourie and Erasmus 2017) This is unlike the open-hearth, whose combustion air is directed to the furnace roof (Derge 1964). Conditions

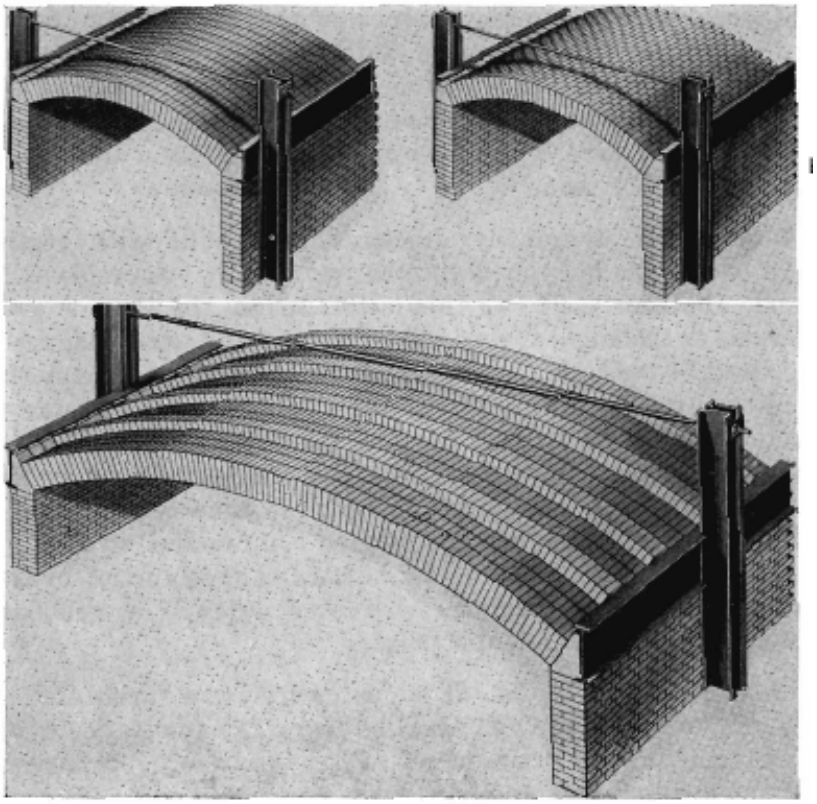

Figure 5.6: Schematic representation of open hearth roof design (Derge 1964).

in the ESS steelmaking furnace therefore can accommodate a fireclay brick as the roof refractory lining. Laboratory experiments would be required to verify the actual performance of fireclay refractory bricks for the roof's configuration.

5.3 Comparison of Inputs

Open hearth steelmaking uses raw materials in a way similar to the proposed ESS steelmaking process. The similarities and differences are discussed in this section.

5.3.1 Pig iron

In the open-hearth steelmaking process, pig iron may be fed in a solid or molten state. In most of the later processes, a separate ironmaking furnace was used to generate a reserve of molten pig iron that is fed to the open-hearth furnace in liquid state. This is a similar feature in the ESS process, the difference being in how pig iron is fed into each furnace. In the open-hearth steelmaking process, a ladle is used to pour the molten pig iron through the charge doors in the front wall into the furnace (Derge 1964). In contrast, the ESS steelmaking furnace is connected to a separate ironmaking unit via a channel, through which pig iron is continuously fed into the furnace (Fourie and Erasmus 2016).

5.3.2 Iron ore

Solid iron ore is fed directly into the molten bath of the open-hearth furnace. The ore melts and dissolves into slag, which then decarburises the alloy (Derge 1964).

In the ESS, iron ore is fed into the furnace to form an inclined heap of material. Exposure to radiation from the hot freeboard melts the ore, and the molten product flows down into a slag layer which is in

contact with the alloy bath (Fourie and Erasmus 2016).

5.3.3 Fluxing material

Lime and silica are added at various stages of a heat in the open-hearth steelmaking process (Derge 1964). This is different from the ESS process in that flux is pre-mixed with iron ore before feeding it into the furnace (Fourie and Erasmus 2016; Fourie and Erasmus 2017).

5.3.4 Reductant

Most open-hearth steelmaking processes did not make use of reductants. This is because iron ore was added directly to the molten bath, where it would react with carbon dissolved in molten alloy. There was therefore no need for any reductant in most open-hearth steelmaking processes (Derge 1964).

The ESS steelmaking process however makes use of reductant, which is pre-mixed with iron ore and flux before feeding into the furnace (Fourie and Erasmus 2016; Fourie and Erasmus 2017). The use of reductant is to reduce iron ore which generates a dominantly iron (II) oxide melt (Fourie and Erasmus 2016). Iron (II) oxide is favourable because it significantly lowers viscosity of steelmaking slags (Mills and Keene 1987). This is expected to improve flow of molten material from the heap surface to the slag and out of the furnace (Fourie and Erasmus 2016).

5.3.5 Combustion air

Preheated air is used in the open-hearth like in the ESS steelmaking process design. The difference lies in the type of pre-heating equipment used. Checker-brick regenerators are used in the open hearth (Derge 1964), whereas more efficient heat exchangers are proposed for the ESS steelmaking process (Fourie and Erasmus 2016; Fourie and Erasmus 2017).

5.3.6 Fuel

In the open-hearth steelmaking process, gas or fuel oil is combusted using burners to maintain the necessary operating temperature of between 1400 and 1600 °C in the molten alloy and slag baths (Derge 1964). In the ESS process, coal burners are to be used instead (Fourie and Erasmus 2016; Fourie and Erasmus 2017) because the furnace is expected to have higher energy efficiency than the open-hearth. In addition to coal combustion, the ESS furnace makes use of a channel induction heating to maintain alloy bath temperatures (Fourie and Erasmus 2016; Fourie and Erasmus 2017), which is unlike the open-hearth.

5.4 Metallurgical Phenomena

5.4.1 Chemical and Physical Reactions

Reactions in the open-hearth are comparable to those in the ESS steelmaking process as discussed in this section.

5.4.1.1 Slag-metal Interface Reactions

In Chapter 7, the mechanisms and kinetics of decarburisation reactions in steelmaking processes are discussed in detail. Considering the nature of these reactions, the differences in slag-alloy reactions between the open-hearth and ESS steelmaking processes lie in the methods by which raw materials are added. In the open-hearth steelmaking process, solid raw material is added directly to the molten bath. Reactions that occur as a result are therefore as follows.

1. Dissolution of solids. Iron ore and fluxes added to the bath will dissolve in already existing molten slag. Some solid particles may reach the interface between alloy and slag, where it interacts with alloy as described in the Decarburisation reaction description. Iron ore dissolves as either iron(II) or iron(III) oxide depending on the slag composition. A higher calcium or magnesium oxide concentration in the slag will favour formation of iron(II)oxide on dissolution. Higher alumina and silica concentrations in the slag will favour iron(III)oxide in the molten slag on dissolution (Fruehan 1998).
2. Decarburisation reaction. Carbon dissolved in alloy interacts with oxygen that is either dissolved in the alloy or carried by solid iron ore and flux.
3. Desulphurisation. Sulphur dissolved in the alloy reacts with CaO dissolved in slag at the slag-metal interface to form calcium sulphide. This product then dissolves into slag and the process is referred to as desulphurisation. Any magnesia present in the slag will have a similar effect to lime. (Refer to Equations 11.8 and 11.9)
4. Dephosphorisation. Phosphorus dissolved in alloy will react with lime dissolved in slag at the slag-alloy interface, depending on the composition of the slag (Refer to Equation 11.10).

In contrast, the ESS steelmaking furnace is not expected to have the same extent of solid-liquid interaction like that observed in the open-hearth process (Fourie and Erasmus 2016; Fourie and Erasmus 2017). This is because solid materials are instead melted on the heap's surface, and the molten product flows into a slag layer (Fourie and Erasmus 2016). Decarburisation reactions will therefore occur purely from the interaction between molten slag and alloy. Dephosphorisation and desulphurisation are expected to be similar to those in the open-hearth.

5.4.1.2 Freeboard Reactions

Freeboard reactions are identical in both processes. For the open-hearth, carbon and hydrogen in gaseous fuel, as well as carbon monoxide from slag-alloy reactions are oxidised to add energy to the systems (Derge 1964).

The difference with the ESS process is that pulverised coal is used instead of gas and fuel oil (Fourie and Erasmus 2016; Fourie and Erasmus 2017). Coal burners are not as efficient as gas burners, but this is not expected to lower the operational efficiency of the ESS process to a great extent (Fourie and Erasmus 2016). Another difference in these reactions is that the ESS process has two sources of carbon monoxide instead of one as in the open-hearth. Carbon monoxide for the ESS is generated through slag-alloy interface, and raw material heap surface reactions which are described by Equations 11.5, 11.6 and 11.7.

5.4.1.3 Other Reactions

The open-hearth steelmaking process does not include the use of an induction heater and so does not feature the electromagnetic heating reactions of the ESS furnace. The open-hearth also does not feature any thermal decomposition of iron ore and flux which is expected to occur at the raw material heap surface of the ESS furnace.

5.4.2 Mass Transfer

Mass transfer phenomena in steelmaking processes is investigated and discussed in Chapter 7.

5.4.3 Heat Transfer

Heat transfer phenomena are similar in the open-hearth and ESS steelmaking processes. There is radiation, conduction and convection between furnace walls and process material. A significant difference between the processes is the presence of a solid raw material heap in the ESS furnace which is not found in the open hearth. This heap is expected to provide some insulation as is described in Section 11.8.

5.5 Summary

An summary of features in open-hearth steelmaking and their relevance to the ESS process is shown in Table 5.1. The score of relevance refers to the extent that the feature can be used in developing a model for the ESS steelmaking process and is quantified as follows.

1. Relevant. The feature will be used explicitly in the model.
2. Partially relevant. Some aspects of the feature will be considered in developing the model.
3. Not relevant. The feature will be omitted from the model. Either it does not exist, or it is so different from the ESS furnace, that another approach is be used.

Table 5.1: Summary of features of the open-hearth furnace and their relevance to the ESS steelmaking furnace.

Feature	Relevance			Reason for relevance score
	1	2	3	
Process:				
Batch processing			✓	The ESS process is designed to be a continuous processing unit. Feeding of solid raw material may be done batch-wise, but decarburisation of pig iron is done continuously.
Separate pig iron melting furnace	✓			The ESS process also makes use of a separate ironmaking furnace to generate the molten pig iron that is refined with it.
Ladle refining after steel tapping.	✓			The ESS will also use ladle refining for final adjustments of the steel product. Its main use in the steelmaking process is to decarburise pig iron.
Off-gas recycling	✓			The ESS steelmaking process will make use of an external heat exchanger to pre-heat combustion air.
Geometry:				
Furnace floor		✓		The ESS furnace has a flat floor inclined at 5° to the horizontal. This is dissimilar to the open-hearth furnace, however, the refractory materials in the ESS furnace will be similar those used in the open-hearth.
Front wall			✓	The ESS furnace does not have charge doors in its front wall design. The refractory lining geometry and materials used differs significantly.
Rear wall		✓		The ESS furnace has a vertical rear wall. It is however susceptible to attack from basic oxides like in the open-hearth. Materials used for the ESS steelmaking furnace will be similar, but the geometry will differ.

Continued on next page

Table 5.1 – continued from previous page

Feature	Relevance			Reason
	1	2	3	
End walls			✓	End wall designs in the ESS furnace are dissimilar to those in the open-hearth. The refractory materials used also differ significantly.
Roof	✓			The ESS furnace also has an arched roof. More advanced refractory materials will be used instead of those common to the open-hearth steelmaking process.
Inputs and Outputs:				
Pig iron		✓		Molten pig iron is used in the ESS steelmaking process. Solid pig iron cannot be used, which is dissimilar to the open-hearth steelmaking process.
Iron ore		✓		The ESS steelmaking process also uses solid iron ore as the oxidant for decarburization. The process flow in the ESS dictates that iron ore is melted away from the molten bath, whereas in the open-hearth it is added as a solid directly to the molten bath.
Fluxes		✓		Flux is also used in the ESS steelmaking process. However, instead of feeding in separate stages as is done in the open-hearth process, it is pre-mixed with iron ore and reductant before feeding semi-continuously to the furnace hearth. This is dissimilar to open-hearth furnace steelmaking.
Reductant			✓	Unlike the open-hearth, the ESS steelmaking is designed to make use of reductants.
Combustion air	✓			Preheated combustion air is used similarly in both the ESS and open-hearth process.
Combustion fuel		✓		Fuel is used similarly in both processes, but the open-hearth uses gas and fuel oils, whereas the ESS uses pulverised coal for fuel.
Metallurgical Phenomena:				
Chemical reactions		✓		The majority of reactions that occur in the open-hearth are also found in the ESS steelmaking process. Reactions such as solid ore and flux dissolution into slag are unlikely and will be excluded in model development for the ESS steelmaking process.

Continued on next page

Table 5.1 – continued from previous page

Feature	Relevance			Reason
	1	2	3	
Mass transfer		✓		Some of the mass transfer phenomena in the open-hearth apply to the ESS steelmaking process. These will be applied during model development. Irrelevant forms of mass transfer will be excluded.
Heat transfer		✓		As with mass transfer, basic principles of heat transfer will be used in developing the ESS steelmaking process model. Aspects of open-hearth heat trasnfer phenomena that are applicable to the ESS process such as refractory material composition will be included in the model and irrelevant aspects such as charge door geometry will be excluded.

Chapter 6

Channel Induction Furnaces in Steelmaking

This chapter presents a comparison of channel-type induction furnaces used in foundries and melt shops melting steel scrap. Only features that are relevant to the ESS steelmaking process are considered.

6.1 Scope of Comparison

Channel induction furnaces are used for melting steel scrap and bars for use in foundries and melt shops The furnaces are not used for "steelmaking" as it is defined in this research. For this reason, a comparison of process flow to the ESS steelmaking process is not relevant and is not considered in this chapter. A comparison of inputs and outputs of channel induction heaters in melting processes is also not relevant because the furnaces use only scrap and small amounts of flux, with no iron ore or reductants.

With respect to geometry, there are similarities between the two furnaces and so this aspect will be discussed in detail. Reactions in channel induction furnaces used for melting are mostly dissimilar to the ESS process and so are excluded in the comparison made in this chapter. Mass transfer related to decarburisation will be described with greater detail in Chapter 7, and so is also excluded from this comparison. Only heat transfer and fluid flow in the heating channels of the furnace are relevant metallurgical phenomena, and will be compared to the ESS steelmaking process.

6.2 Geometrical Comparison

Figure 6.1 shows a cross section of a channel induction heating furnace example typically used in steel foundries and workshops (Edited figure. Original figure extracted from article by Goldstein 2014). This is an example design where a single-cored induction heater is placed below the alloy bath that it is supplying heat energy to. It was selected for analysis by virtue of its similarities with the induction heating configuration in the ESS steelmaking furnace.

In the ESS furnace, a double cored induction heater is used (Fourie and Erasmus 2016; Fourie and Erasmus 2017). An example of such a configuration is shown in Figure 6.2 (Ottojunker 2018). The numbers in this figure indicate the following:

1. Intake or uptake passage.
2. Refractory material.
3. Laminated iron core with transformer oil.
4. Water-cooled flange.
5. Water-cooled copper protective jacket for high operational safety.
6. Water-cooled spool made of copper special profile for high efficiency.

7. Water-cooled steel housing.

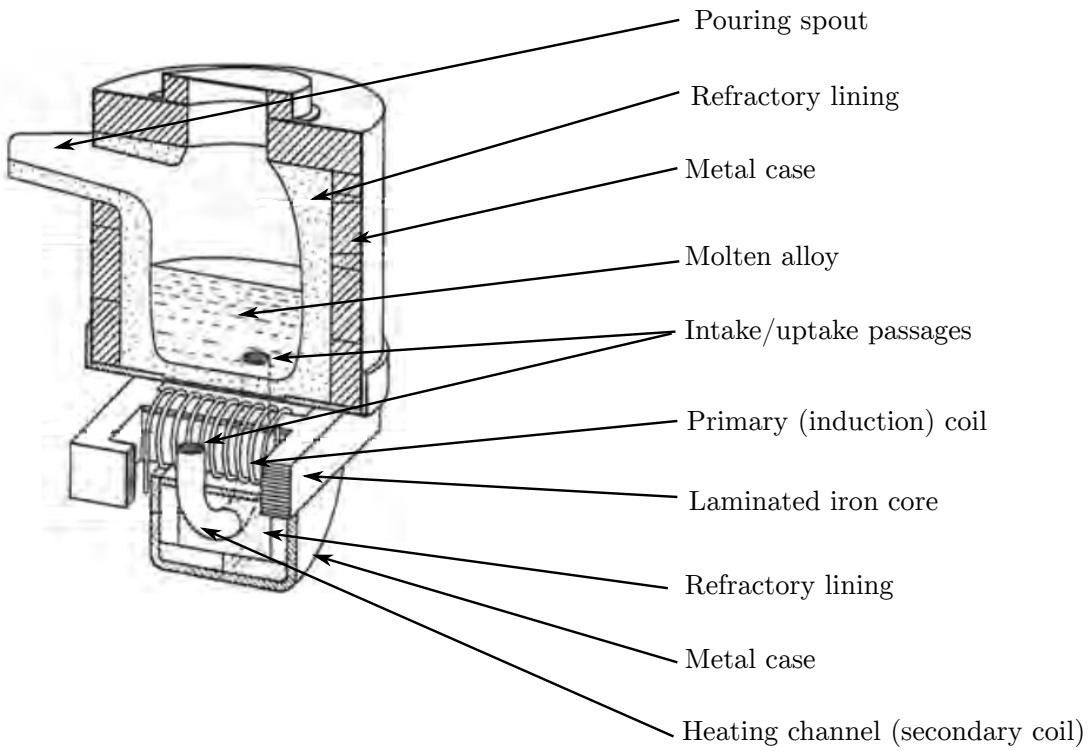

Figure 6.1: Schematic cross section of a channel induction heating furnace (Goldstein 2014).

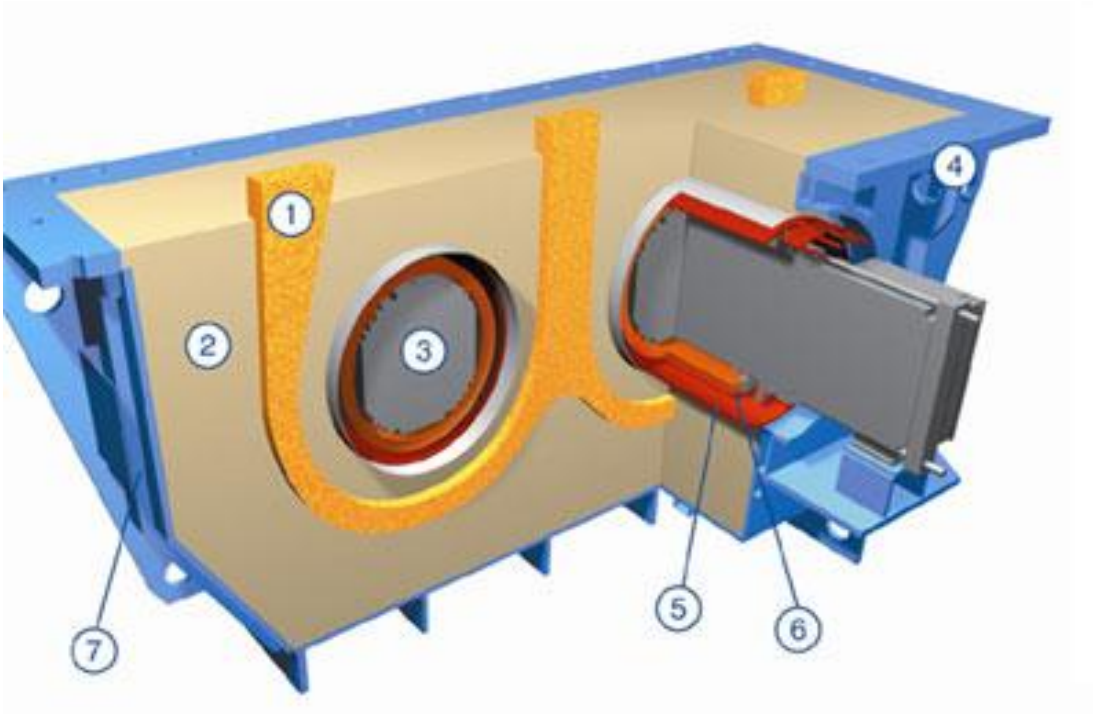

Figure 6.2: Schematic cross section of a double-cored channel induction heater (Ottojunker 2018).

With respect to the ESS furnace, the passages are configured such that the middle is for alloy intake into the heater and the two outer passages are outlets that return alloy back to the bath in the furnace above it This was shown in Figure 3.5 (Fourie and Erasmus 2016; Fourie and Erasmus 2017).

6.3 Metallurgical Comparison

6.3.1 Fluid flow

Figure 6.3 is a schematic representation of metal flow in a double-cored channel induction furnace (Edited image. Original image source: Win 2015).

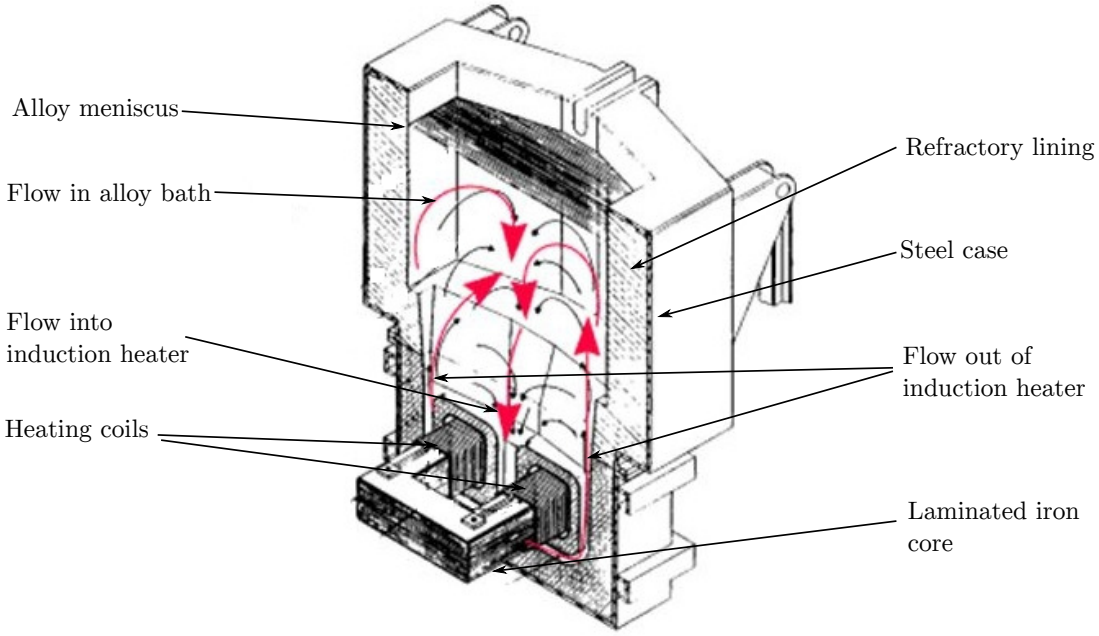

Figure 6.3: Schematic representation of molten alloy flow in a channel induction furnace (Win 2015).

Heating the alloy increases its temperature and lowers its density. Alloy in the heating channel is forced to rise by natural convection through these channels to re-enter the reservoir of molten alloy above it (Yue, Zhang, and Pei 2017). In the ESS furnace, the middle passage is an inlet for cooler alloy to enter into the channels in the same way shown in Figure 6.3 (Fourie and Erasmus 2016; Fourie and Erasmus 2017). The subsequent flow of molten iron causes stirring in the bath and therefore improves mixing and homogeneity.

6.3.2 Heat Transfer

Electromagnetic induced joule heating occurs when an externally applied magnetic field induces an alternating current in a conductor. Eddy currents are generated in the material and ohmic heating of that conductor occurs (EncyclopediaBrittanica 2017). Ohmic heating is described by Joule's first law (also known as the Joule-Lenz law), which is defined mathematically by Equation 6.1.

$$P = I^2 R \tag{6.1}$$

Where:

P is the rate of heat dissipation by the conductor in Watts (W)
I is the current passed through the conductor in Amperes (A)
R is the electrical resistance of the conductor in Ohms (Ω)

Current is passed through a primary coil which generates a magnetic field. A current is induced in the alloy contained by the channel by the generated magnetic field and flow of this current results in ohmic heating as described by Joule's first law.

Numerical definitions of electromagnetic heating for modelling purposes has a large scope, and would require a separate, more extensive study. For this reason, the ESS steelmaking furnace model developed in this research did not include a detailed description of the induction heating phenomenon. Instead, it was taken that, in the ESS steelmaking process, a heater supplying 200 kW of heating power to the alloy would be used (Fourie and Erasmus 2016).

6.4 Summary

A summary of phenomena in channel induction furnaces is given in Table 6.1. The score of relevance refers to the extent that the feature can be used in developing a model for the ESS steelmaking process and is quantified as follows.

1. Relevant. The feature will be used explicitly in the model.
2. Partially relevant. Some aspects of the feature will be considered in developing the model.
3. Not relevant. The feature will be omitted from the model. Either a different steelmaking process will be used, or assumptions made when developing the model.

Table 6.1: Summary of features of the channel induction furnace and their relevance to the ESS steelmaking furnace.

Feature	Relevance			Reason for relevance score
	1	2	3	
Process:			✓	Channel induction furnaces are not used for "steelmaking" as defined in this research. This feature is therefore irrelevant to the ESS steelmaking process model.
Geometry:			✓	The ESS steelmaking process model developed was simplified to the extent that geometry and physical configuration of the heater play no role in the model. For this reason, this feature is irrelevant to the ESS steelmaking process model in this research.
Fluid flow:			✓	Fluid flow in the induction heater requires more extensive research, such as computational fluid dynamics studies. Although fluid flow will most likely have an effect on steady state operation, the scope is too large to include in this research. It is therefore excluded from this study with some assumptions and simplifications made as a compromise for this omission.
Heat transfer:		✓		Numerical modelling of heat transfer also has too large a scope to include in this research. Simplifications and assumptions were made to exclude in-depth consideration of the feature without compromising the process model, or the results obtained from this research.

Chapter 7

Decarburisation in Steelmaking

To develop an ESS steelmaking process model, a solid understanding of decarburisation of molten iron-carbon alloys was required. A literature review was therefore done to investigate this phenomenon.

7.1 Oxygen Potential and Decarburisation

In steelmaking processes, oxygen is introduced to a high-carbon iron alloy by contacting it with either a gas or slag containing a species that can oxidise. "Bath steelmaking" refers to processes where oxygen is introduced via a slag layer, and "oxygen steelmaking" refers to processes where oxygen is introduced by a gas phase injected into alloy (Larsen 1956). Figures 7.1 and 7.2 show the differences in the processes schematically.

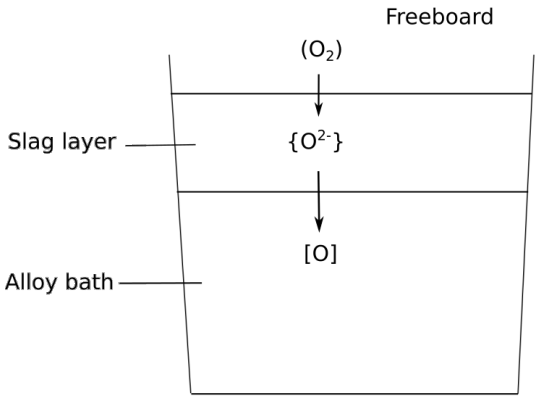

Figure 7.1: Oxygen dissolution mechanism in bath-steelmaking processes

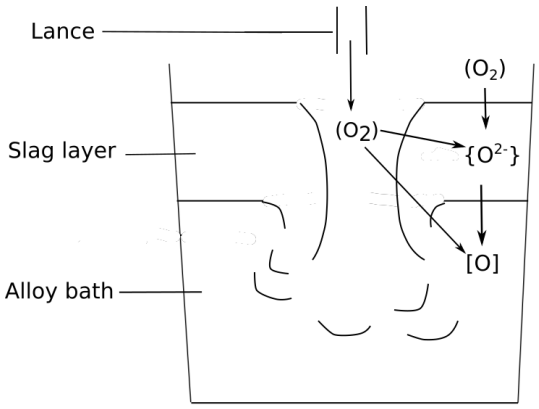

Figure 7.2: Oxygen dissolution mechanisms in oxygen-steelmaking processes.

Gas, slag and alloy are immiscible fluids, and so oxygen must be transferred to the alloy across interfaces where the fluids are in contact. This creates the need for a higher oxygen potential in gas and slag than alloy, so that oxygen can be transferred to alloy for decarburisation to occur (Larsen 1956).

The simplest means to achieve this is by generating slag with high oxygen potential. This is done by having a high concentration of reducible oxides (e.g. iron II and III oxide) which dissolve at the slag-alloy interface as metallic iron and mono-atomic oxygen into the molten alloy (Larsen 1956).

Another pathway observed for the dissolution of oxygen into alloy in bath steelmaking, is by dissolving oxygen gas into slag, and then from slag into the alloy (Woolley and Pal 1999a).

In oxygen steelmaking processes the high velocity jet of oxygen gas is blown into the alloy, which promotes its direct dissolution into the alloy. The jet also oxidises iron and other elements and so a slag is inevitably produced (Larsen 1956). In latter stages of the process, a significant amount of slag will have

formed, enough to make slag-to-alloy dissolution the more dominant oxygen source. This why even when pure argon gas is used in the final stages of a basic oxygen steelmaking furnace (BOF), decarburisation still continues to occur, albeit at a lower rate than the initial stage (Woolley and Pal 1999a).

Once dissolved in the bath, the oxygen reacts with carbon to form carbon monoxide gas at a suitable surface, which typically is somewhere on the refractory lining. The bubbles then grow as more of the reaction occurs and eventually escape the alloy bath once they have reached a diameter large enough to allow buoyancy forces to act on and lift the bubble from the reaction surface to an external environment (Larsen 1956).

This view of the physical sub-processes involved in decarburisation provides a very useful method to analyse the phenomena in steelmaking processes. The challenge faced in this research was accessibility to relevant information that would allow for modelling work to be done. In this light, this review of decarburisation literature was structured so as to present theory on decarburisation in a more accessible manner.

The overall decarburisation reaction is accepted in literature to occur as shown in Equation 7.1.

$$[C] + O \longrightarrow (CO) \tag{7.1}$$

Where [C] represents carbon dissolved in the liquid metal bath, O is oxygen that is either dissolved in the molten slag layer as FeO, or gaseous O_2 in gas-alloy reaction interfaces, and (CO) is the gaseous carbon monoxide product of the reaction

For any particular steelmaking process some or all of the following steps are involved:

1. Mass transfer of:
    1.1. oxygen in slag to the surface where slag meets alloy;
    1.2. oxygen in alloy to the interface where carbon monoxide gas bubble is formed; or
    1.3. carbon in alloy to the interface where carbon monoxide gas bubble is formed.
2. Dissolution of:
    2.1. FeO from slag into alloy as metallic iron and mono-atomic oxygen;
    2.2. gaseous oxygen (O_2) into slag with the aid of $Fe_3{}^+$ ions; or
    2.3. gaseous oxygen (O_2) into alloy as mono-atomic oxygen.
3. Oxidation of:
    3.1. dissolved carbon at reaction sites; or
    3.2. carbon monoxide at gas-metal interfaces.
4. Reduction of FeO and Fe_2O_3 at reaction sites.
5. Nucleation, growth and escape of carbon monoxide and carbon dioxide gas bubbles from the molten bath into the external environment.

The exact steps and the order in which they occur depend on furnace design and process material used (Larsen 1956).

Larsen (1956) mentions that in terms of heat transfer calculations, the open-hearth process should have been impractical and not possible. The fact that process temperatures could be maintained with a gas burner above a slag layer that is low in thermal diffusivity and conductivity, was an unanswered challenge. The author attributed this to the fact that the process was viewed as homogeneous (occuring within the alloy and slag), which greatly simplified calculations, but presented the aforementioned problems, which hindered further development of the process from a research perspective. With the analysis, the author presented a rate-limiting theory that laid the foundation for the aforementioned steps that occur in the decarburisation reaction. In his theory, reactions in the process had to be heterogeneous (different sub-reactions at unique positions), with the controlling species being oxygen (Larsen 1956).

Other researchers then followed the same line of thought, and for the majority of their investigations, came to the conclusion that oxygen mass transfer in slag was the rate-limiting step for concentrations

below 40 wt%FeO slags. For the cases above this concentration, the rate-limiting step was found to be mass transfer in the alloy bath. Mathematical models for mass transfer rates in both slag and alloy were developed to estimate possible decarburisation rates for steelmaking processes and these are discussed in the remainder of this chapter.

7.2 Slag Oxidation by Gaseous Oxygen

Literature with kinetics and rate equations for this reaction were not found in this research because for most investigations, the rate-limiting step was mass transfer of oxygen either in the slag, alloy or gas phases. The dissolution is accepted to occur so quickly at steelmaking temperatures, that it is not the rate-limiting step. The information is presented here to give a view on the possibility of slag oxidation by oxygen gas in steelmaking processes, and its importance to decarburisation.

If the gas above a slag bath is highly oxidizing, oxygen may dissolve into the slag as was postulated by Woolley and Pal (1999a), via electrochemical phenomena at the gas-slag and slag-alloy interfaces. In their research, the cathodic half reaction is described by Equation 7.2.

$$\frac{1}{2}(O_2) + 2e^- \longrightarrow \{O^{2-}\} \tag{7.2}$$

The anodic half reaction was proposed to be the oxidation of another oxygen ion at the slag-alloy interface, where the oxygen atom dissolves into the alloy as shown by Equation 7.3.

$$\{O^{2-}\} \longrightarrow [O] + 2e^- \tag{7.3}$$

Woolley and Pal (1999a) proposed this to be possible due to the ionic nature of slag, which makes it an electrical and ionic conductor. Electrons produced in the anodic half reaction are free to travel through slag, to the gas-slag interface where they are consumed by the cathodic half reaction. This was validated by an experiment where solid, electrically conducting rods or plates that were placed in contact with both slag and alloy significantly improved the rate at which decarburisation occurred (Woolley and Pal 1999a). The solid conductors became a short circuit path for electrons to travel between reaction sites instead of through the relatively less electrically conductive slag.

7.3 Oxygen Mass Transport in Slag

Oxygen mass transfer is the most studied step in literature as it is often postulated to be the rate limiting step for cases where slags have less than 40 wt% FeO (Philbrook 1961; Darken 1964; Robertson and Staples 1974; Min and Fruehan 1992; Paul, Deo, and Sathyamurty 1994; Woolley and Pal 1999b; Woolley and Pal 1999a; Woolley and Pal 2002). In motionless slag baths, diffusion is proposed to be the dominant mode by which mass transfer occurs (Philbrook 1961; Darken 1964). Since the oxygen is in ionic form, it is associated with metallic cations in solution, and so diffusion is the motion of cation-anion pairs through slag (Min and Fruehan 1992; Paul, Deo, and Sathyamurty 1994; Woolley and Pal 1999b). Mass transfer rates of oxygen in slag are therefore dependent on diffusion rates of the cation in the pair, because it is usually the heavier and hence slower diffusing species in slag (Min and Fruehan 1992; Paul, Deo, and Sathyamurty 1994; Woolley and Pal 1999b).

For steelmaking processes, reactions at the slag-alloy interface consume oxygen (discussed in Section 7.4). Also, gas directly above the slag can be oxidising as was discussed in section 7.4. There is therefore a chemical potential gradient of oxygen going down from the slag meniscus, to the slag-alloy contact surface (Woolley and Pal 1999b).

In investigations by Larsen (1956), the existence of a chemical potential gradient was shown by the temperature differences in the slag layer of an open-hearth system. The fact that there was a temperature

profile such as that shown in Figure 7.3 meant that there had to be some boundary-limited processes occurring at the slag-alloy contact surface.

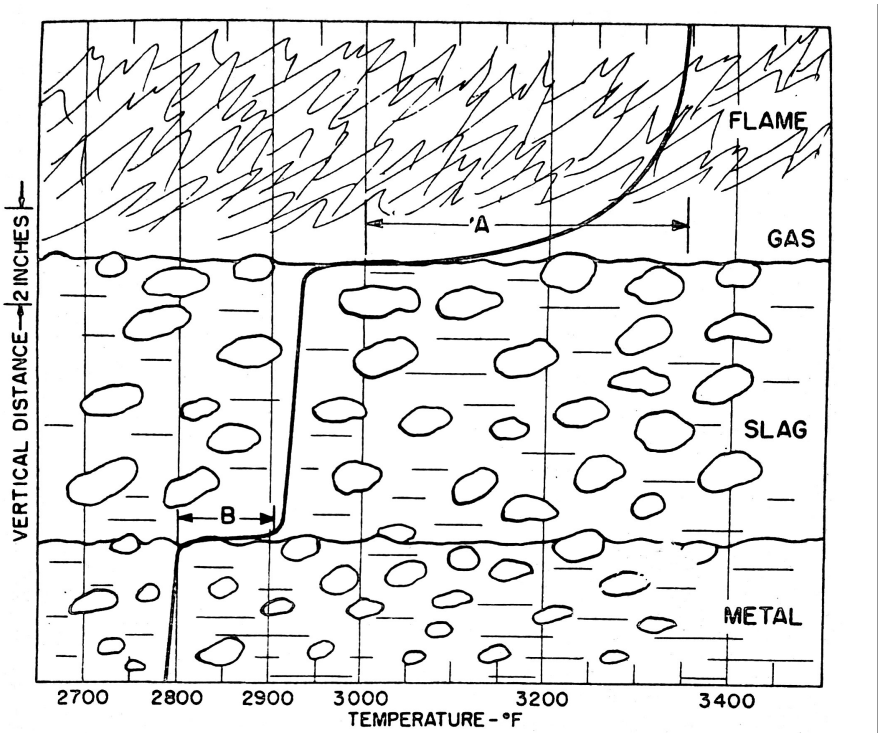

Figure 7.3: Temperature profile of alloy, slag and gas in an open-hearth steelmaking furnace (Larsen 1956).

Philbrook (1961) hypothesised a mathematical description that can be used to describe decarburisation rate in $\mathrm{kg\,s^{-1}}$ as shown by Equation 7.4.

$$\text{Rate} = k_i \cdot A \cdot \Delta C_i \tag{7.4}$$

Where k_i is the mass transport coefficient in $\mathrm{m\,s^{-1}}$, ΔC_i is the concentration difference that creates a driving force for mass transfer of i in $\mathrm{kg\,m^{-1}}$ and A is the interfacial area where i is being consumed in $\mathrm{m^2}$. The values obtained from this model hypothesis were lower than what was physically observed in open hearth furnaces. This was attributed to the fact that open-hearth steelmaking baths have what is called a "carbon boil", where evolution of carbon dioxide from decarburisation reactions add stirring, which enhances mass transfer rates. To account for this convective or mechanical stirring Philbrook (1961) hypothesized that the mass transfer coefficient h_i, varied with fluid velocity as shown in Equation 7.5. The parameters and their units were not explicitly stated in the article, but it was suggested that they would have to be determined empirically from data during a specific furnace's operation, since they will vary with the type of steelmaking process studied (Philbrook 1961).

$$k_i = aV^m \tag{7.5}$$

In Equation 7.5 a is a proportionality constant dependent on fluid properties, diffusion rate of reacting species and geometry of the slag and alloy bath, V is the velocity of the fluid, which is fast enough to result in turbulent flow, and m is an exponent dependent on flow of fluids carrying reactants and the resultant stirring caused by it.

In investigations by Darken (1964) Equation 7.6 was proposed as the molar mass transfer rate (in mol/s) through alloy, slag and gas for steelmaking processes.

$$\dot{n}_i = A_{int} \cdot \frac{D_i}{\delta_i} \cdot (C_i - C_i^*) \tag{7.6}$$

Where A_{int} is the reaction interface area (m^2), D_i is the diffusion coefficient ($m^2\,s^{-1}$), δ_i is the boundary-layer thickness (m) and C_i and C_i^* are the molar bulk and interfacial concentrations of species i (mol/m^3). This is similar to Equation 7.4 presented by Philbrook (1961), except that mass transfer coefficient h_i is replaced by diffusivity across a boundary layer and the concentration gradient across it. With furnace parameters as shown in Table 7.1, mass transfer rate of FeO in slag was calculated to be approximately 0.11 mol/s for an open-hearth steelmaking furnace during a carbon boil (Darken 1964).

Table 7.1: Furnace parameters used in decarburisation investigations found in literature (Darken 1964).

Parameter	Value
Capacity	30 t
Slag FeO concentration	20 wt%
Slag FeO activity	0.4
Slag density	$3.5\,t/m^3$
CaO/SiO_2 ratio	2
Alloy C concentration	0.5 wt%
Alloy density	$7.0\,t/m^3$
Pressure of CO gas bubble in the bath	1.5 atm
Diffusion coefficient ($D_1 i$)	$1.0 \times 10^{-6}\,cm^2\,s^{-1}$
Boundary layer width (δ_i)	1.2×10^{-4} m

Investigations by Darken (1964) were done with relatively motionless alloy and slag baths. In bath steelmaking processes, the bath is stirred by carbon monoxide bubbles formed in decarburisation reactions moving through and out of the slag. This stirring is known to improve mass transfer rates as was shown in investigations done by Robertson and Staples (1974). In their experiments, the aim was to determine mass transfer coefficients across bubble-stirred interfaces, using molten lead-salt and aqueous-amalgam systems. The results obtained suggested that mass transfer coefficient (k) was related to gas bubble-flow rate (Q) according to Equation 7.7.

$$k^2 \propto \frac{DQ}{d_{cell}^2} \tag{7.7}$$

Where D is the diffusion coefficient of the diffusing species ($m^2\,s^{-1}$), Q is the gas bubble flow rate from any number of sources ($m^3\,s^{-1}$), d is the diameter of the cell (i.e. experimental reaction chamber) measured in m^2. This equation implies that rate of decarburisation is proportional to the square root of gas bubble flow rate across the reaction interface. Equation 7.7 was transformed to 7.8, where B is a proportionality constant and was successfully applied to open-hearth steelmaking conditions, using parameters obtained from experiments using amalgam-aqueous and lead-molten salt systems.

$$k^2 = B\frac{DQ}{d_{cell}^2} \tag{7.8}$$

The values of B were shown to be different for metal and slag diffusion control, as shown in Table 7.2.

Table 7.2: Proportionality constant (B) values under different conditions (Robertson and Staples 1974).

	Low depth	High depth
Slag control	$40\,cm^{-1}$	$50\,cm^{-1}$
Alloy control	$80\,cm^{-1}$	$120\,cm^{-1}$

Applying Equation 7.8 and parameters used by Larsen (1956) to an open-hearth steelmaking process, mass transfer rates were calculated (Robertson and Staples 1974). Results obtained from the sample calculation showed that the equation applied to steady state boils, where decarburisation rate was generally

observed between 0.15 to 0.20 wt%C/h. This back-calculated rate coefficient was close to observed values in experiments done by Robertson and Staples (1974), using an amalgam-aqueous system, which was accepted as validation of Equation 7.8.

In investigations by Min and Fruehan (1992) mass transfer of FeO in slag to the slag-metal interfaces was formulated based on diffusion of iron oxide (FeO) through slag. FeO is believed to diffuse as Fe^{2+} and O^{2-} ion pairs, but the phenomena was simplified to combined FeO mass transport. The molar flux of FeO was described by Equation 7.9. FeO^e was taken to be the concentration of FeO in slag that is at equilibrium with an overlying CO gas at 1 atm pressure, which was further approximated to be zero. With this model, an increase in bulk FeO concentration or gas-slag interfacial area, results in increased mass transfer rate of FeO in slag, which leads to higher rates of decarburisation. This is in agreement with results observed in previous experiments by researchers such as Philbrook (1961), Darken (1964), and Robertson and Staples (1974).

$$J_{FeO} = \frac{m_s \cdot \rho_{slag}}{M_{FeO} \cdot 100}(\%FeO - \%FeO^e) \tag{7.9}$$

In Equation 7.9, m_s is the mass transfer coefficient of FeO in slag, estimated to be 1×10^{-4} to 1×10^{-5} m s^{-1}, ρ_{slag} is slag density in kg m^{-3}, M_{FeO} is molecular weight of FeO in kg mol^{-1} and %FeO and $\%FeO^e$ are percentage concentrations of FeO in the bulk slag and gas-slag interface respectively.

Paul, Deo, and Sathyamurty (1994) did investigations under conditions where mass transfer rate of FeO in slag was the rate-limiting step using a kinetic model they developed from theory. With regard to decarburisation, FeO mass transfer was modelled to follow Equation 7.10, where A_{gs} is gas-slag interfacial area (m^2), k_{FeO} is mass transfer coefficient of FeO in slag (m/s) and C^s_{FeO} and C^i_{FeO} are the molar concentrations of FeO in bulk slag and at the gas-slag interface respectively in mol m^{-3}.

$$-\frac{\partial n_{FeO}}{\partial t} = A_{gs} \cdot k_{FeO} \cdot [C^s_{FeO} - C^i_{FeO}] \tag{7.10}$$

The model was used to determine the mass transfer coefficient k_{FeO}, for the following conditions stated by a separate author, whose research was not found in this literature search. Calculated values of the mass transfer coefficient were observed between 2.4×10^{-5} and 10.63×10^{-5} m s^{-1}. Variations in the value were attributed to dependence on FeO concentration and slag temperature during the experiments (Paul, Deo, and Sathyamurty 1994).

Woolley and Pal (2002) did experiments to investigate the kinetics of reduction of iron-oxide slag and decarburisation of iron carbon alloys. In their research, decarburisation was defined as the reduction of FeO in slag by carbon in liquid-iron droplets, which applies to slag-alloy emulsions such as those observed in BOF steelmaking. FeO reduction was defined as reduction of FeO from slag by an underlying Fe-C alloy bath, which applies to bath steelmaking process such as with the open-hearth. In their investigations a relationship between molar rate of reaction and molar slag FeO concentration was found as described by Equation 7.11.

$$Rate = k \cdot C_{FeO} \tag{7.11}$$

Where k is the reaction rate constant in m s^{-1}, and C_{FeO} is the average molar concentration of FeO in the slag (mol m^{-3}). For their experiments, the apparent rate constant at time t was defined using Equation 7.12, where m_{slag} is total mass of slag in kg, ρ_{slag} is density of the slag in kg m^{-3}, A_{SMI} is planar area of the slag-metal interface in m^2, $\%O_{Fe}$ is mass percent of oxygen in the slag associated with iron, and t is time in s.

$$k(t) = -\frac{10^{-6} m_{slag}}{\rho_{slag} A_{SMI}} \frac{\partial \ln \%O_{Fe}}{\partial t} \tag{7.12}$$

The value for the apparent rate constant was approximately equal to the FeO mass transfer coefficient in slag. Using results from the experiment, they substituted values in to Equation 7.8 from Robertson and Staples (1974). They calculated the parameter B using dimensionless correlations to a value of 0.4 cm^{-1} and substituted the value into Equation 7.8. B was much lower for their experiments than values obtained

by Robertson and Staples (1974) for both low and high-depth slag control, but when substituted into Equation 7.8, resulted in a rate constant very close to that calculated in slag-metal systems by other researchers.

Mass transfer of oxygen can also be analysed from an iron-oxygen diffusion pair perspective. Since the slower ion is usually the cation, diffusivity of oxygen can be calculated from as that of the cation. In the case of steelmaking slags, the cation of interest is of iron II and III. The diffusivity of these cations and oxygen in slags has been studied by a number of authors. The values and equations which were found in literature are summarized in Table 7.3, along with their source citations (Woolley and Pal 2002).

Table 7.3: Diffusivity of oxygen and iron ions in liquid slags.

T °C	**Chemistry**	**D** m^2/s	**Reference**
1615	$\frac{Fe^{2+}}{Fe_{Total}}$	$D = 3.0(\pm 1)10^{-7}$	Sayad-Yaghoubi, Sun, and Jahanshahi (1997)
1500	$CaO\text{-}SiO_2\text{-}MnO\text{-}FeO_x$	$[1.7 to 4.3]\,(\pm 0.4)\ 10^{-10}$	Dolan and Johnston (2004)
1600	60.9 to 65.4 wt%SiO_2 4.5 to 15.9 wt%FeO 30.1 to 23.2 wt%CaO	$D = 2 \times 10^{-10}$ to 1.5×10^{-9}	Keller and Schwerdtfeger (1986)
1253 to 1535	Molten $CaFeSiO_4$	$logD_{Fe} = -\frac{(10700 \pm 1600)}{RT} - 1.93 \pm 0.37$ 3.67×10^{-10} to $1.49 \times 10^{-9}\,cm^2/s$	Agarwal and Gaskell (1975)
1430 to 1550	$0.1 < \frac{Fe^{3+}}{Fe_{Total}} < 0.4$	$D = (6.60 \pm 1.15)10^{-3} \exp -\frac{(10700 \pm 1600)}{RT}$	Mori and Suzuki (1968)

7.4 Dissolution of Oxygen from Slag to the Alloy

Oxygen dissolution at slag-metal interfaces has been shown to be electrochemical in nature from galvanostatic (fixed current) and potentiostatic (fixed voltage) experiments done by Woolley and Pal (1999a). The iron-oxygen redox was described to occur as shown by the half reactions in Equations 7.13 and 7.14, where curly braces denote dissolution in slag ({}) and square brackets denote dissolution in the alloy bath ([]).

$$\{Fe^{2+}\} + 2\,e^- \longrightarrow [Fe] \tag{7.13}$$

$$\{O^{2-}\} \longrightarrow [O] + 2\,e^- \tag{7.14}$$

Experiments done in the investigations were set up as follow:

1. Base experiments - FeO containing slag overlying an Fe-C bath:

   (a) Crushed, solid slag added to a carbon saturated molten iron bath maintained at 1400 to 1600 °C;
   (b) Pellets of pure iron oxide added to molten slag layer overlying a carbon supersaturated liquid iron bath maintained at 1400 °C.
2. Addition of TiO_2
3. "Internal circuit": Base experiments with solid iron plates or molybdenum rods made to contact slag and alloy.
4. "External circuit": Base experiments with solid graphite rod in contact with alloy only and solid iron rod in contact with slag only simultaneously.
5. External circuit experiment with:
   (a) Voltmeter connected to both iron and graphite to measure open-circuit voltage; and
   (b) Ammeter connected to both iron and graphite to measure short-circuit current.
6. External circuit with direct current voltage source connected to iron and graphite:
   (a) Base "external circuit" with DC; and
   (b) External circuit with DC arc, with iron rod raised out of slag to conduct current through an arc.

From experiments in Item 3 of the list, it was established that the rate of reaction was increased when there was an internal circuit added. This was because the rod or plate in the slag increased the surface area where iron could be reduced and oxygen oxidised. The rod or plate also provided a path way for electrons to travel deeper in to the slag layer as shown in Figure 7.4 (Woolley 1998).

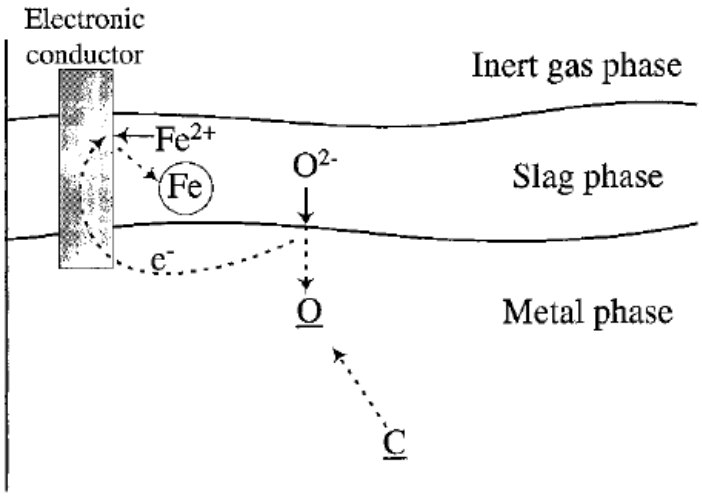

Figure 7.4: Enhancement of iron-oxygen redox reactions using an electrode (Woolley 1998).

Experiments 6a and 6b showed that the rate could be significantly increased by applying a DC current with an anode placed in the alloy bath.

In investigations by Min and Fruehan (1992), another reaction was shown to occur at the gas-slag interface, when there is carbon monoxide present in the gas phase. In their experiments, an iron-carbon alloy droplet was placed in an FeO containing slag. X-ray tomography showed a gas halo developed around the alloy after some time. It was postulated that CO_2 was reduced at the gas-alloy interface by carbon dissolved in alloy (Equation 7.16). The carbon monoxide product of this reaction diffused through the gas halo to reach the gas-slag interface, where it is then oxidised by FeO to form CO_2 (Equation 7.15).

$$[C] + (CO_2) \longrightarrow 2\,(CO) \tag{7.15}$$

$$CO + FeO \longrightarrow Fe + CO_2 \tag{7.16}$$

The CO_2 product then travels back to the gas-alloy interface and is reduced once again to CO gas. This process continues until there is no more carbon in the alloy or oxygen ions in the slag, or the gas bubble escapes through the effect of buoyancy forces. These mechanisms of decarburisation are shown in Figure 7.5.

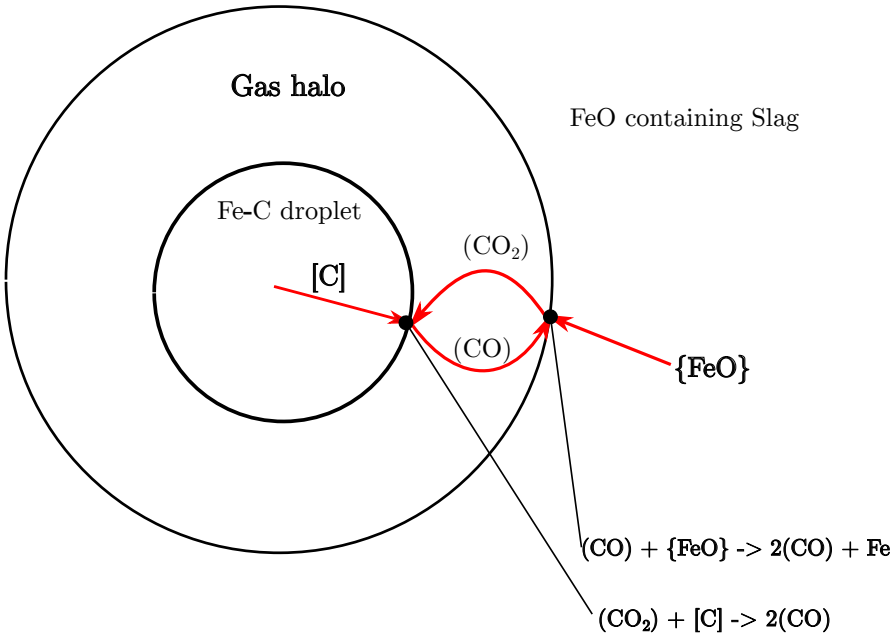

Figure 7.5: Mechanism of decarburisation of an alloy droplet as proposed by Min and Fruehan (1992).

For the case where CO_2 dissociation was the rate-controlling step, the rate was found to follow Equation 7.17.

$$Rate = k_{CO2} \cdot A \cdot K \cdot C(wt\%FeO) \tag{7.17}$$

Where k_{CO2} is the rate constant for dissociation of CO_2, K is the equilibrium constant for the reaction in Equation 7.16, A is the gas-metal interface area and C is an equilibrium constant relating weight percent of FeO to its activity. The rate constant was also found to be affected by surface active elements such as sulphur which occupy reaction sites and limit the rate at which oxygen dissolves into the alloy (Min and Fruehan 1992).

7.5 Oxygen Mass Transport in Molten Iron

From a process level perspective, oxygen mass transfer in molten iron is hardly ever a rate-limiting step. Most researchers have therefore excluded it from their research and model development processes. Fundamentally, mass transport of oxygen is via diffusion and is most important at gas-metal and slag-metal contact surfaces. The difference in chemical potential between the bulk alloy and gas-metal contact surface is the driving force for diffusion and so the flux can be determined using Equation 7.18.

$$J_{[O]} = k \cdot A \cdot (C^b - C^i) \tag{7.18}$$

Where k is mass transfer coefficient (m/s), A is the area of the particular interface to which oxygen is being transferred, C^b and C^i are molar bulk and interfacial concentrations respectively in mol/m^3.

Oxygen diffusivity parameters have been investigated by many other researchers and are presented in Table 7.4 as taken from an article by Ono (1977).

Table 7.4: Diffusivity parameters for oxygen in liquid iron as extracted from 7.6.

Temperature (°C)	**Diffusivity** ($cm^2\,s^{-1}$)	
	D_o (m^2/s)	Q (kJ/mol)
1550	$(19 \pm 7) \times 10^{-5}$	
1560	$(2.3 \pm 0.3) \times 10^{-5}$	
1600	$(2.7 \pm 0.5) \times 10^{-5}$	
1610	$(12 \pm 3) \times 10^{-5}$	
1620	$(15 \pm 1) \times 10^{-5}$	
1550 to 1680	3.34×10^{-3}	50.21
T_{melt} to 1700	3.18×10^{-3}	50.21

With the diffusivity determined, the mass transfer coefficient can be calculated for scenarios where there is gas bubble stirring (Either from Equation 7.8 as was described by Robertson and Staples (1974) or from the Equation 7.23 derived through dimensional analysis given by Hack and Ende (2014)).

It was found that oxygen concentration in an alloy bath is usually higher than that expected at equilibrium with a given carbon content (Larsen 1956). In previous studies by Taylor and Chipman (1942), the oxygen concentration in liquid iron with an overlying pure FeO slag was estimated to follow Equation 7.19, which was related to the temperature of the alloy (T_{alloy}).

$$log(\text{wt\%[O]}) = 2.765 - \frac{6380}{T_{alloy}} \tag{7.19}$$

Further studies by Bishop et al. (1956) incorporated the activity of iron(II)oxide and the CaO/SiO_2 ratio of a slag overlying a still molten alloy bath at 1600 °C, and obtained the plot shown in Figure 7.6. The values were extracted digitally, and data fitted to a sigmoid relationship shown in Equation 7.20. Constants a, b, c and d vary with $CaO{:}SiO_2$ ratio and FeO mass concentration as shown in Table 7.5.

$$0.2 \times \text{wt\%O} + log(\text{wt\%O}) = a_{FeO} \cdot e^{2.73 - \frac{6372}{T_{alloy}}} \tag{7.20}$$

$$a_{FeO} = a - (b \cdot \exp -c \cdot \frac{wt\%CaO}{\text{wt\%SiO}_2}^{\,d}) \tag{7.21}$$

These equations provided a more accurate way of estimating the concentration of oxygen composition, and therefore the estimated rate of oxygen mass transfer in molten alloy of bath steelmaking processes.

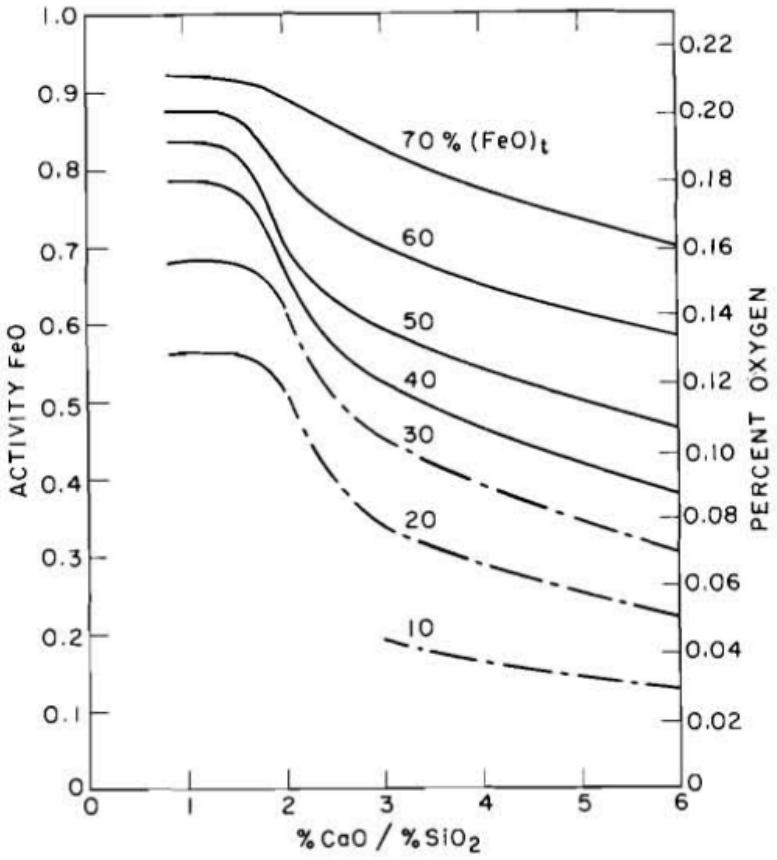

Figure 7.6: Results from experiments by Bishop et al. (1956) on the oxygen concentration in molten alloy as a function of FeO concentration and lime to silica ratio in molten slag at 1600 °C.

Table 7.5: Constants for the sigmoid equation fitted on data from experiments done by Bishop et al. (1956) shown in Figure 7.6.

FeO wt%	a	b	c	d
10	5.83×10^{-1}	5.89×10^{-1}	8.43×10^{-1}	-6.63×10^{-1}
20	5.66×10^{-1}	3.34×10^{-1}	1.98×10^{1}	-3.61
30	6.84×10^{-1}	3.80×10^{-1}	1.36×10^{1}	-3.07
40	7.92×10^{-1}	4.15×10^{-1}	7.91	-2.7
50	8.46×10^{-1}	3.71×10^{-1}	7.15	-2.8
60	8.83×10^{-1}	3.19×10^{-1}	6.30	-2.28
70	9.23×10^{-1}	3.49×10^{-1}	6.89	-1.53

7.6 Dissolved Carbon and Oxygen Reaction and the Formation of Bubbles

Because carbon is removed from the bath by oxidation, the product of the reaction is carbon monoxide and carbon dioxide gases. The ratio of carbon monoxide to dioxide is dependent on the oxygen potential of the alloy bath (Woolley and Pal 1999a). For most steelmaking processes, the more abundant product is carbon monoxide and so a small amount of carbon dioxide is formed.

Fruehan and Pistorius (2014) suggested a first approximation of the maximum gas bubble diameter

that would result in a bubble escaping the alloy bath using Equation 7.22.

$$d_b = \left[\frac{6\sigma d_o}{g\rho_L}\right]^{\frac{1}{3}} \tag{7.22}$$

Where σ is the liquid surface energy ($1.8\,\mathrm{J\,m^{-2}}$ for liquid iron), d_o is an orifice diameter (such as in the refractory lining), g is acceleration due to gravity, ρ_L is the alloy density, which is about $7.0\,\mathrm{g/cm^3}$ for liquid iron.

The generation of the gas bubbles results in stirring of the bath. The effect of stirring on reaction rate was studied by Robertson and Staples (1974) where the evolution rate of gas bubbles affects the mass transfer coefficients of species according to Equation 7.8 discussed in Section 7.3. This implies an auto-catalytic process, where increased decarburisation rate, is an increase in bubble formation rate and vice-versa. Therefore if diffusivity of a species is known, a more realistic mass transfer coefficient can be estimated using an expected gas bubble evolution rate.

In computer simulations of a bottom blown steel refining ladle reported in the chapter by Hack and Ende (2014), a relationship between mass transfer coefficients versus ladle conditions was derived from dimensional analysis and was represented by Equation 7.23

$$k = \frac{0.08}{m}\sqrt{14.23\frac{QTA_{top}}{N^{\frac{1}{4}}}\log\left(1+\frac{h}{1.5P_o}\right)} \tag{7.23}$$

here Q is the argon gas flow rate through the alloy, m is the mass of steel in the ladle, T is the alloy temperature, A_{top} is area of the top alloy surface, N is number of porous plugs supplying the argon gas, h is the depth of gas injection and P_o is the ambient pressure above the vessel. Calculation of the mass transfer coefficients in slag and metal were in agreement with values from real ladle refining processes.

7.7 Overall Rate Constant

The apparent or overall rate constant can be determined either from a weighted average, or slowest step calculation. In the weighted average method, the contributions of each rate constant is included and overall rate constant calculated as shown in Equation 7.24.

$$k_o = \frac{1}{\sum \frac{1}{k_i}} \tag{7.24}$$

Where k_o is the overall or apparent rate constant and k_i are the rate constants for individual steps in the overall decarburisation reaction.

In the slowest-step method:

$$k_o = k_{min} \tag{7.25}$$

Where k_{min} is the lowest rate constant.

An example of the weighted-average method is in the work done by Paul, Deo, and Sathyamurty (1994), where a general kinetic model for decarburisation in a basic oxygen process was developed. With the model, the authors observed the following:

1. At <5 wt%FeO concentration, overall reaction rate was controlled by a mix of FeO mass transport and gas-metal reaction rates.
2. Between 5 wt%FeO and 40.0 wt%FeO, all three mechanisms had an influence on the rate of reaction and a mixed control mechanism was calculated.
3. Above 40 wt%FeO, overall reaction was controlled by the reactions at the gas-metal and gas-slag interface.

Similar work was done by Min and Fruehan (1992) and for their experiments, were mainly under slag mass transfer control.

The slowest-step approach was used by Woolley and Pal (1999b) in their model development. In their investigations the rate-limiting step was also oxygen mass transfer in slag.

Rates were similar in all cases where there was slag mass transfer control, with the apparent rate coefficient lying between 10^{-5} and 10^{-4} m/s

7.8 Summary

Decarburisation in steelmaking involves a number of steps that depend on processing equipment and raw materials used. In design, analysis and optimization, mass and energy balances tend to assume homogeneous emulsions of immiscible phases in reactions. It can be useful to include kinetics in steady state calculations for a bath steelmaking process such as the ESS Furnace, so as not to over-estimate potential performance of a particular furnace.

Some rate equations were found for mass transfer of oxygen in slag and alloy, and carbon in alloy. The effect of gas-bubble stirring on mass transfer was also reviewed. No information on slag-metal and gas-metal interface reaction rates for bath steelmaking processes were found at the time. This was due to limited access to literature that may have the information. Most of the information found was for investigations where mass transfer was the rate-limiting step. A more comprehensive literature search is required to obtain information on the rates of gas-metal and slag-metal reactions. For steelmaking processes in which expected slag compositions are below 40 wt%FeO, it is likely that chemical reaction rates will not be controlling, but rather, the rate at which species diffuse to respective reaction sites during steady state processing.

Part III

Research Approach and Methodology

Chapter 8

Research Approach

This chapter describes the approach used to do this work. Figure 8.1 provides an overview of the steps taken. Each of the steps is described in the remainder of this chapter.

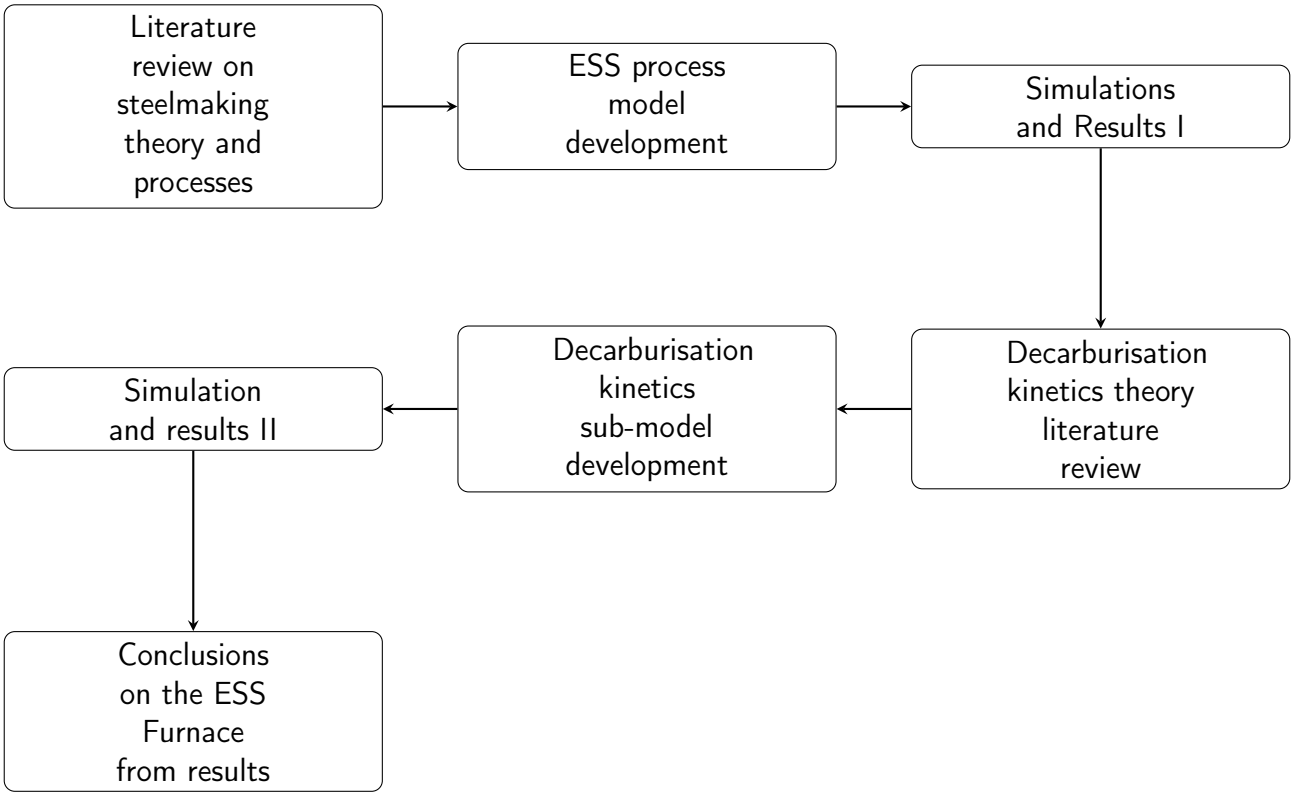

Figure 8.1: Research approach flow diagram.

8.1 Literature Review on Steelmaking Theory and Processes

The first step was a literature review to investigate steelmaking theory. Information about the ESS furnace was obtained from literature and through private communications with inventors of the furnace. Open-hearth furnace steelmaking literature was then reviewed, since it is similar in some respects to the ESS furnace. Information about induction heating furnaces was then obtained from literature, since the ESS furnace uses channel-type induction heating technology in its design.

8.2 ESS Process Model Development

A mass and energy balance model of the ESS steelmaking process was developed. The model's purpose was to gain insight into the expected steady-state behaviour of the furnace.

8.3 Simulations, Results I

Simulations were done to study the steady-state behaviour of the ESS steelmaking process. Results revealed the need to better understand decarburisation kinetics theory for bath steelmaking processes in order to include it in the study and make more informed decisions regarding the process from work done in this research.

8.4 Decarburisation Kinetics Theory Literature Review

A literature review was then done to better understand decarburisation kinetics. Mathematical descriptions that describe rates of decarburisation were investigated to develop a sub-model that would be included into the steady-state mass and energy balance model.

8.5 Decarburisation Kinetics Sub-model Development

A decarburisation kinetics sub-model was developed with selected mathematical descriptions from literature. This was incorporated into the steady-state mass and energy balance model of the ESS process.

8.6 Simulations, Results and Analysis II

Simulation experiments were done with hypothetical and real material assays found in literature. The results provided a basis for the conclusions made about the ESS process when applied to steelmaking.

8.7 Conclusions and Recommendations from Results

Conclusions about the ESS steelmaking furnace concept were made based on the modelling work. Recommendations for further research work were made after conclusions were reached.

Chapter 9

Research Methodologies

A mix of qualitative and quantitative research methods were used to gather information that could be used in this project for the reasons described in this section.

9.1 Gathering of Information

The primary source of information was through conversation with designers of the ESS furnace, and review of articles published by them. It was therefore necessary to include the qualitative type of research in order to organise information from direct communication with the designers about the ESS furnace to gain their understanding of the process and document it responsibly.

Due to similarities with the open hearth furnace and features similar to induction furnaces, literature around these processes was also reviewed in order to understand metallurgical features, that will possibly play a role in the ESS steelmaking furnace. Decarburisation kinetics theory was reviewed in order to gain a deeper understanding of the rates at which the reaction can occur, so that this may be included in the ESS steelmaking model. Correlational quantitative research was therefore used for this part of the work.

9.2 Model Development

The research method used was adapted from the work done by Zietsman (2004). The modelling approach for the steady state process model is similar to that used by Pauw (1989) and Zietsman (2004). This approach has been chosen because of the nature of the ESS furnace, which allows coarse discretisation into specific regions, which can be used to develop a steady state mass and energy balance model. To account for the effects of decarburisation kinetics, sub-models of these phenomena was developed and included in the mass and energy balance model of the ESS steelmaking furnace. Simulations were then done with the model, and results used to predict potential behaviour of the furnace under steady state operation. This part of the work required both experimental and correlational research methods to achieve the goals of this project.

Part IV

Process Modelling

Chapter 10

Model Specification

10.1 Modelling Aims

The aim of this modelling work is to develop a mass and energy balance calculator that includes decarburisation kinetics, which simulated the steady state operation of the ESS steelmaking furnace based on information obtained from literature and the designers of the furnace.

10.2 Identification

The model is identified as follows:

Full model name: ESS mass and energy balance model
Model codename: ESS-MEB

10.3 Purpose

The purpose of this model is to calculate mass and energy balances for use in investigating whether it is possible to decarburise pig iron from 4.0 to 0.25 wt%C, at a steel production rate of $10.0\,\mathrm{t\,h^{-1}}$, when using raw materials that are produced locally in South Africa.

10.4 Scope

The process model is focussed on phenomena that occur within the furnace walls. For this reason, explicit descriptions of raw material preparation, induction heating in the channels, exhaust gas heat exchangers and post treatment of products are excluded from the model. Assumptions and simplifications presented in Sections 13 and 14 were used to approximate performance without having to explicitly describe the excluded features.

The decarburisation kinetics sub-model focuses on decarburisation reaction only. Other reactions such as desulphurisation and dephosphorisation were not included.

10.5 Modelling Approach

The flow sheet modelling approach described in Section 4.5, was used to develop the ESS steelmaking process model.

10.5.1 Result Specification

The results required from this model included the following.

1. The quantity of prescribed iron ore, flux and reductant required to decarburise molten pig iron from it's initial carbon-saturated state to less than 0.25 wt%C.
2. The quantity of combustion air and pulverised coal required to maintain sufficient energy in the system during steady state operation.
3. The quantity and quality of molten material produced at the heap's surface in order to achieve the decarburisation state in Item 1 of this list.
4. An estimation of rates at which decarburisation phenomena will occur during steady state operation, given the conditions in Item 3 of this list.
5. The quality and quantities of hot metal, slag and exhaust gas that can be produced during steady state operation, which includes chemical composition and mass flow of the materials.
6. An estimation of heat production or consumption at the raw material heap surface and slag-alloy interface.
7. An estimation of heat losses that will be observed during steady-state operation, given the materials used in, and the dimensions of the furnace's refractory materials.

Chapter 11

System Analysis

This chapter describes the ESS steelmaking concept. Analyses of the process flow, furnace design, material inputs and outputs, and metallurgical aspects is provided to as much detail as was provided for research at the time this project was done.

11.1 Process Description

The ESS furnace was proposed to be suitable for producing low carbon steel in a continuous iron and steelmaking process as shown in Figure 11.1. Molten pig iron is fed directly to the ESS from an ironmaking or scrap melting furnace. Envirosteel has an in-house ironmaking furnace design which is recommended for use in this steelmaking process configuration. However, other ironmaking sub-processes can also be used, as long as a continuous supply of molten pig iron can be supplied to the ESS. Solid iron-ore, flux and reductant are also added to the ESS furnace's heap surface and are melted to produce an iron-oxide rich slag, which flows down to the alloy bath and sits above it. Oxygen is transferred from the slag to alloy and reacts with carbon dissolved in it, which decarburises the alloy in a similar way to open-hearth steelmaking and the product is low-carbon hot metal. The hot metal is tapped from the furnace into a ladle where its chemical composition is adjusted to the desired final specification using alloying agents in the form of solid ferroalloys. If required, further decarburisation can be done manually in the ladle metallurgy stage using oxygen lances as stated by the designers of the furnace. The final hot metal product is then cast and rolled to produce the final solid steel sheets or bars as required by customers.

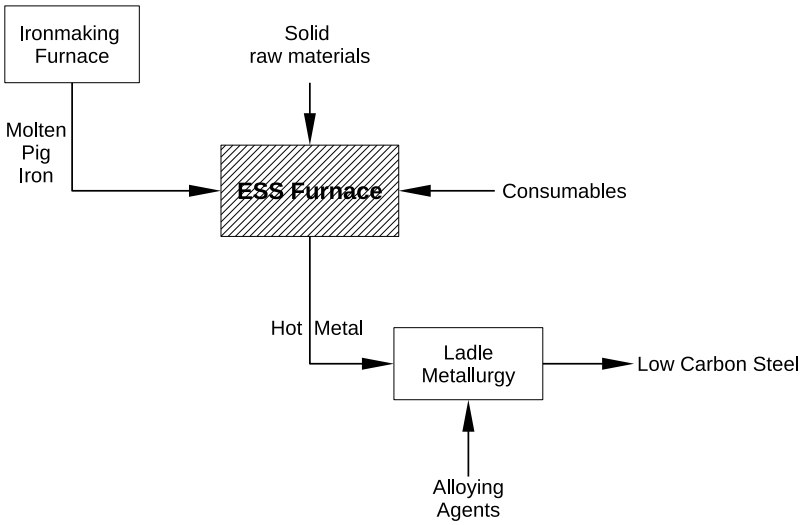

Figure 11.1: Flow diagram of the ESS steelmaking process concept.

11.2 Furnace Model Geometry

ESS steelmaking furnace dimensions used in this research are shown in Table 11.1 and Figure 11.2 is provided for reference to some of the dimensions described in the table.

Table 11.1: Dimensions of the ESS Steelmaking furnace used in this work.

Dimension	Symbol	Value
Internal furnace length (from slag-tapping to alloy-tapping wall)		4.0 m
Internal furnace width	W1	4.0 m
Furnace floor angle	A1	5.0°
Height of exposed hot wall	H1	2.5 m
Height of exposed cold wall	H2	1.2 m
Internal roof radius	R1	2.5 m
Wall and roof refractory lining width		0.4 m
Slag layer width (top meniscus)	W2	2 m
Slag-alloy interface width	W3	1.8 m
Heap top surface width	W4	2.4 m
Heap angle of repose	A2	33°
Calculated freeboard volume		46.0 m^3
Number of induction heating segments		1

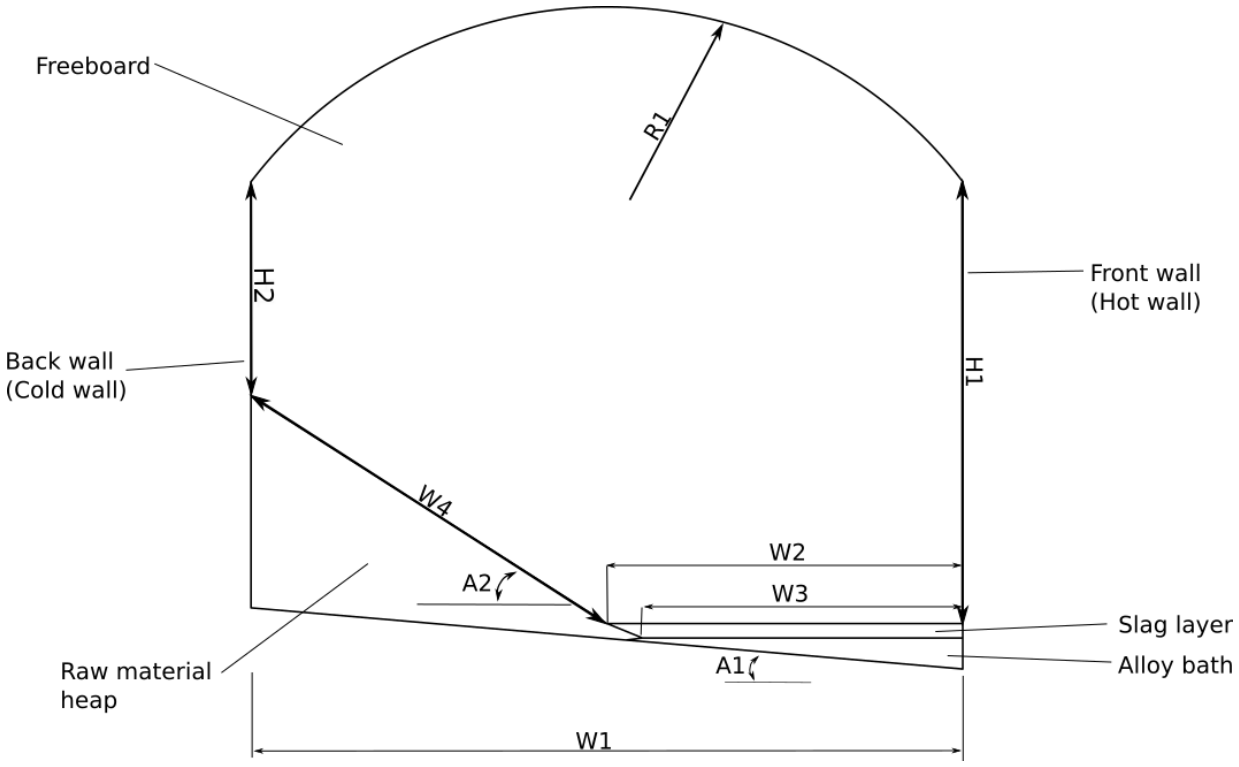

Figure 11.2: Reference diagram for dimensions of the ESS furnace studied in this project.

The proposed total refractory lining thickness of the furnace walls and roof is 40 cm while the steel plates that form a case around the refractory material is 5 cm thick (Fourie and Erasmus 2016). The thickness of refractory material in the floor was not specified for this work. It is expected that the floor will have a much thicker refractory material layer than the walls and roof, which will be layered on top of a steel support structure.

11.3 Inputs

Inputs to the ESS furnace include solid raw material, molten pig iron and consumables. These are described individually in the remainder of this section.

11.3.1 Molten Pig Iron

Molten, carbon-saturated pig iron which is produced in a separate process is the main raw material input of the process. The molten pig iron is fed directly into the ESS furnace hearth at a proposed feed rate of $10\,\mathrm{t\,h^{-1}}$, with an input temperature between 1500 to 1550 °C (Fourie and Erasmus 2016). This feed rate is for a furnace that is sized as specified in Section 11.2.

11.3.2 Solid Raw Material

Solid raw material feed is mainly iron ore, with flux and reductant added to assist with improved furnace operation as will be discussed in Section 11.5. The iron ore is the source of iron oxide in slag, which is used as the main oxidant in removing carbon dissolved in the molten pig iron feed. A proposed advantage of the ESS furnace is its ability to use fine particle raw materials after an agglomeration step such pelletising (Fourie and Erasmus 2016). Sintering and re-grinding are not necessary steps in the process, which has the potential to save energy overall (Fourie and Erasmus 2016).

11.3.3 Consumables

Consumables used in the ESS steelmaking furnace are air, fuel and electricity. Air provides oxygen for expected combustion reactions in the furnace freeboard and can be preheated for improved thermal efficiency in the furnace. The temperature of preheated air is expected between 600 to 800 °C (Fourie and Erasmus 2016), depending on the efficiency of heat exchangers which use exhaust gas to preheat the incoming fresh air. Pulverised coal is used as fuel in the proposed coal burners, whose tuyeres are embedded in the hot wall as described in Section 3.1. The coal burner flame and fresh hot air supplement energy in the furnace and maintain required operating temperatures of between 1500 to 1550 °C (Fourie and Erasmus 2016). Electricity is used by the ESS furnace to power a channel induction heater, which helps to regulate the alloy bath temperature to required specification. A 200 kW induction heater is proposed for the furnace design as specified in Section 11.2 (Fourie and Erasmus 2016).

11.4 Outputs

Outputs of the ESS furnace are low-carbon steel, slag and exhaust gas, whose expected quantities are discussed in this section.

11.4.1 Low Carbon Steel

The ESS steelmaking furnace is designed to produce low-carbon steel with less than 0.25 wt%C in composition (Fourie and Erasmus 2016). The tap temperature of this alloy is expected to be above 1510 °C, which is the liquidus temperature of an iron-carbon alloy with 0.25 wt%C (Fourie and Erasmus 2016).

11.4.2 Slag

Slag is produced in the furnace when iron ore and flux melt on the solid raw material heap surface. The molten slag is used in decarburisation reactions and spent slag is tapped continuously from the furnace

at temperatures between 1530 and 1600 °C (Fourie and Erasmus 2016) at the slag tapping end of the reactor. Tapped slag is expected to be mostly calcium oxide, around 15.0 wt%FeO and silica (Fourie and Erasmus 2016).

11.4.3 Exhaust Gas

Exhaust gas produced by reactions exits the furnace through an off-gas chute in the slag tapping end wall, with an expected exit temperature of between 1600 to 1900 °C. The gas will consist mostly of N_2, CO_2 and CO (Fourie and Erasmus 2016).

11.5 Metallurgical Phenomena

Metallurgical phenomena which are expected to occur during steady operation of the furnace are described in this section.

11.5.1 Chemical Reactions and Phase Changes

Physical and chemical reactions occur in the following regions:

1. Freeboard volume - These are combustion reactions, where oxidation of gaseous components are a source of heat energy for the furnace.
2. Raw material heap surface - Melting and partial reduction of iron oxide is the dominant reaction at this interface. There may be other reactions such as calcination if there are carbonates present in the raw material feed mix.
3. Slag-alloy bath - The predominant reactions are that of molten iron oxide removing carbon from the alloy bath which is referred to as decarburisation.
4. Induction heating channels. In this region molten alloy is heated in order to maintain suitable temperatures in the alloy bath during steady state operation.

The following convention is used to represent process material phases, in reaction equations described in this research:

- {X} - X is dissolved in slag.
- [X] - X is dissolved in molten alloy.
- (X) - X is a gas.
- X - X is a solid.

11.5.1.1 Raw Material Heap Surface Reactions

Solid material on the heap surface is exposed to radiation which results in dehydration, calcination, decomposition, partial reduction, melting and dissolution reactions.

Dehydration and calcination occurs at the top most part of the heap, where fresh raw material first lands and is exposed to radiation from the freeboard. If carbonate fluxes such as $CaCO_3$, $MgCO_3$ and $CaMg(CO_3)_2$ are used, calcium or magnesium oxides and carbon dioxide gas are produced. Further exposure of the material to radiation is expected to result in decomposition and partial reduction of iron ore. With these reactions, the material will remain in the solid solid state. Chemical equations for these reactions are as follows:

1. Calcination reactions.

$$CaCO_3 \xrightarrow{\Delta H_{rad}} CaO + (CO_2) \tag{11.1}$$

$$MgCO_3 \xrightarrow{\Delta H_{rad}} MgO + (CO_2) \tag{11.2}$$

$$MgCa(CO_3)_2 \xrightarrow{\Delta H_{rad}} MgO + CaO + 2\,(CO_2) \tag{11.3}$$

2. Decomposition:

$$Fe_2O_3 \xrightarrow{\Delta H_{rad}} 2\,FeO + \frac{1}{2}\,(O_2) \tag{11.4}$$

3. Partial reduction

$$Fe_2O_3 + C_{reductant} \longrightarrow 2\,FeO + (CO) \tag{11.5}$$

Further radiation and contact with liquid slag at the bottom part of the heap will result in melting reactions. The molten product is expected to flow into the slag layer because of the inclined heap surface. Gas products formed in the reactions are released into the freeboard volume.

11.5.1.2 Slag-alloy Interface Reactions

The foremost reaction in this region is decarburisation of molten alloy, which occurs when iron oxides dissolved in the slag react with carbon dissolved in the alloy. The products are liquid iron, which stays in the bath and carbon monoxide gas, which bubbles through slag and is released into the freeboard. These reactions are described by Equations 11.6 and 11.7.

$$[C] + \{\,Fe_2O_3\,\} \xrightarrow{\Delta H_{reaction}} 2\,\{FeO\} + (CO) \tag{11.6}$$

$$[C] + \{FeO\} \xrightarrow{\Delta H_{reaction}} [Fe] + (CO) \tag{11.7}$$

Iron oxide reduction is an endothermic reaction, and hence the $\Delta H_{reaction}$ values are positive.

Desulphurisation may also occurs at the slag-alloy interface, if slag conditions are conducive for the reactions described by Equations 11.8 and 11.9 to proceed. Although thermodynamics and kinetics of sulphur removal are not yet fully understood, it is proposed that one or both of the reactions in Equations 11.8 and 11.9 are responsible for desulphurisation (Posch et al. 2002).

$$\{CaO\} + [S] \xrightarrow{\Delta H_{reaction}} \{CaS\} + [O] \tag{11.8}$$

$$\{MgO\} + [S] \xrightarrow{\Delta H_{reaction}} \{MgS\} + [O] \tag{11.9}$$

Low concentrations of iron oxide slag have been observed to promote removal of sulphur dissolved in alloy into the slag (Posch et al. 2002). This may be difficult to achieve in the ESS furnace, since slag is expected to contain a relatively large amount of iron oxides during steady operation.

Dephosphorisation may also occur when lime is added to the raw material feed mix. Lime is understood to promote recovery of phosphorous to slag in steelmaking applications, according to the reaction shown in Equation 11.10 (Basu 2007). An oxidising environment is also necessary, which can be provided by the iron oxide rich slag in the ESS steelmaking process.

$$3\,\{CaO\} + 5\,\{FeO\} + 2\,[P] \xrightarrow{\Delta H_{reaction}} \{3\,CaO \cdot P_2O_5\} + 5\,[Fe] \tag{11.10}$$

11.5.1.3 Freeboard Reactions

Combustion of carbon monoxide in the freeboard generates energy to drive decarburisation reactions. Control of air input to the furnace is necessary to ensure the freeboard atmosphere has more oxygen for combustion of carbon monoxide and pulverised coal. Combustion of pulverised coal at the burners is shown by Equation 11.11. Combustion of volatiles and carbon monoxide from the heap surface are shown by Equation 11.12. Subscripts "HMI" denotes heap-melting and and "SAI" denotes slag-alloy interface reactions

$$C_{fixed-carbon} + C_{volatiles} + 2\,H_{volatiles} + S_{volatiles} + \frac{5}{2}\,(O_2) \longrightarrow 2\,(CO) + (H_2O) + (SO_2) \tag{11.11}$$

$$(CO_{HMI}) + (CO_{SAI}) + C_{volatiles,HMI} + 2\,H_{volatiles,HMI} + S_{volatiles,HMI} + \frac{9}{2}\,(O_2) \longrightarrow 3\,(CO_2) + (H_2O) + (SO_2) \tag{11.12}$$

11.5.1.4 Induction Heating Channel reactions

Only heating of alloy is required in the induction heating channels. Any other possible reactions such as chemical and physical wear of refractory material by alloy, is undesirable. This can be mitigated by appropriate selection and use of a suitable refractory lining material. Another type of interaction found in this project's literature search is when a refractory lining acts as a catalytic surface for the nucleation and growth of carbon monoxide gas bubbles in bath steelmaking furnaces (Larsen 1956). Carbon and oxygen dissolved in molten alloy diffuse to such nucleation sites on the refractory and react to form carbon monoxide. If these bubbles grow to a sufficiently large diameter, they will disrupt the continuous flow of molten iron in the channel and disconnect the secondary circuit. This therefore interrupts normal operation of the induction heater and result in inefficient heating in the channels. This can be avoided by using a sufficiently smooth refractory lining, which will limit gas bubble formation within them. Another alternative is making a large channel which can allow bubbles to form and escape the channel without breaking the molten iron secondary circuit.

11.6 Fluid and Particulate Flow

11.6.1 Solid Materials

Fine particles of pre-mixed iron ore, fluxes and reductant are added through feed chutes that are aligned on the furnace roof close to the cold wall. Before reaching steady state operation, the materials are added until a heap is formed. Positioning of feed chutes should result in a near uniform distribution of raw material along the cold wall. As shown in Figure 3.3, the heap rests against the cold wall and slopes down towards the slag layer. The heap angle is dependent on the solid raw material particles' natural angle of repose, which is estimated to be approximately 30° for an iron ore, reductant and flux mix. During feeding, the solid material will land on the highest point of the heap. It is proposed that as soon as the material lands on the heap surface, calcination, partial reduction and melting reactions begin (Fourie and Erasmus 2016). Some material may not melt immediately, but will move down the surface along with molten material to reach the slag layer.

11.6.2 Liquids

Liquids in the furnace system are molten slag and alloy, whose flow fluid flow is discussed individually in this section.

11.6.2.1 Molten Alloy

Flow of molten alloy in the furnace hearth can be divided into the following types:

1. Net alloy flow from the slag-tapping end wall, to the steel tapping end wall of the furnace;
2. Alloy recirculation due to induction heating; and
3. Localised eddy currents due to gas bubbles rising through the molten slag and alloy bath.

Flow of steel during tapping is excluded from the list and is not investigated in this research.

Net Alloy Flow There is nett alloy flow from the slag-tapping, to the steel tapping end wall (Fourie and Erasmus 2016). This is because fresh molten pig iron is fed into the hearth at the slag-tapping end, and refined steel extracted at the steel-tapping end of the furnace. Factors that have so far been identified to have an effect on the rate of this flow are:

1. Molten pig iron feed rate;
2. Liquid alloy formation at the slag-alloy interface; and
3. Steel tapping rate.

The furnace is designed such that $10\,\mathrm{t\,h^{-1}}$ of pig iron fed to the furnace. Since more liquid alloy is generated in the slag-alloy interface, the tapping rate of low-carbon steel is expected to be higher than $10\,\mathrm{t\,h^{-1}}$ (Fourie and Erasmus 2016).

Alloy Recirculation Due To Induction Heating As described in Section 11.2, three passages are installed for every 4 m length of the hot wall. One down passage directs molten alloy from the bath into induction heating channels, where alloy is heated and then rises by natural convection through two up passages to re-enter the alloy bath. As alloy re-enters the furnace, it spreads over the molten alloy surface (Fourie and Erasmus 2016). It is cooled down due to reactions at the slag-alloy interface and so becomes more dense and flows down toward the furnace floor. It then flows along the floor, back to where the down passage is located, where it re-enters the induction heating channels (Fourie and Erasmus 2016). There is therefore, circulation of alloy from the hot wall towards the cold wall along the alloy bath meniscus, and then back to the hot wall along the furnace floor to re-enter the down-passage to the induction heating channels. This re-circulating flow is shown schematically by Figure 11.3. The rate of this circulatory flow is largely dependent on the amount of heat supplied to the molten alloy in the induction heating channels.

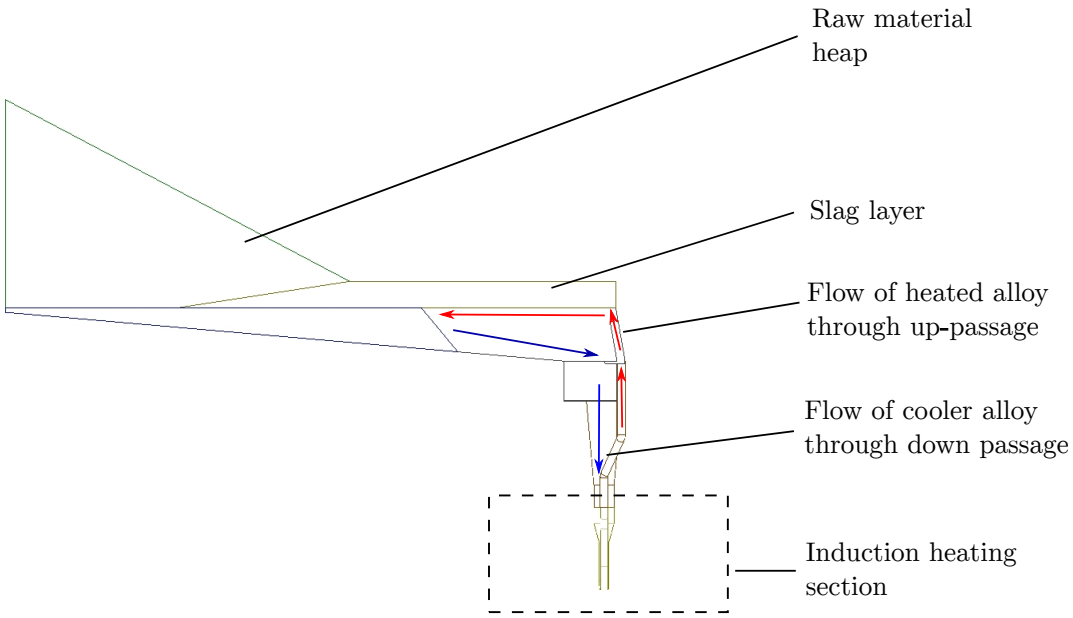

Figure 11.3: Schematic representation molten alloy flow in alloy bath due to influence of induction heating, as see from the alloy-tapping end. (Fourie and Erasmus 2016).

Localised Flow in the Alloy Bath Carbon monoxide bubbles formed in slag-alloy interface reactions will rise through the alloy bath causing movement in small volumes of molten alloy . The result of this movement is localised stirring and mixing of the alloy bath. The exact pattern of this flow was not investigated in this project.

11.6.2.2 Molten Slag Flow

The main flow profile of slag in the ESS furnace hearth is a result of:

- Molten material produced on the solid heap surface flowing onto the alloy bath. Because slag has a lower density than alloy it will float on top of the alloy during steady state operation.
- Tapping of slag at the slag-tapping end wall.

A second type of flow is the result of carbon monoxide gas bubbling upwards from slag-alloy interface reaction sites, up into the freeboard volume of the furnace.

Slag Flow from the Raw Material Heap to the Alloy Bath nett flow of molten oxides from the heap surface is dependent on the following:

1. Rate at which solid raw material melts on the heap surface (i.e. The heap melting interface);
2. Viscosity of this molten product; and
3. The natural angle of repose of the solid material below the heap surface;

The rate at which material on the heap surface melts is dependent on composition and rates of heat radiation to the heap surface. The viscosity is dependent on the composition and temperature of the molten material.

Slag Mixing Due to Bubbling Localised stirring of slag is caused by carbon monoxide gas bubbles formed at slag-alloy interface reactions, rising up and moving through the slag layer. The true nature of this fluid flow was not investigated in this research, but it is expected that there will be short-range eddy current flow in small volumes throughout the slag bath.

Nett Slag Flow The nett flow of slag is from the raw material heap towards the slag tap hole at the slag tapping end wall. This is the same wall where molten pig iron is fed into the furnace. There is therefore, a counter-current flow between slag and alloy in the furnace. This is by design and is meant to improve rates of decarburisation during steady state operation (Fourie and Erasmus 2016).

11.6.3 Gaseous Material Flow

The overall view of gas flow in the furnace system is shown schematically in Figure 11.4 (Fourie and Erasmus 2016).

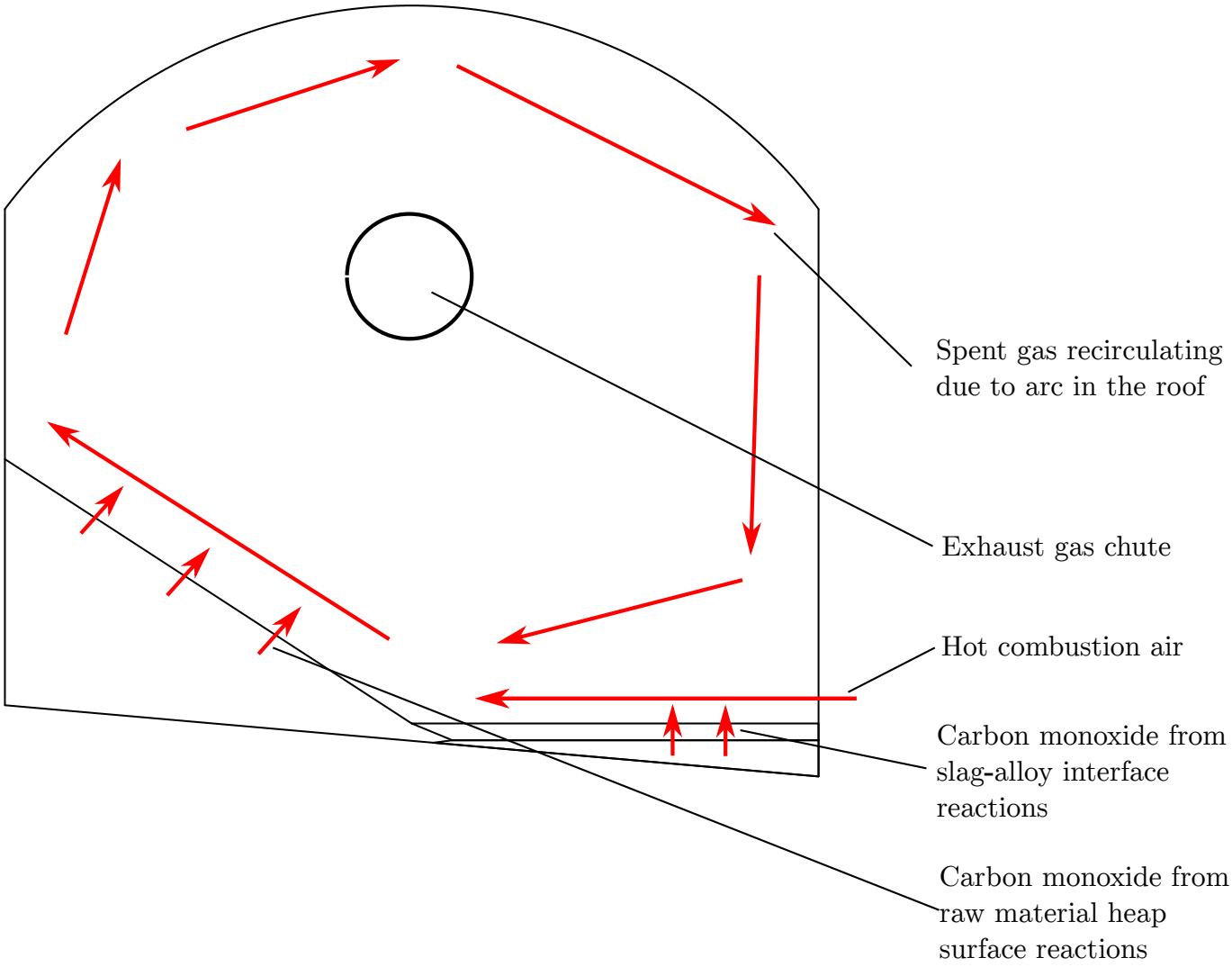

Figure 11.4: Schematic representation of gas flow in the freeboard of the ESS furnace (Fourie and Erasmus 2016).

Three major streams of gas are expected in the furnace system during steady state operation. The first stream is that of combustion air fed into the furnace freeboard through tuyeres placed in the hot wall above the slag surface. Because of the heap's geometry and the arched furnace roof, spent gas is made to circulate in the freeboard before exiting through the exhaust gas chute. This recirculating spent gas mixes with the constant stream of incoming fresh combustion air (Fourie and Erasmus 2016).

The second stream of gas is carbon monoxide formed from decarburisation reactions at the slag-alloy interface. This stream mixes with incoming combustion air, and reacts with oxygen carried by by it (Fourie and Erasmus 2016).

The third stream is formed by various reactions at the raw material heap surface. The main components of this gas will be carbon dioxide and monoxide depending (Fourie and Erasmus 2016). The exact composition will be dependent on the solid raw material mix used during operation.

The combined effect of these gas flow phenomena is a helical nett flow in the freeboard volume, which flows from the combustion air input tuyeres, circulates in the freeboard volume and then exits via the exhaust gas chute (Fourie and Erasmus 2016).

11.7 Mass Transport

The sites where mass transport is of importance to successful decarburisation in the ESS steelmaking furnace are as follows:

1. Alloy bath
2. Slag layer
3. Raw material heap surface

Fluid flow type and diffusion play a major role in mass transport rates and their exact effect is also dependent on various factors such as fluid temperature and viscosity. Factors affecting mass transfer in each of the aforementioned regions of the ESS furnace are described in the remainder of this section.

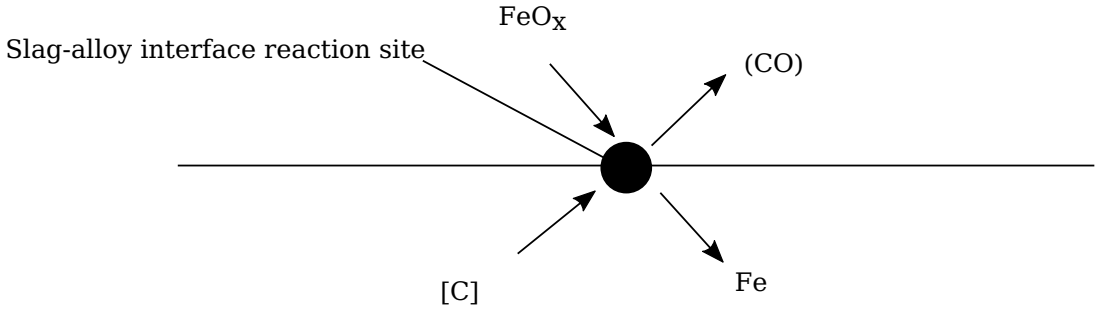

Figure 11.5: A schematic representation of mass transfer phenomena in the slag and alloy bath of the ESS steelmaking process.

11.7.1 Alloy Bath

Carbon, phosphorous, silicon and sulphur dissolved in alloy react with oxides in slag at the slag-alloy interface (Fourie and Erasmus 2016). The consumption of these species generates chemical potential gradients which promote mass transfer from the bulk alloy to reaction sites of the slag-alloy interface across a diffusion boundary layer.

Referring to figure 11.3, upon entry from induction heating channels, alloy will have concentration similar to the bulk concentration of the alloy. This flow of alloy and that caused by rising carbon monoxide gas bubbles, reduces the effective diffusion boundary layer thickness,which is expected to promote rates of mass transfer in the alloy bath and improve performance of the furnace to levels beyond open-hearth furnace steelmaking (Fourie and Erasmus 2016).

11.7.2 Slag Layer

Mass transfer in the slag is dependent on chemical composition, fluid flow and temperature of the slag. The ESS steelmaking furnace, makes use of a thin slag layer during steady state operation, which will improve mass transfer rates within the slag (Fourie and Erasmus 2016). The advantage of maintaining a thin slag layer is that it will be easily disturbed by rising gas bubbles from slag-alloy reactions and so will have a considerable amount of stirring. This will reduce the effective boundary layer thickness and therefore promote mass transfer of species from the bulk slag to the slag-alloy interface. Refining in the ESS furnace is therefore expected to be more efficient than other bath processes such as the open-hearth steelmaking process (Fourie and Erasmus 2016).

11.7.3 Raw Material Heap Surface

Mass transfer plays a role in the heap where carbon in reductant reacts with iron ore particles during partial reduction reactions as described in Section 11.5.1.1. For the ESS furnace, it is proposed that

fine particles are more suitable for use in the heap (Fourie and Erasmus 2016). Fine particles are an advantage in that they significantly increase the reaction-site surface area, and so greatly improves the rates of reaction. Iron ore particle reduction is understood to follow a shrinking core model. The reducing gas is carbon monoxide which is produced when carbon in reductant is oxidised by air, which follows the shrinking particle model of reaction (Hamadeh, Mirgaux, and Patisson 2018).

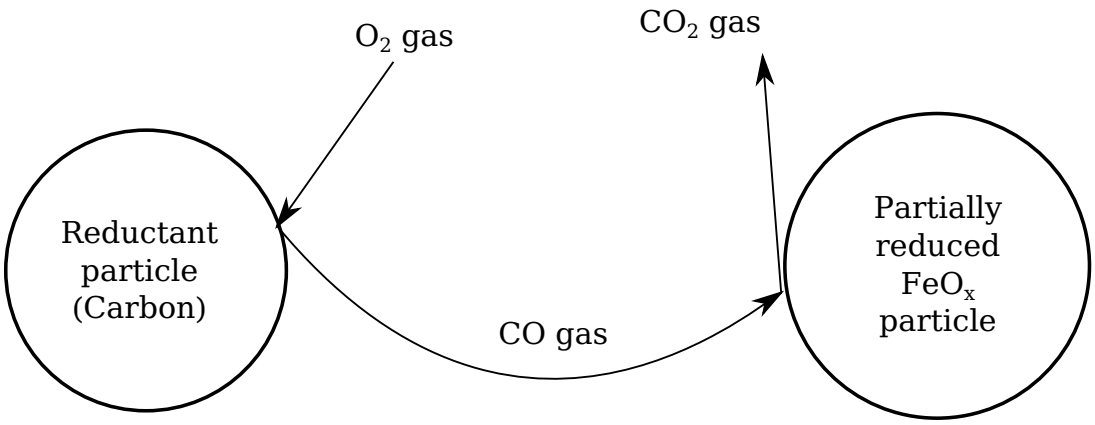

Figure 11.6: A schematic representation of mass transfer phenomena in iron reduction reactions at the raw material heap surface of the ESS steelmaking process.

11.8 Heat Transfer

This section describes heat transfer phenomena in selected regions which are expected have an influence on steady-state performance of the ESS steelmaking furnace.

11.8.1 Freeboard

Heat in the freeboard is generated through combustion of the following:

1. Carbon monoxide gas evolved in decarburization reactions at the slag-alloy interface;
2. Carbon monoxide gas evolved by reduction reactions on the raw material heap surface; and
3. Coal injected into the freeboard using pulverised coal burners.

Energy from these combustion reactions is transferred to the refractory lining, raw material heap and the slag layer. Radiation will be the dominant method of heat transfer from the freeboard during steady state operation. Convection heat transfer will occur to a lesser extent between gas and the raw material heap, furnace roof and walls (Fourie and Erasmus 2016). Figure 11.7 is a schematic cross-section of the furnace as seen from the alloy-tapping end wall, which shows an overall view of heat transfer phenomena expected to occur under steady-state operation. The numbered components in the figure are as follows:

1. Heat transfer from freeboard gas to cold wall.
2. Heat transfer from freeboard gas to roof.
3. Heat transfer from freeboard gas to hot wall.
4. Heat transfer from freeboard gas to raw material heap surface.
5. Heat transfer from freeboard gas to slag.
6. Heat generated from combustion of CO gas from the slag-alloy interface transferred to the freeboard.
7. Heat generated from combustion of CO gas from raw material reduction transferred to the freeboard.
8. Heat generated from combustion of pulverised coal injected with combustion gas transferred to the freeboard.

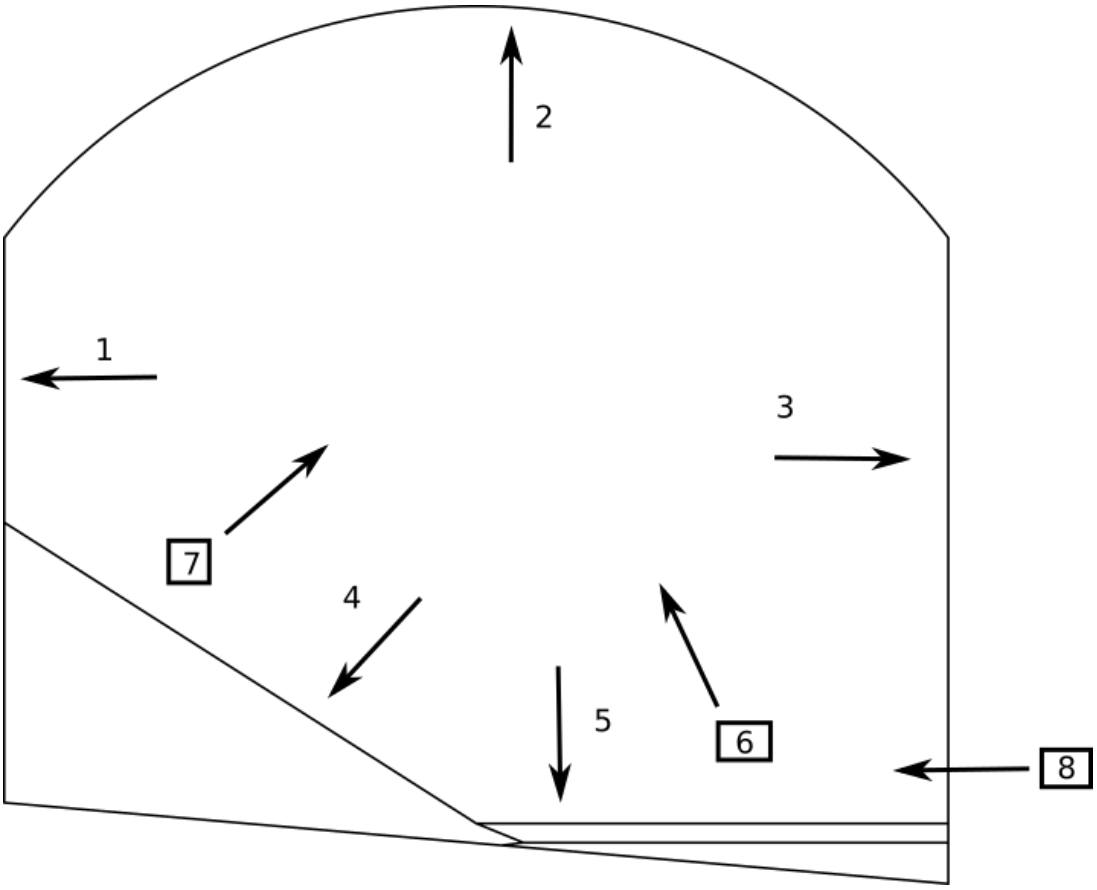

Figure 11.7: Schematic representation of heat transfer in the furnace freeboard.

Excluded from Figure 11.7 is heat transfer from the furnace's steel shell to the external environment, which is discussed in a later section. Complete combustion in the freeboard is proposed to result in high volumes of CO_2 and H_2O, whose unsymmetrical nature tends to promote radiative heat transfer through the gas. Total heat flux density from the freeboard is expected to lie between 100 and 180 kW/m^2, depending on temperatures of the different furnace regions (Fourie and Erasmus 2015). Each region's heat transfer phenomena is described in the remainder of this section.

11.8.2 Raw Material Heap

Heat is transferred to the heap in two ways. The major method is radiation from the highly emissive flame in the freeboard and from hot refractory surfaces. Convection from combusted gas flowing over the heap surface also contributes to heating, but to a much lesser extent. The heat drives dehydration, decomposition, partial reduction and melting reactions in a thin layer of solid material at the heap surface. This layer is therefore referred to as an "active" portion of the heap (Fourie and Erasmus 2016; Fourie and Erasmus 2017). Low thermal conductivity of solid raw materials is expected to insulate half of the furnace floor and cold wall. Furthermore, no reactions are expected to occur in this region and it is therefore referred to as a "dead" portion of the heap (Fourie and Erasmus 2016; Fourie and Erasmus 2017).

Figure 11.8 is a schematic cross-sectional view of the heap, showing heat transfer phenomena that are expected. Descriptions for the numbered components in Figure 11.8 are as follows:

1. Radiation exchange with the freeboard. Combustion flames and hot refractory surfaces will radiate heat to the heap surface. Batch addition of fresh raw material cools the heap's surface, providing the necessary temperature gradient for radiation to occur.
2. Convection heat transfer from spent gas to raw material heap surface. Hot gas flowing over the heap surface will result in forced convection heat transfer between the two mediums.

3. Heat transferred when molten material flows from the heap surface to the slag bath. When material is melted on this surface, it flows down to the slag as described in Section 11.6. The heat stored in this molten material is therefore transferred with it, from the heap to the slag layer.

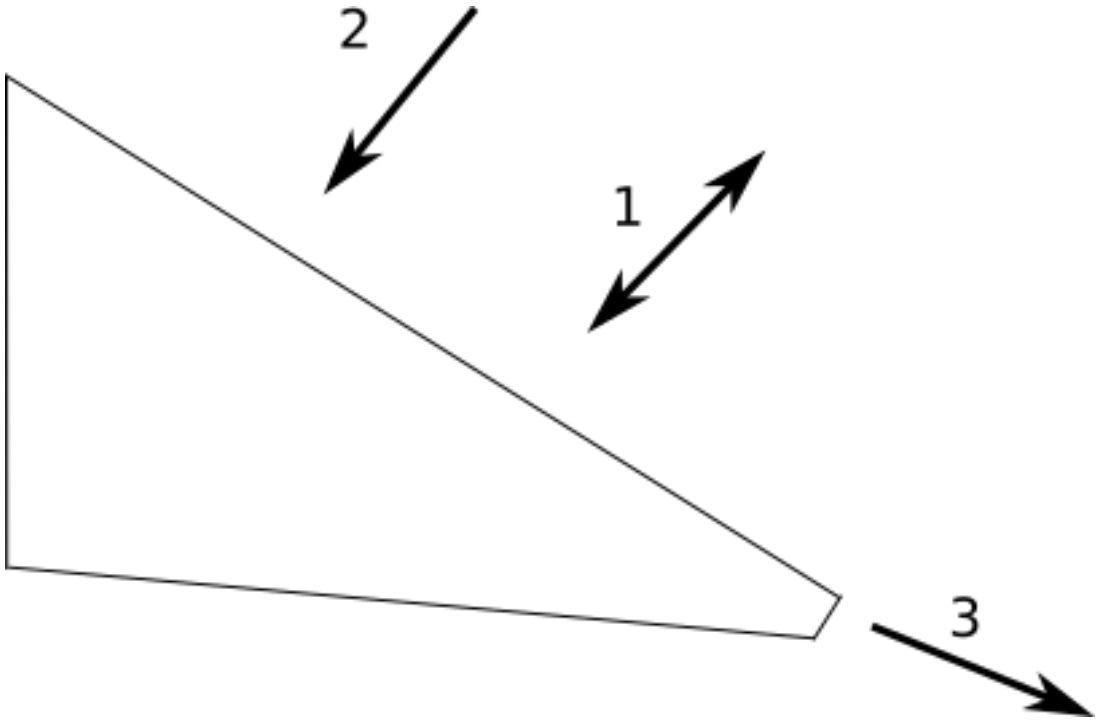

Figure 11.8: Schematic representation of heat transfer phenomena in the raw material heap

11.8.3 Slag Layer

A thin slag layer of approximately 8.3 cm, is maintained during steady operation, and so there is a small contact area between slag and the refractory lining (Fourie and Erasmus 2016). This is intended to reduce heat losses to the refractory lining, but has the added advantages for mass transfer in the slag (Fourie and Erasmus 2016). In open hearth steelmaking applications, a thin slag layer is known to improve heat transfer through slag from the freeboard to the alloy bath (Larsen 1956; Philbrook et al. 1951; Derge 1964; Schane and Willard 1959). Endothermic refining reactions at the slag-metal interface also remove heat from the slag layer and alloy bath.

Figure 11.9 is a schematic cross section of the slag showing expected heat transfer phenomena in the ESS process. Descriptions for the numbered components in Figure 11.9 are as follows:

1. Radiation exchange with the freeboard. The nett direction of heat transfer is dependent on the temperatures of the slag layer and refractory lining and freeboard regions. Favourable conditions for the ESS furnace are when the slag is at a lower temperature than the freeboard. The resultant temperature gradient, allows for heat transfer to the slag rather than in the opposite direction. The slag therefore becomes a heated insulating jacket for the alloy beneath it. Less energy is therefore required to heat the metal via induction heating and electrical energy consumption is therefore reduced (Fourie and Erasmus 2016; Fourie and Erasmus 2017).
2. Heat lost or gained from slag-alloy reactions. Reduction of iron (II) and (III) oxide is endothermic and robs the slag and alloy of heat. Oxidation of carbon is exothermic and will add heat to the slag. The nett heat transfer from these reaction will therefore depend on the rates of these slag-alloy reactions (Fruehan 1998).
3. Heat loss to the refractory lining. Heat is transferred to the external environment through the refractory lining and steel shell. The steel shell is cooled naturally by air on the outside surface (Fourie and Erasmus 2016; Fourie and Erasmus 2017).

4. Heat exchange with the raw material heap. The slag layer is in contact with the cooler raw material heap and so conductive from the slag to the heap may occur. There is flow of material from melting reactions on the heap surface to the slag, which will add heat to it. The nett heat transfer will therefore depend on the balance between addition and removal of heat by these two phenomena.

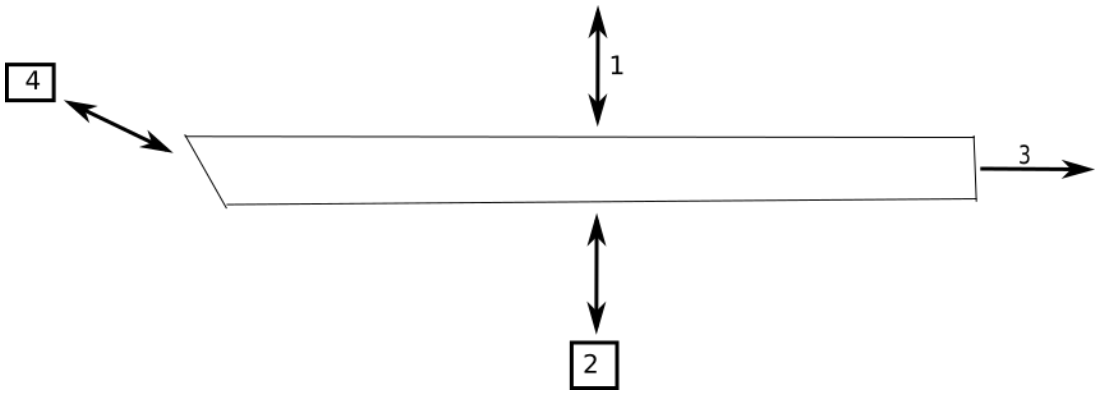

Figure 11.9: Schematic representation of heat transfer phenomena in the slag layer.

11.8.4 Alloy Bath

The alloy bath loses heat through contact with the refractory, the raw material heap and through endothermic reduction of iron oxide during steady-state operation. Heat is added through the oxidation of carbon dissolved in the alloy.

In steelmaking, more heat escapes through the alloy bath than slag because it has higher thermal conductivity (Fruehan 1998). The effect of heat loss to the alloy is minimised in the ESS furnace by induction heating and an insulating layer of slag (Fourie and Erasmus 2016). Figure 11.10 is a schematic representation of heat transfer in the liquid metal component. Descriptions for the numbered components in Figure 11.10 are as follows:

1. Conduction and convection from alloy bath to refractory floor and walls. There is a large area of contact between the alloy bath and refractory floor and hot wall and so there will be significant heat transfer between these regions.
2. Heat loss when alloy leaves the bath and enters the induction heating channels. Heat stored in this alloy moves out with alloy that leaves the bath through down channels and flows into induction heating channels.
3. Conduction from alloy bath to raw material heap. Where there is contact between the alloy bath and the raw material heap, it is expected that heat will be transferred through convection and conduction to the heap, since the latter is the cooler region.
4. Heat transfer through refining reactions at the slag-metal interface. Reduction of iron oxide in the slag will rob the alloy bath of heat, while oxidation of carbon will add heat. The nett flow of heat will depend on the rates of these reactions.
5. Molten alloy entering the molten bath from induction heating channels. Alloy that is heated in the induction heating channels flows through up-passages and enters the alloy bath. This serves to regulate the alloy bath temperature during steady operation (Fourie and Erasmus 2016).

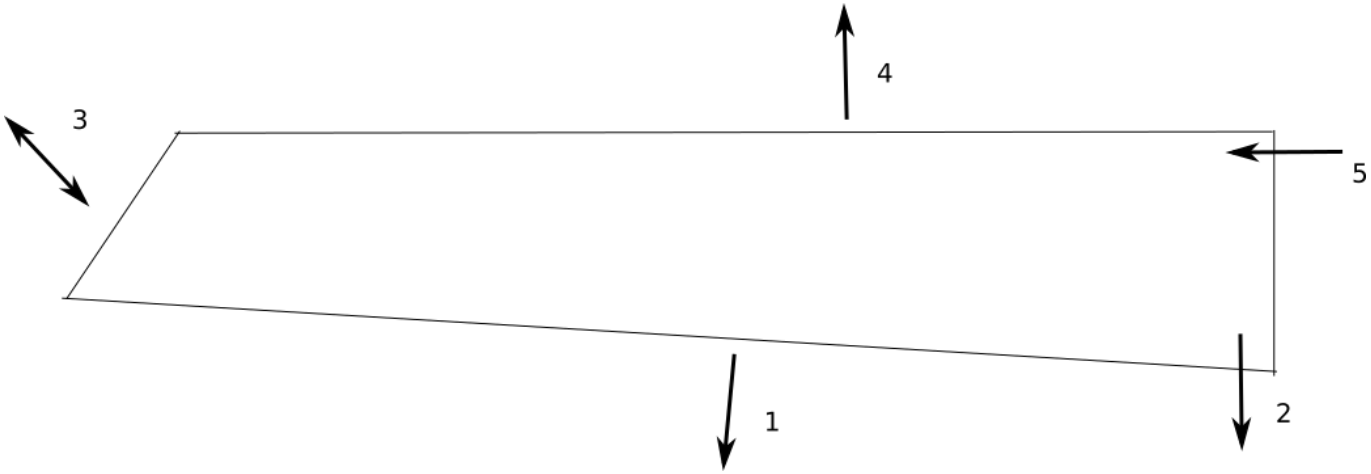

Figure 11.10: Schematic representation of heat transfer associated with the molten alloy bath.

11.8.5 Induction Heating Channels

Electrical power is supplied to a primary coil which transfers electromagnetic energy to the alloy in the induction heating channel which acts as a secondary coil. The electromagnetic energy results in joule heating of the alloy. The proposed power input to the alloy via each induction heater is 200 kW. This is expected to heat alloy in the channels by up to 50 °C (difference between alloy inlet and outlet temperatures in the heating channel), depending on mass flow rate through the channel. . This will help regulate alloy bath temperatures to the desired range of 1550 °C to 1600 °C. The induction heaters were put outside the scope of this research and so heat transfer in this region was not investigated in detail.

11.8.6 Refractory Lining

A refractory lining must contain as much heat as possible within the furnace for efficient operation. Heat transfer occurs to and from the ESS furnace refractory lining as shown in the schematic cross-sectional view in Figure 11.11.

Descriptions for the numbered components in Figure 11.11 are as follows:

1. Convective and radiative heat exchange with the external environment. This has to be minimised as much as possible to increase efficiency of the furnace and reduce electricity and coal consumption.
2. Heat exchange with the freeboard and heated surfaces. Hot gas, combustion flames and heated raw material and slag surfaces will radiate heat to the exposed refractory material. Convective heat transfer will also occur from hot gas flowing close to the refractory lining.
3. Heat exchange with the heap. Conductive heat exchange between the refractory lining and solid heap will occur to a very small extent in comparison to other heat exchanges. For this reason, the heap is considered an insulator which adds on to the name "dead heap" that the region is given (Fourie and Erasmus 2016).
4. Conductive and convective heat exchange will occur between the alloy bath and the refractory lining where there is contact between the two materials.
5. Conductive and convective heat exchange will also occur between the slag layer and the refractory lining.

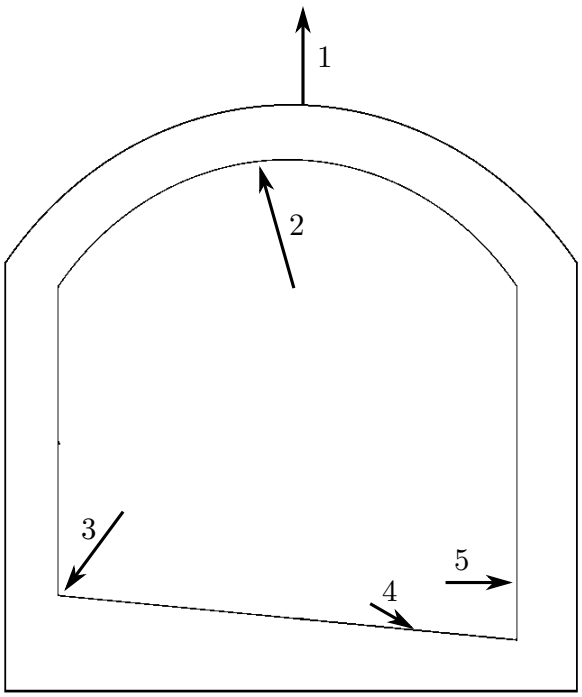

Figure 11.11: Schematic representation of heat transfer phenomena in the refractory lining.

Chapter 12

Key Phenomena

A summary of phenomena and features of the ESS steelmaking process that will be used in developing the model is presented in Table 12.1.

Table 12.1: Summary of features in the ESS steelmaking process used in developing the process model.

Feature	Relevance			Reason for relevance score
	High	Med	Low	
Process:				
Processing strategy	✓			The model has to simulate continuous instead of batch processing.
Pre-furnace processing			✓	Preparation of raw materials is not of interest in this research.
Exhaust gas processing			✓	The precise methods of pre-heating combustion air using exhaust gas is not of interest in this research.
Post processing			✓	Processing of slag and steel after tapping does not influence furnace performance in the context of this research.
Geometry:				
Heap-freeboard contact area	✓			Direct influence on heap surface melting rate.
Alloy-slag contact area	✓			Direct influence on decarburisation rate.
Alloy-refractory contact area	✓			Direct influence on heat losses from the furnace.
Slag-freeboard contact area	✓			Indirect influence on decarburisation rate.
Freeboard-refractory contact area	✓			Direct influence on heap surface melting and heat losses. Indirect influence on decarburisation rate.

Continued on next page

Table 12.1 – continued from previous page

Feature	Relevance			Reason
	High	Med	Low	
Refractory external surface area	✓			Direct influence on heat losses and heat retention. Indirect influence on decarburisation rate.
Refractory thickness	✓			Direct influence on heat losses. Indirect influence on decarburisation rate.
Freeboard volume	✓			Direct influence on energy supply. Indirect influence on decarburisation rate.
Heap-alloy contact area			✓	Low influence on decarburisation rate.
Heap-refractory contact area			✓	Low influence on decarburisation reactions.
Heap-slag contact area			✓	Not relevant in the scope of this study.
Fluid and particulate flow:				
Solid raw material		✓		Indirect influence on heat transfer and decarburisation rate.
Molten alloy flow	✓			Direct influence on decarburisation rate.
Molten slag flow	✓			Direct influence on decarburisation rates.
Gas flow	✓			Direct influence on energy production and decarburisation rate.
Physical and chemical reactions:				
Heap surface reactions	✓			Direct influence on decarburisation rate.
Slag-alloy interface reactions	✓			Direct influence on decarburisation rate.
Freeboard combustion reactions	✓			Direct influence on energy production and decarburisation rate.
Induction heating channel reactions			✓	Not desired, must be avoided.
Mass transfer:				
Mass transfer at the slag-alloy interface	✓			Direct influence on decarburisation rate.
Mass transfer at the heap surface			✓	Out of scope for this research.
Mass transfer in the freeboard			✓	Negligible effect on energy production.
Heat transfer:				
Freeboard to heap	✓			Direct influence on decarburisation rate.
Freeboard to slag	✓			Indirect influence on decarburisation rate.

Continued on next page

Table 12.1 – continued from previous page

Feature	Relevance			Reason
	High	Med	Low	
Freeboard to refractory lining	✓			Direct influence on energy retention. Indirect influence on decarburisation rate.
Alloy to refractory lining	✓			Direct influence on energy retention. Indirect influence on decarburisation rate.
Slag to alloy	✓			Direct influence on decarburisation.
Slag to refractory lining	✓			Direct influence on energy retention. Indirect influence on decarburisation.
Heap to refractory lining			✓	Negligible rates.
Slag to heap			✓	None.
Alloy to heap			✓	None.

Chapter 13

Assumptions

Assumptions made about the ESS steelmaking process are presented in this chapter. These were made so that modelling would be possible, despite a lack of information about certain aspects of the process.

The assumptions are given a special numbering format for ease of referencing in Chapter 15. For each assumption stated, a justification is provided, following which, the validity and impact of the assumption on calculation results from the model is evaluated.

A1. Homogeneity in Respective Material Regions

Statement: Each material region will be homogeneous in nature within its boundaries under steady state operation of the furnace.

Justification: The alloy bath will be continuously mixed by induction heating flow and gas bubbles rising through it. The slag layer is mixed by the same gas bubbles flowing through it and so there will be a fair amount of mixing throughout the bulk of the material. Freeboard gas flows at a speed that will cause sufficient mixing to approximate homogeneous properties in these regions. Solid raw material is mixed well and pelletised before it is fed into the furnace and so can be considered homogeneous.

Validity: The assumption is not valid because none of these regions will be uniform throughout their respective volumes of existence.

Impact: Calculations mass and energy balance calculations made with the model will give average values for a particular period of simulation time, which is useful only when determining steady state operation of the furnace.

A2. Thermodynamic Equilibrium in Slag-alloy interface Reactions

Statement: Thermodynamic equilibrium is achieved in slag-alloy interface reactions, except in the case of decarburisation.

Justification: Decarburisation has been observed to occur slower than other reactions such as desulphurisation and dephosphorisation in steelmaking processes, so it can be safely assumed that reactions will reach equilibrium before carbon. Furthermore, there

is usually a larger amount of carbon than minor impurities, which means the latter will be consumed faster than carbon over a period of time.

Validity: This assumption is valid only under specific conditions in steelmaking. The scenarios in this research are similar to a carbon boil in open-hearth steelmaking, where the statement has been shown as valid (Larsen 1956).

Impact: This assumption allows for the inclusion of only decarburisation kinetics in the model. Kinetics of other reactions, which are not yet well understood, can then be excluded without increasing the model's inaccuracy.

A3. Complete Melting on Heap Surface

Statement: Solid raw material fed into the furnace will melt completely before reaching the heap toe

Justification: Heat transfer to the heap surface is expected to raise its temperature such that fresh solid raw material will melt very fast as soon as it lands on the heap.

Validity: Under successful steady state operation, this statement is valid. Material will most likely melt seconds after settling on the heap surface.

Impact: This assumption removes the need to simulate solid particles flowing into the slag layer. This greatly simplifies modelling slag in that solid phases can be excluded from the slag during equilibrium calculations in the model.

A4. Inactive Raw Material Heap Below Surface

Statement: A large portion of the solid raw material heap below the surface is inactive chemically and physically.

Justification: The heap volume is large enough to act as a barrier to heat. No reactions will occur in this region since it is far from the heap surface, which is chemically active because of radiation from the freeboard. Furthermore, fresh raw material is added continuously to the heap. Constant renewal of this surface will therefore limit exposure of material below to any radiation during steady state operation.

Validity: This statement is partially valid. When considering chemical reactions, they will most likely occur at the hottest part of the heap, which is at the surface. Here, the main reaction is melting of iron ore which is highly endothermic and therefore consumes most of the heat radiated to it rather than allow conduction to the material below it. This means below the active surface layer there will not be an adequate amount of heat in the material to drive reactions. It is not valid however, because some heat will be transferred through this region to the refractory wall. The amount

of heat transferred through the heap will be negligible however, in comparison to heat transfer in other regions of the furnace.

Impact: Assuming an inactive heap simplifies the model by removing the need to simulate heat transfer through a porous solid medium. This would require a separate more involved study using discrete-element modelling. Ignoring this portion will mean energy balance calculations will give an under estimation of expected heat losses.

A5. No Retention of Material at Reaction Sites

Statement: Materials do not remain at any reaction site before, after or during the reaction. Reactants arrive to the site, react quickly and then the products immediately move away from the reaction site into respective phase regions.

Justification: This assumption was made, to satisfy the condition that reaction sites have no state, and therefore hold no material at any point in time. This means materials will always be found in their respective bulk phases and nowhere else. Thus a mass balance can be calculated, while including phenomena that occur in intermediate zones such as the heap-melting and slag-alloy interfaces.

Validity: This is not a valid assumption seeing as most reactions are under mass transfer control and removal of products from reaction sites contributes significantly to the rate of mass transfer. However, considering the length of the time-step to be used during simulations with the model, the high operating temperatures of the furnace and thorough mixing in fluid regions, the error incurred by adopting this assumption is most likely to have minimal impact on the system.

Impact: The influence of product residence times at reaction interfaces cannot be directly implemented in this model, which will most probably result in error when investigating phenomena. It is expected to be a very minimal result particularly for fluid regions where there is a great deal of mixing to actively remove products from reaction sites.

A6. Zero Refractory Wear During Simulation Duration

Statement: There is no refractory wear of any form, in the time period over which the model approximates process states.

Justification: Refractory wear is not of consideration in investigations to be conducted and as such is excluded.

Validity: The statement is invalid because refractory wear will occur during processing. However, the 1 h simulation time step selected is too short a period for significant wear to occur under steady operation, if a suitable refractory was selected for use during operation.

Impact: The error in calculation results will be minimal.

A7. Sufficient Radiation to Heap Surface for Melting

Statement: The heap surface is exposed to sufficient radiation at all times, such that any material that settles on it, will melt and flow down to the slag-alloy interface.

Justification: Assuming sufficient radiation allows adding heap surface temperature as an independent variable for investigations, without the need for a detailed heat transfer model to estimate the said temperature.

Validity: This is invalid, radiation plays a major role on the heap surface temperature.

Impact: Energy analysis of the process may produce results showing consumptions that are higher than the furnace's actual capabilities.

A8. Thermodynamic Equilibrium Achieved at Reaction Interfaces

Statement: Thermodynamic equilibrium will be achieved at all interfaces where there is a material input.

Justification: This assumption will allow for calculation of reaction products without the requirement of explicitly calculating rates of reaction according to principles in classic physical chemistry.

Validity: This statement is partially valid for high temperature processes.

Impact: Assuming fast reactions neglects the effects of chemical reaction kinetics, which may play an important role. This could lead to over estimation of rates in places such as the heap surface, where reactions may be slower for the pelletised solid raw material feed.

A9. Refractory Surface Temperature

Statement: The temperature of the refractory surface and its neighbouring regions are equal under steady state operation.

Justification: This will eliminate the need to determine the actual temperatures of the surface explicitly, which would require a more involved heat transfer model.

Validity: This is invalid. The actual furnace's refractory surface temperatures will differ from the neighbouring region.

Impact: Heat transfer calculations will have a margin of error included by making this simplification. The significance of this error will have to be determined using a more detailed heat transfer model.

A10. Adiabatic Slag-alloy Interface Reaction Zones

Statement: Reactions between molten slag and alloy will occur in an adiabatic zone with no energy losses to the surroundings via convection, conduction or radiation heat transfer.

Justification: This assumption is for setting up calculations for the reactions in such a way that change in heat is carried only by materials and not through direct heat exchange. It was made so as to avoid the complexity of assuming a temperature of the slag-alloy interface reactions, which will vary depending on which reaction surface is being considered.

Validity: This cannot be proven directly, and so the validity is unknown.

Impact: The impact cannot be quantified because validity is unknown.

Chapter 14

Simplifications

Simplifications were made in order to increase practicality of modelling and eliminate variables or equations that are too complex to include in the steady state mass and energy balance model scope in this research work. These are presented in this chapter, with the justification and impact of making the simplification described.

S1. Planar Surfaces at Reaction Interfaces

Statement: Reaction interfaces are perfectly planar.

Justification: Simplifying to planar surface areas eliminates the need to approximate the real areas of reaction sites.

Impact: Using planar surface areas may greatly underestimate mass and heat transfer, particularly at the slag-alloy and heap surface reaction interfaces. Underestimation may not be favourable to understanding the process. The furnace may not perform better than what is calculated with the model, but rather blind researchers and the designers to other issues that will arise due to over-performance.

S2. Induction Heating as a Direct Power Source in the Alloy Bath

Statement: Induction heater is simplified to a power source placed directly in the alloy bath.

Justification: Modelling flow to and from induction heating channels requires complex calculations, since flow due to electromagnetic induction heating is complex in nature. These calculations can therefor be excluded from the model in this research and focus placed on decarburisation potential of the furnace from phenomena occurring within the furnace itself.

Impact: Induction heating may play a significant role in decarburisation in the actual furnace, since heated metal enters the alloy bath directly below the alloy meniscus. The model may greatly under estimate decarburisation kinetics, if the flow from the induction heating plays a major role in improving rates of iron oxide dissolution at the slag-alloy contact surface.

S3. Efficient Heat Exchangers

Statement: Heat exchangers used in the actual furnace will have the capability to pre-heat combustion air to any desired temperature.

Justification: This simplification allows the input temperature of combustion air to be set as a dependent variable when investigating the effects of air temperature on the furnace energy balance with the model.

Impact: The air temperature may have a limit to which it can be heated, which if overestimated, will incorrectly assume that the furnace can be successfully run under the temperatures proposed.

S4. Single Combustion Sub-region in Freeboard

Statement: All gaseous materials and combustion fuel will mix and react in a single discrete portion of the freeboard.

Justification: Combining the combustion regions will reduce the number of calculations required in the model. Furthermore, the entire freeboard has been assumed homogeneous (Assumption A.1) and therefore this simplification holds.

Impact: The fact that combustion occurs in different areas may lead to incorrect energy balance calculations which will give a wrong evaluation of furnace performance from an energy perspective.

S5. FeO and Fe_2O_3 Oxidants

Statement: FeO and Fe_2O_3 are the only active oxidants for the decarburisation reaction.

Justification: This allows exclusion of complex phases in the decarburisation kinetics sub-model

Impact: If other chemical phases are present in slag that actively participate in decarburisation, the rates calculated by the model will be lower than those would be observed in an actual furnace.

S6. Gas Bubble Volume Flow Rate Through Slag and Alloy

Statement: The volume flow rate of gas through slag and alloy can be approximated as the total molar volume of CO gas that can be formed over the simulation time step, moving through the bath.

Justification: By approximating this flow rate, calculation of gas bubble formation rates can be made without having to consider surface tension and viscosity effects on bubble nucleation, growth and escape from the alloy and slag bath.

Impact: The model essentially calculates decarburisation rates with the highest possible stirring from gas bubble flow rate, which may not be the case in the ESS furnace. The volume flow rate will in fact be directly proportional to the rate of decarburisation, which requires iterative calculations to determine in this model's set up.

Chapter 15

Model Formulation

In this chapter details are provided about how the model was formulated and given a mathematical description, such that it could be implemented in software.

15.1 Model Overview

15.1.1 Process Flow

Figure 15.1 is an overview of material flow in the process model. Colours of the arrowed lines in the diagram represent the following:

Blue - Gaseous material
Black - Solid material
Red - Molten oxides (ie. slag)
Green - Molten alloy

Italicised names in descriptions that follow are those present in Figures 15.1 and 15.2.

Iron Ore, *Flux* and *Reductant* are combined and added to an isothermal *Heap Melting Interface*, and the product of this calculation is split into three material streams, namely gas, "active" and "inactive" slag. A more detailed description of this split will be discussed in a later section.

Pig Iron is combined with active slag in an isenthalpic *Slag-Alloy Interface*. The result of the calculation is split into slag, alloy and gas. The slag is captured in the *Slag Tapping Ladle* and alloy in the *Alloy Tapping Ladle* material output.

Combustion Air and *Combustion Fuel* combine with gaseous products from *Heap-Melting Interface* and *Slag-Alloy Interface* in the isothermal *Freeboard Combustion Interface*, where reactions between constituents of these streams are simulated at an approximated freeboard temperature. Gaseous products from this calculation are transferred to the *Exhaust Gas Chute* material output, which simulates gases leaving the actual ESS steelmaking furnace system to the surroundings.

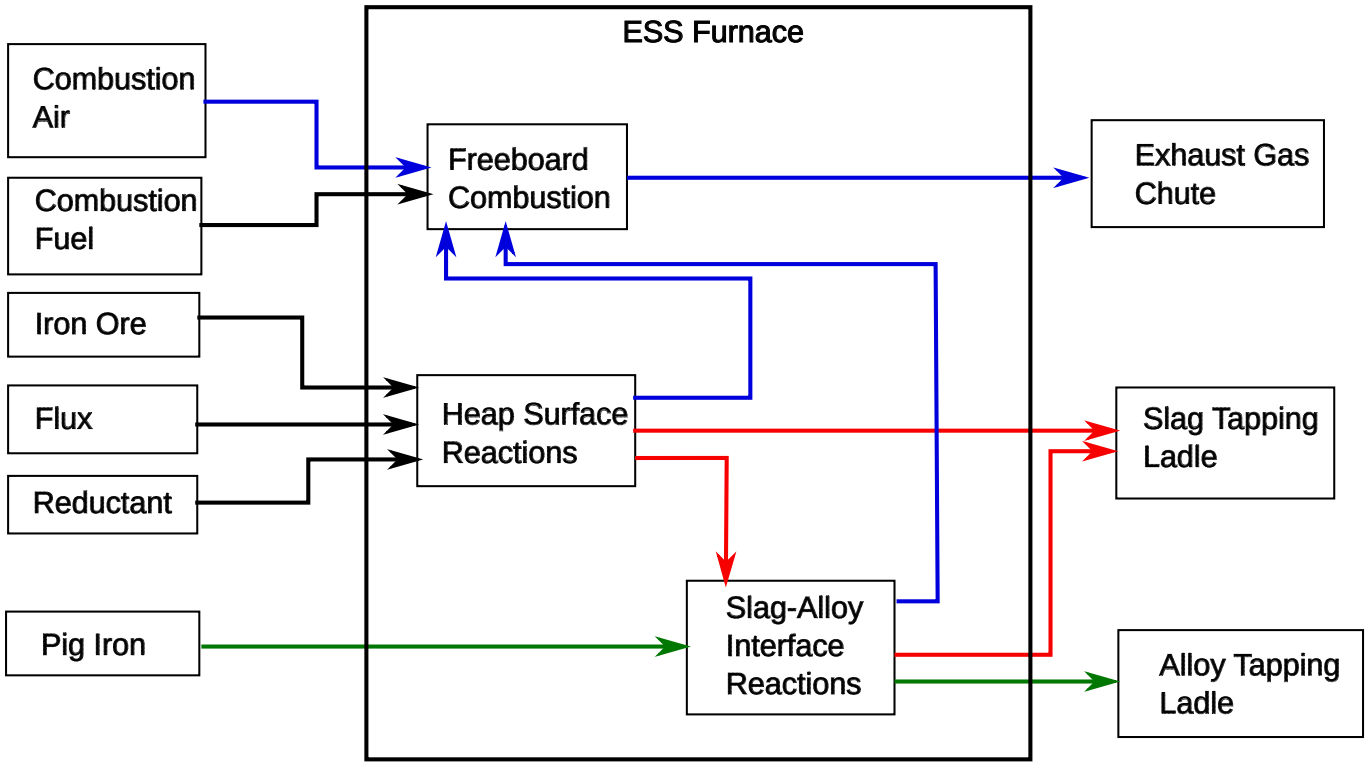

Figure 15.1: Schematic representation of material flow in the ESS steelmaking model.

Figure 15.2 is an overview of energy flow in the ESS steelmaking furnace process model. Energy inputs are induction heating of alloy and that from all material inputs. Material outputs carry energy out of the furnace alongside heat losses. *Freeboard Combustion Interface* is an internal energy inputs, while *Slag-alloy Interface* and *Heap Melting Interface* are both internal energy outputs.

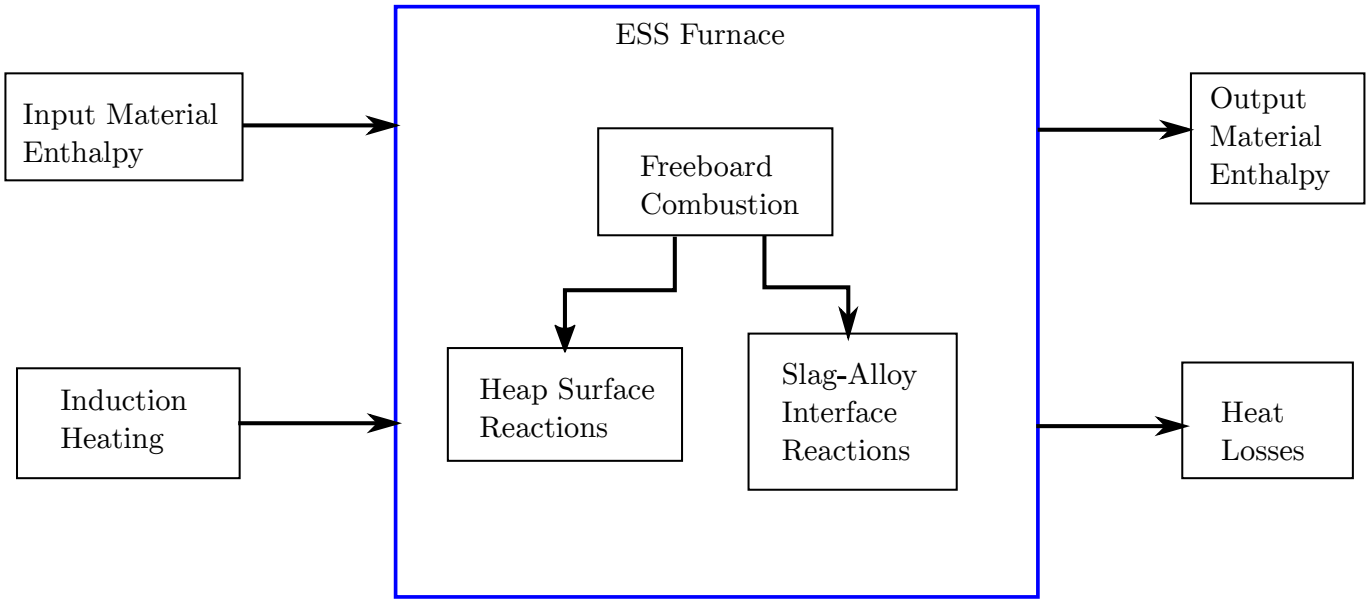

Figure 15.2: Schematic representation of energy flow in the ESS steelmaking model.

15.1.2 Mass and Energy Conservation

A mass and energy balance is calculated in the process model using steady state mass and energy conservation Equations 15.1 and 15.2.

$$\dot{m}_{ca} + \dot{m}_{cf} + \dot{m}_{io} + \dot{m}_{fl} + \dot{m}_{rd} + \dot{m}_{pi} = \dot{m}_{eg} + \dot{m}_{st} + \dot{m}_{at} \tag{15.1}$$

Each term $\dot{m}_i$ is the rate of change in mass of the system introduced by material *i*. Subscripts for the materials are: *ca* for combustion air; *cf* for combustion fuel; *io* for iron ore; *fl* for flux; *rd* for reductant; *pi* for pig iron; *at* for tapped alloy; *eg* for exhaust gas and *st* for tapped slag.

$$\Delta\dot{H}_{bal} = \Delta\dot{H}_{mi} + \Delta\dot{H}_{ih} + \Delta\dot{H}_{fbc} + \Delta\dot{H}_{mo} + \Delta\dot{H}_{hl} + \Delta\dot{H}_{hmi} \pm \Delta\dot{H}_{sai} \tag{15.2}$$

Each term $\Delta\dot{H}_i$ is the rate of change in heat made to the system by *i*. Subscripts are: *bal* for balance in energy (deficit, excess or zero); *mi* for energy associated with material inputs; *ih* for induction heating; *fbc* for freeboard combustion reactions; *mo* for material outputs; *hl* for calculated heat losses; *hmi* for heap surface melting interface reactions and *sai* for slag-alloy-interface reactions.

15.2 Process Materials

15.2.1 Pig Iron

Pig iron used in the model has chemical and physical attributes as shown in Table 15.1.

Table 15.1: Physical and chemical properties of pig iron used in the model.

Property	Value
Physical State	Liquid
Default Temperature	1550.0 °C
Chemical Composition	C - 4.0 wt% Si - 3.0 wt% S - 0.03 wt% P - 0.1 wt% Fe - balance

15.2.2 Iron Ore

Sishen iron ore was selected for use in the model whose assay is as shown in Table 15.2 (Geyer 2011), and temperature set at 30 °C.

Table 15.2: Sishen iron ore sample assay used in the process model. Composition is stated on a dry basis.

Component Name	Chemical Formula	Composition (wt%)
Hematite	Fe_2O_3	95.68
Quartz	SiO_2	2.36
Corundum	Al_2O_3	1.32
Lime	CaO	0.04
Periclase	MgO	0.03
Manganosite	MnO	0.03
Phosphorous	P	0.04
Sulphur	Monoclinic S	0.02
Chromite	Cr_2O_3	0.02

15.2.3 Flux

Pure burnt lime (CaO) and silica (SiO_2) at 30 °C, were the only fluxes used in the model.

15.2.4 Reductants and Combustion Fuel

The type of reductant used in the model has properties as shown in Table 15.3 and is a sample assay of coal from a coal mine in the Tshikondeni coal mining region of South Africa. Since a pulverised coal burner will be used in the ESS steelmaking furnace, the same material is used as combustion fuel in the model. Material properties and assay (dry-basis) of the coal are shown in Table 15.3.

Table 15.3: Properties of Tshikondeni coal used in this research.

Material Property	Units	Value
Gross Calorific Value	MJ/kg	35.8
Physical State		Pulverised solid
Proximate Assay		
Fixed Carbon	Mass %	61.3
Moisture	Mass %	0.6
Ash	Mass %	17.7
Volatiles	Mass %	20.4
Ultimate Assay		
C	Mass %	90.1
H	Mass %	4.9
O	Mass %	1.2
N	Mass %	2.1
S (Pyrite)	Mass %	0.9
S (Organic)	Mass %	0.8
Ash analysis		
SiO_2	Mass %	59.30
Al_2O_3	Mass %	27.17
Fe_2O_3	Mass %	3.30
P_2O_5	Mass %	0.41
CaO	Mass %	3.01
MgO	Mass %	0.99
Na_2O	Mass %	2.16
MnO	Mass %	0.03
BaO	Mass %	0.17
FeS	Mass %	3.46

15.2.5 Combustion Air

Preheated atmospheric air was used as combustion air for the model, whose chemical and physical properties as shown in Table 15.4.

Table 15.4: Chemical and Physical properties of combustion air used in the process model. Composition is stated on a dry basis.

Property	Value
Physical State	Gas
Temperature	500.0 to 900.0 °C
Composition	N_2 - 76.0 wt% O_2 - 23.0 wt% CO_2 - 1.0 wt%

15.2.6 Refractory Lining

Specific materials for the refractory lining to be used in the actual ESS furnace were not provided for this research. To this effect, a hypothetical specification was used for this process model, with the materials selected for the whose information was found in literature such as the work by Vert (2016). This is not a refractory recommendation, but rather a solution to having a lack of information and time during this research project. Assays of materials selected for the ESS process model are shown in Table 15.5 and thermal conductivities shown in Table 15.6.

Table 15.5: Materials selected for various sections in the refractory lining.

Section	Material	Reason for choice
Furnace roof	Magnesite	High resistance to disintegration by carbon deposition in CO-containing atmosphere. Good spalling resistance. Relatively light-weight.
Working lining of the floor, hot and cold wall	Magnesite	Good resistance to chemical attack by FeO-CaO slags, Fe-C alloys and CaO-FeO-C containing dust. High spalling resistance under conditions proposed for steady state operation of the ESS furnace.
Insulation layer for the floor, hot and cold wall	Insulating Firebrick	Lower thermal conductivity reduces heat losses through it. Low density will make the furnace lighter. High Structural integrity at temperature will give the walls the required rigidity.
Steel shell	ASTM A36 structural steel	A multi-purpose steel used for most major construction projects.

Table 15.6: Materials selected for the refractory lining.

Material	Property	Value	Data Sources
Magnesia brick	Density	2900.0 kg m^{-3}	Vert (2016), Carniglia and Barna (1992), Benavidez et al. (2015), Powell, Ho, and Liley (1966)
	Thermal conductivity	3.5 W m^{-1} K	
	Melting temperature	2850 °C	
	Tamman temperature	2070 °C	
	Chemical composition	MgO - 100%	
Insulating Firebrick	Density	2900.0 kg m^{-3}	Vert (2016), Carniglia and Barna (1992), Benavidez et al. (2015), Powell, Ho, and Liley (1966)
	Thermal conductivity	0.6 W m^{-1} K	
	Solidus temperature	1900 °C	
	Tamman temperature	1600 °C	
	Chemical composition	Al_2O_3 - 60% SiO_2 - 40%	
ASTM A36 steel	Condition	As fabricated	Brockenbrough (1999)
	Density	7850.0 kg m^{-3}	
	Thermal conductivity	50.0 W m^{-1} K	
	Max. $T_{service}$	400.0 °C	
	Solidus temperature	1460.0 °C	
	Chemical composition	0.25-0.290 wt%C 98.0 wt%Fe 0.20 wt%Cu 1.03 wt%Mn 0.040 wt%P 0.280 wt%Si 0.050 wt%S	

15.3 Formulated Geometry

This section presents formulated geometry of specific regions that for which information was not provided or found in literature.

15.3.1 Alloy Bath

The alloy bath is maintained at approximately 10 t during steady state operation. Molten iron has a density of about 7000 kg m^{-3} at 1600 °C. The volume of the alloy bath is therefore expected to be about 1.28 m^3. The length of the bath along the hot wall is 4.0 m, which gives cross-sectional area dimensions as shown in Figure 15.3, when viewed from the alloy-tapping end wall.

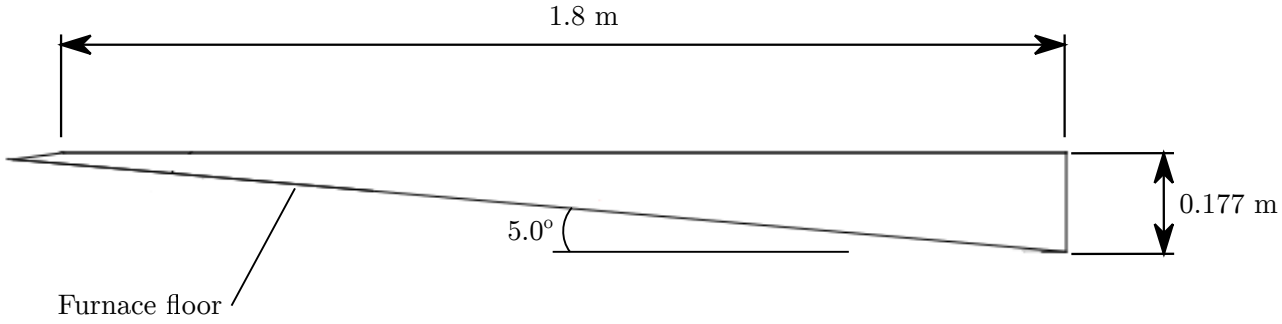

Figure 15.3: Dimensioned cross section of alloy bath as viewed from the alloy-tapping end wall.

15.3.2 Slag Layer

The density of steelmaking slags is between 2.1 kg m^{-3} to 2.4 kg m^{-3} (Mills and Keene 1987). The furnace's slag tap-hole is installed such that approximately 0.6 m^3 of slag is maintained above the 10 t alloy bath during steady-state operation. With a furnace length of 4.0 m, the slag height will therefore be approximately 0.08 m on the face in contact with the hot wall.

15.3.3 Raw Material Heap

Solid particles in the heap mixture are expected to have a 30° to 35° angle of repose, depending on the mix ratios. With the proposed 2.0 m heap width and 4.0 m furnace length, the approximate volume of the heap is 4 m^3. The surface exposed to radiation from the freeboard has an area of approximately 7 m^2 assuming that the surface is perfectly flat (Assumption S.1).

15.3.4 Freeboard

The volume of the freeboard region for the model is set at 46 m^3 according to proposed furnace dimensions (Fourie and Erasmus 2016).

15.3.5 Refractory Lining

The refractory lining is split into sections as shown in Figure 15.4 for heat transfer calculation purposes in the model. Names and surface areas of numbered sections shown in the figure are as follows:

1. Roof arch = 18.55 m^2
2. Hot wall exposed to freeboard radiation = 10.00 m^2
3. Hot wall in contact with slag layer = 0.32 m^2
4. Hot wall in contact with alloy bath = 8.71 m^2
5. Floor and cold wall in contact with alloy bath = 7.20 m^2
6. Cold wall covered by raw material heap = 13.20 m^2
7. Cold wall exposed to radiation from the freeboard = 4.80 m^2

Thickness of materials in each section of the refractory lining is formulated in the remainder of this section. These values are used only for purposes of the model. The actual thickness of sections will require a more in-depth study in order to have an appropriate configuration for the actual furnace.

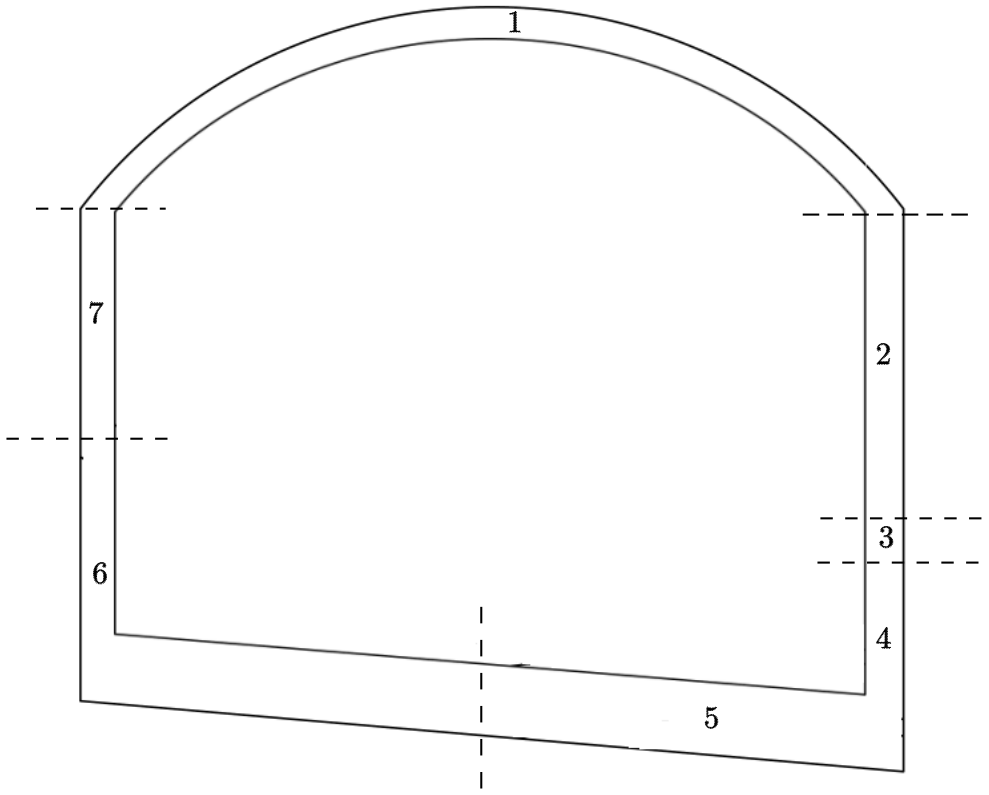

Figure 15.4: Divisions of the refractory lining for heat transfer calculations.

15.3.5.1 Roof Arch Thickness

The roof arch for the ESS process model is composed of only gunned magnesia. This is taken from some basic open-hearth furnace configurations found in literature (Section5.2). The configuration used is shown in Figure 15.5.

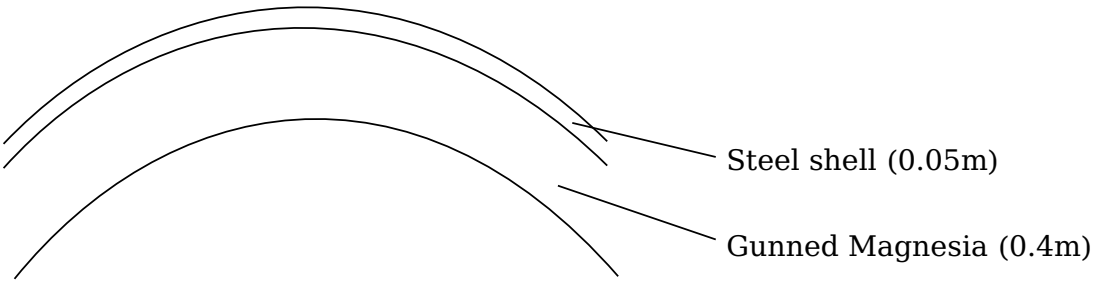

Figure 15.5: Configuration of the roof refractory materials for the ESS steelmaking process model.

15.3.5.2 Wall Thickness

The hot, cold and end walls of the ESS furnace in the model has a working lining made of pure periclase (MgO), which is laid against fireclay bricks and supported by the A36 steel shell. The configuration and thickness of the walls is shown in Figure 15.6.

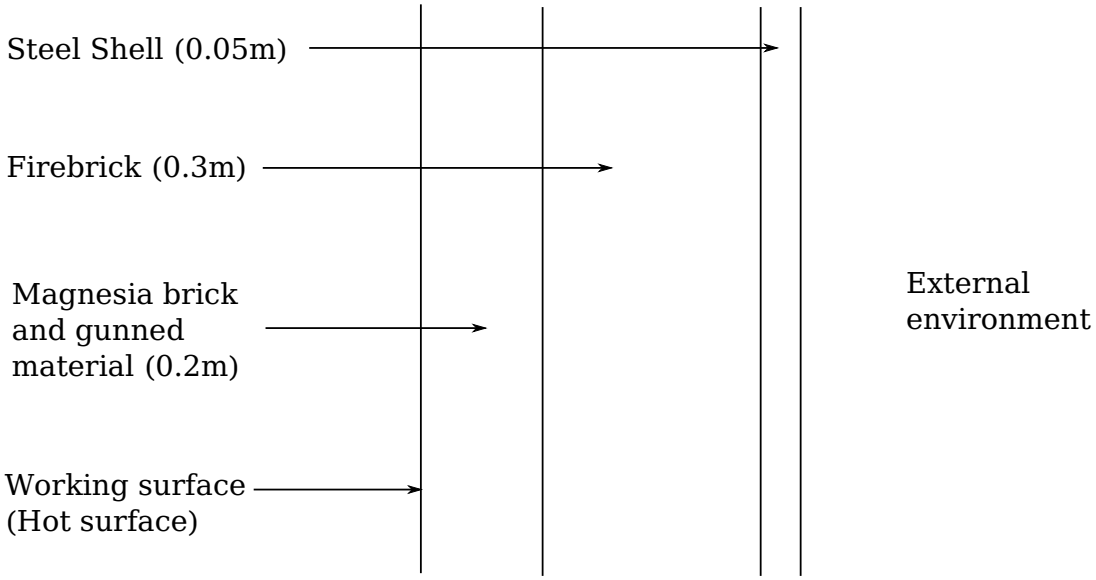

Figure 15.6: Configuration of the hot wall refractory materials for the ESS steelmaking process model.

15.3.5.3 Furnace Floor Thickness

The furnace floor will have a magnesia working surface, which sits above fireclay bricks as shown in Figure 15.7.

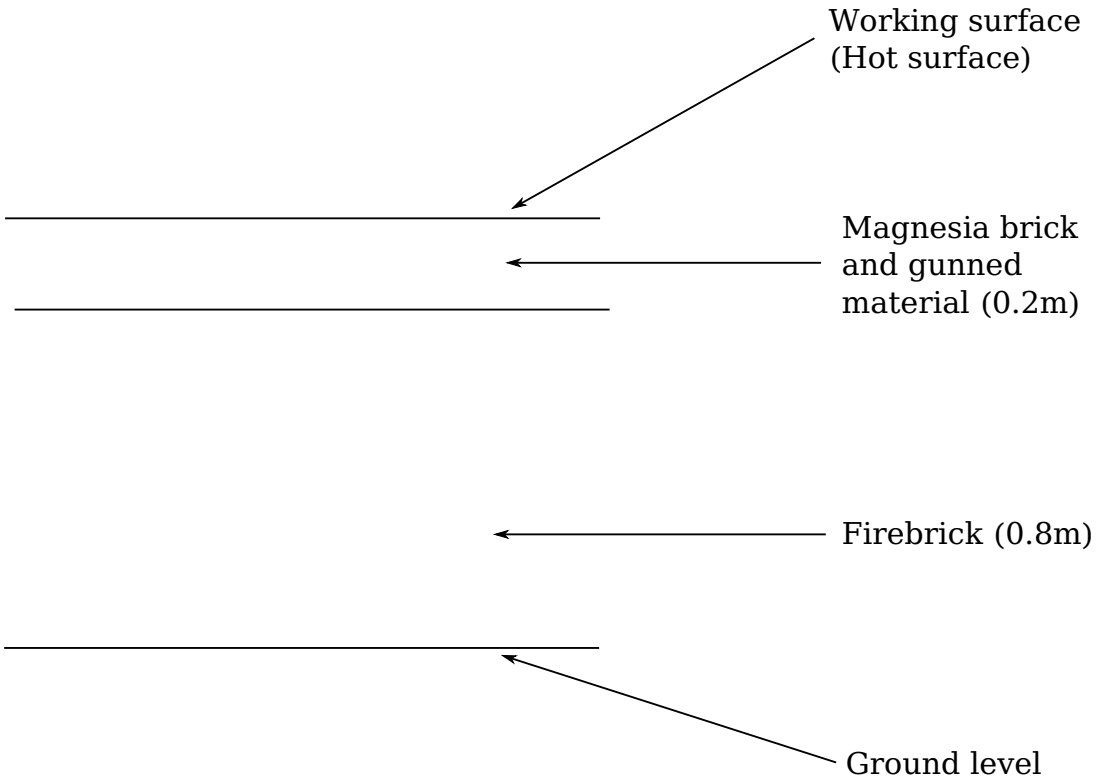

Figure 15.7: Configuration of the floor refractory materials for the ESS steelmaking process model.

15.4 Fluid and Particulate Flow

Detailed fluid and particulate flow was not simulated by the model. A flow sheet modelling approach was used instead, which makes use of flow streams, where mass flow rates are of greater interest than

flow types and regime, such as in Computational Fluid Dynamics (CFD). Materials are expected to flow between regions as follows.

1. Solid raw material flows from a source outside the furnace onto the raw material heap surface. This will not be added explicitly to the model.
2. Slag is generated on the heap surface, which flows down to the slag layer to participate in slag-alloy interface reactions. The rate at which this should occur is not known and so was made an independent variable in the model for simulation investigations.
3. Spent slag from the slag-alloy interface exits the furnace through a slag tap-hole to a ladle.
4. Pig Iron flows from an external source into the alloy bath to participate in slag alloy interface reactions.
5. Refined alloy from the slag-alloy interface exits the furnace through a tap-hole to a ladle.
6. Combustion gas flows from the furnace exterior into the furnace's freeboard to participate in freeboard combustion interface reactions.
7. From the freeboard, gas exits through an exhaust chute to the furnace exterior.
8. Combustion fuel (pulverised coal) is introduced through a pulverised coal burner from an external source into the freeboard.
9. Gas bubble flow rate through the slag and alloy bath. This is discussed in Section 15.4.1.

Only pig iron feed mass flow rate was specified in this research which was $10.0\,\mathrm{t\,h^{-1}}$ as proposed by designers of the ESS furnace. Other flow rates were investigated in simulation experiments, whose details are described in Chapter 18.

15.4.1 Gas Bubble Flow Rate

Gas bubble volume flow rate was reduced to the highest possible flow rate in the bath (Simplification S.6). The ideal gas law in Equation 15.3 was therefore used to calculate gas bubble volume flow rate through the bath ($\frac{dV_{CO}}{dt}$), by making volume (V) the subject of 15.3 and differentiating with respect to time (dt), which yields Equation 15.4.

$$P \cdot V = n \cdot R \cdot T \tag{15.3}$$

$$\frac{dV_{CO}}{dt} = \frac{R \cdot T_{bath} \cdot \frac{dn_{CO}}{dt}}{P_{bubble}} \tag{15.4}$$

The gas bubble pressure (P_{bubble}), was estimated as the absolute pressure a the alloy-refractory contact surface. Since the greatest portion of this surface is the furnace floor, the effect of bubbles that could form on the hot and end walls was excluded, and the pressure therefore was calculated using Equation 15.5, where ρ_{slag} and ρ_{alloy} are the densities, d_{slag} and d_{alloy} the depth of molten slag and alloy respectively, and P_{atm} is atmospheric pressure. The furnace operates in an "open" manner, since exhaust gas is allowed to exit freely from the furnace, so atmospheric pressure can be assumed to exist in the freeboard.

$$P_{bubble} = P_{atm} + \rho_{slag} \cdot g \cdot d_{slag} + \rho_{alloy} \cdot g \cdot d_{alloy} \tag{15.5}$$

Molar flow rate of CO gas ($\frac{dn_{CO}}{dt}$), was calculated using Equation 15.6, with Simplification S.6, where $n_{C,alloy}$, is the total available carbon in the molten alloy bath that can be removed through decarburisation.

$$\frac{dn_{CO}}{dt} = \frac{n_{C,alloy}}{\Delta t_{simulation}} \tag{15.6}$$

15.5 Mass Transport

Only mass transfer steps in the decarburisation reaction are considered in the model. The calculation and use of these rates are discussed in the remainder of this section.

15.5.1 Rate Calculations

Mass transfer in steelmaking process was discussed in Chapter 7, where literature to date states that rates of this phenomena are dictated by diffusion. Equation 7.4 was postulated by several authors as the rate at which a chemical component will diffuse through a solvent under steady state in steelmaking baths. It is repeated in this section for convenience. It was selected for use in the model when determining the rate limiting step in the decarburisation kinetics sub-model, which would fit into the overall ESS steelmaking model.

$$\text{Rate} = k_i \cdot A_{SMI} \cdot \Delta C_i \tag{7.4}$$

The available area for the reaction A_{SMI} was taken as the planar area of contact between the slag and alloy, whose value was simplified to the planar area based on Simplification S.1.

Stirring of molten baths reduces boundary layer thickness and enhances rates of reaction (Robertson and Staples 1974). The ESS steelmaking furnace's molten bath is expected to have a carbon boil during steady operation, which will add the effect of stirring to the bath. With this theory, the model in this research used diffusion based mass transfer rate calculations that are enhanced by bubbling of CO gas through the slag and alloy bath. Equation 7.8 was used to calculate the mass transfer rate constant k_i, which is enhanced by bubble induced stirring.

$$k^2 = B\frac{D_i \cdot Q}{d^2_{cell}} \tag{7.8}$$

The d^2 parameter, which represents the area of contact between the immiscible fluids, was replaced with the slag-alloy contact surface, simplified as a planar area (Simplification S.1). Volume flow rate of gas bubbles (Q) calculation is discussed in Section 15.4.1 of this document. Since the ESS furnace has an approximate 8 cm slag, and 17.7 cm alloy height it is expected that the process will operate under slag control. Therefore the B parameter chosen for use in Equation 7.8 was for low depth slag control 40 cm^{-1} as stated in Chapter 7, with reference to the values given in literature (Robertson and Staples 1974). The Diffusion rate (D_i) at which species i (i.e. either iron oxide, carbon or oxygen) will diffuse through its *solvent* (slag or alloy) to respective reaction surfaces, was defined in the model using Equation 15.7.

$$D_i = D_{o,i} \cdot e^{\frac{-Q_{d,i}}{R \cdot T_{solvent}}} \tag{15.7}$$

Activation energies for diffusion ($Q_{d,i}$) and diffusivity coefficients (D_o, i) were obtained from literature and $T_{solvent}$ is the estimated temperature of each solvent.

15.5.1.1 Oxygen Concentration in the Alloy Bath

Mass transfer is dependent on the concentration gradient between the bulk alloy and the concentration at the reaction surface where oxygen is consumed. The concentration of oxygen was calculated using Equation 7.19 as discussed in Section 7.5.

15.5.2 Molar Relationship of Decarburisation Reaction Steps

An important observation that was made from decarburisation kinetics literature is that these steps have a 1:1 molar relationship. That is to say, for every mole of FeO transferred to the slag-metal interface:

1. One mole of FeO dissociates at the slag-alloy interface and dissolves into the alloy bath.

$$\{\text{FeO}\} \longrightarrow [\text{Fe}] + [\text{O}] \tag{15.8}$$

2. One mole of O diffuses through the alloy bath to gas-alloy interface.
3. One mole of C diffuses through the alloy bath to gas-alloy interface.

4. One mole of C and O respectively react at the gas-alloy interface to generate one mole of CO.

$$[C] + [O] \longrightarrow (CO) \tag{15.9}$$

5. One mole of CO gas escapes the slag-alloy system to enter the freeboard.

For steelmaking process it is believed that steps 1, 4 and 5 occur fast enough that they are never the rate limiting steps. To this effect, only mass transfer was considered for the decarburisation kinetics sub-model in this research.

With regard to the presence of Fe_2O_3 dissolved in slag, it has been observed that the species reacts faster than FeO at the slag-alloy interface (Woolley and Pal 1999b). The reaction occurs as shown in Equations 11.6, repeated here for convenience.

$$[C] + \{Fe_2O_3\} -> 2\{FeO\} + 1(CO) \tag{11.6}$$

This still follows the 1:1 molar relationship, where one mole of Fe_2O_3 is transferred to and dissociates at the slag-alloy interface.

This relationship simplifies the process of converting the limiting sub-reaction rate to a mass flow rate, which can then be converted to a mass flow rate of slag (active slag) from the heap melting interface, to the slag-alloy interface in the ESS process model.

15.5.3 Use of Mass Transfer Kinetics to Determine Active Slag Flow Rate

The mass transfer kinetics equations were used to formulate the decarburisation kinetics sub-model as described in this section.

15.5.3.1 Step 1. Calculate Limiting Rate

The limiting rate of decarburisation is calculated according to equations described in Section 7. The steps involved for decarburisation were identified as follows:

1. Mass transfer of iron oxide through slag to the slag-alloy interface.
2. Dissociation and dissolution of iron oxide into alloy.
3. Mass transfer of oxygen to gas-alloy interfaces.
4. Mass transfer of carbon to gas-alloy interfaces.
5. Reaction between carbon and oxygen at gas-alloy interfaces.
6. Growth and escape of carbon monoxide bubbles out of the slag-alloy system into the freeboard.

These rates are all calculated as mass flow rates in $kg\,h^{-1}$ and the smallest value is the used as the limiting rate (m_{lim}) of the decarburisation reaction.

15.5.3.2 Step 2. Set the Mass Flow Rate of Active Slag

The limiting mass flow rate calculated in Step 1 is then used to obtain an equivalent mass flow rates of Iron(II) and Iron(III) oxide to the slag-alloy interface. Assumption S.5 allows consideration of only these two chemical phases and no other when calculating this step. This step makes use of a material splitter as devised by Pauw (1989) where the fraction of Fe_2O_3 and FeO are calculated using the following procedure.

1. Determine the total mass of Fe_2O_3 available in the slag (m_{t1}) and compare with (m_{lim}).

(a) If the m_{lim} is greater than (m_{t1}), calculate the difference in mass between the two values (m_{rem}). This difference represents a deficit iron oxide required to reach the limiting rate, which will be supplemented by FeO. Set the fraction of Fe_2O_3 that will be split as active slag ($f_{Fe_2O_3}$) to unity. This step enforces that, if the limiting rate of decarburisation calculated in Section 15.5.3.1 is larger than the Fe_2O_3 available in the slag, then all of it will participate in slag-alloy interface reactions.

(b) If the m_{t1} is less than m_{lim}, set $f_{Fe_2O_3}$ to the value calculated in Equation 15.10, and set m_{rem} to zero.

$$f_{Fe_2O_3} = \frac{m_{t1}}{m_{lim}} \tag{15.10}$$

This step enforces that, if the limiting rate m_{lim} is less than the total Fe_2O_3 available, only m_{lim} kg of it will participate in slag-alloy interface reactions, while the rest reports to inactive slag.

2. Compare m_{rem} with the mass of FeO available in the slag (m_{t2}).

(a) If the m_{t2} is less than m_{rem}, set the fraction of active Fe_2O_3 in the material splitter to f_{FeO}.

$$f_{FeO} = \frac{m_{t2}}{m_{rem}} \tag{15.11}$$

This step enforces that if the FeO cannot supply the required deficit m_{rem}, then only the available amount of FeO will be transferred.

(b) If the m_{rem} is greater than (m_{t2}), set the fraction of active Fe_2O_3 in the material splitter to unity. This step enforces that if the deficit to achieve the required limiting rate is greater than the available FeO, then all the FeO will be active. This is highly unlikely, but is added to the model as a way of anticipating this outcome.

3. Calculate the fraction of liquid slag, by dividing the mass transferable from the fractions determined above, by the total amount of iron oxide in the slag, which is shown in Equation 15.12.

$$f_{active\ slag} = \frac{m_{FeO,slag} \times f_{FeO} + m_{Fe_2O_3,slag} \times f_{Fe_2O_3}}{m_{m_{FeO,slag}+m_{Fe2O3,slag}}} \tag{15.12}$$

Metallic phases are set as part of active slag, so that if any are calculated at the heap melting interface, they will be transferred to the slag-alloy interface calculations. All other phases in the slag are assumed inactive as per Simplification S.5.

15.6 Chemical Reactions and Phase Changes

Equilibrium calculations as described in Section 4.3, were used to simulate chemical and physical reactions at the interface region.

15.6.1 Heap Melting Interface Reactions

Reactions at this interface are simulated using an isothermal equilibrium calculation. Material inputs to this region are solid iron ore, flux and reductant, whose ratio can be varied in order to obtain the best combination, that will produce liquid slag and gas products. Metallisation is not desired at this stage, since the use of molten material from this interface is to decarburise pig iron in the bath. Molten iron oxide with no alloy production and entrainment, is therefore the target product of these calculations. The mass flow rate of the mix in the model represents the mass of material that must melt and flow to the slag-alloy interface for successful decarburisation of pig iron.

It is assumed that the heat radiated from the freeboard is sufficient to raise the surface to a temperature at which the desired melting rate can be achieved (Assumption A.7). With this assumption, the heap melting interface is made into an isothermal equilibrium calculation to estimate reaction products.

15.6.2 Freeboard Combustion Reactions

It is assumed that thermodynamic equilibrium is also achieved in the freeboard (Assumption A.8) It is also proposed that the temperature of the freeboard region can reach a maximum of approximately 1900.0 °C under steady state operation, by the furnace designers. With this information, the freeboard combustion interface can be simulated in the model with an isothermal equilibrium calculation, at the proposed temperature.

15.6.3 Slag-alloy Interface Reactions

Active slag and molten pig iron are combined and an isenthalpic equilibrium is done to simulate slag-alloy interface reactions. An isenthalpic equilibrium calculation is chosen because it is a composite of two sub-regions, namely, slag-alloy surface and gas-alloy surface. According to literature as discussed in Chapter 7, different reactions occur in these two sub-regions with the slag-alloy surface reactions being endothermic, and the gas-alloy surface reactions exothermic. It was considered a better choice to assume an adiabatic slag-alloy interface which will calculate temperature changes from the reaction, rather than to base calculations on a value that cannot be obtained by any simple means. The respective slag and alloy streams could then be reset to the desired tap temperature as described in Sections 15.6.4.

15.6.4 Final Slag and Alloy Equilibrium

To account for temperature changes calculated in the slag-alloy interface isenthalpic equilibrium calculation, isothermal equilibrium calculators were added to reset temperatures of slag and alloy outputs respectively. This was a decision made in a revision of this model, after it was observed that some solid iron was being calculated in the slag-alloy interface. The isothermal calculations also became useful in setting the desired temperatures at which the slag and alloy can be tapped, and adjust the energy balance which helps in showing energy changes that can be expected from slag-alloy interface reactions.

15.7 Energy Calculations

Energy flow is divided into three categories in the model. These are namely sources, sinks and transfer. Sources supply energy to, while sinks remove energy from the furnace system under study. Energy transfer refers to energy exchange between regions within the furnace system under study.

15.7.1 Energy Sources

15.7.1.1 Freeboard combustion

The primary energy source for ESS steelmaking the furnace is combustion of pulverised coal and carbon monoxide in the freeboard region. Combustion heat input (ΔH_{FB}) is calculated as the energy change from carbon monoxide ($H_{r,CO}$), pulverised coal ($H_{r,C}$) reactions with combustion air. Nitrogen can also be combusted, but the reaction mostly consumes heat, hence the negative ($\Delta H_{r,N_2}$). This is expressed by equation 15.13.

$$\Delta H_{FB} = \Delta H_{r,C} + \Delta H_{r,CO} - \Delta H_{r,N_2} \tag{15.13}$$

15.7.1.2 Induction heating

Heat supplied to the alloy bath by an induction heater is set at a fixed rate of 200.0 kW for this model and the source is placed directly in the alloy bath Simplification S.2.

15.7.1.3 Carbon-oxygen reaction at Gas-alloy Interfaces

Carbon and oxygen dissolved in the alloy will react at gas-alloy interfaces and supply some energy to the alloy bath. The rate at which this will occur is determined by the rate of reaction between carbon and oxygen at the gas-alloy interfaces.

15.7.1.4 Carbon Oxygen reaction at Heap-alloy Interface

Carbon in reductant reacts with oxygen in iron ore at the heap surface, which supplies some energy to the system.

15.7.1.5 Enthalpy of material inputs

The addition of materials into the furnace is also considered a heat source in the model. This is expressed by Equation 15.14, where each term is the enthalpy of formation of each material at its temperature when added to the furnace. The major heat suppliers in this regard are combustion air and fuel, reductant and molten pig iron.

$$\Delta H_{MI} = \Delta H_{CA} + \Delta H_{CF} + \Delta H_{R} + \Delta H_{PI} + \Delta H_{IO} + \Delta H_{F} \tag{15.14}$$

The subscripts in Equation denote the following:

MI is total energy supplied by material inputs.
CA is energy supplied by preheated combustion air. The required preheat temperature will be investigated in this research.
CF is energy supplied by combustion fuel, which in the case of the model is pulverised coal 30 °C.
R is energy supplied by reductant, which in the case of the model is coal 30 °C.
PI is energy supplied by molten pig iron 1550 °C.
IO is energy supplied by solid iron ore at 30 °C.
F is energy supplied by flux at 30 °C.

15.7.2 Energy Sinks

15.7.2.1 Reactions at the Heap-melting Interface

Apart from the carbon-oxygen reaction, partial reduction and melting of iron ore, flux and ash also occurs at the heap-melting interface. These use up energy in the furnace and are therefore energy sinks in the ESS steelmaking process model.

15.7.2.2 FeO Reduction at Slag-alloy Interface

Similar to partial-reduction at the heap surface, iron oxide reduction at the slag-alloy interface is an endothermic reaction. It is therefore another energy sink in the furnace model.

15.7.2.3 Enthalpy of Material Outputs

Slag, alloy and gas leaving the furnace, carries with it a significant amount of energy since it is at high temperature. The extraction of these materials from the furnace system in the model is therefore a heat sink.

15.7.2.4 Energy Losses to the Environment

Heat given off to the external environment is not reusable in the furnace system, which makes it an energy sink in the process model.

15.7.3 Energy Transfer

Heat transfer was only explicitly defined in the calculation of heat losses to the external environment using steady state one-dimensional heat transfer principles. This heat transfer rate (q) is expressed using thermal resistance (R_{tot}) and temperature gradient (ΔT) as shown in Equation 15.15.

$$q = \frac{\Delta T}{R_{tot}} \tag{15.15}$$

There are three paths by which heat is transferred through the refractory layer to the external environment, which are as follows:

1. **Freeboard-slag-external environment**. By virtue of Assumption A.9, radiation resistance is ignored on both the internal and external surfaces, which simplifies formulation of heat transfer to the circuit diagram shown in Figure 15.8.

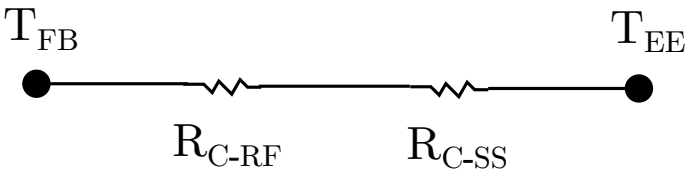

Figure 15.8: Circuit diagram for freeboard to external environment heat transfer.

In the figure, T_{FB} and T_{EE} are the temperatures of the freeboard and external environment respectively. R_{C-RF} is the thermal resistance to conduction of the refractory layer calculated using Equation 15.16, in which L_{RF} is the cross-sectional width, k_{RF} is the thermal conductivity and A is the surface area of refractory material.

$$R_{C-RF} = \frac{L_{RF}}{k_{RF} \cdot A} \tag{15.16}$$

R_{C-SS} is the thermal resistance to conduction steel shell calculated using Equation 15.17, where L_{SS} is the width, k_{RF} is the thermal conductivity, A is the surface area of steel shell.

$$R_{C-SS} = \frac{L_{SS}}{k_{SS} \cdot A} \tag{15.17}$$

2. **Freeboard-slag-external environment**. The circuit diagram shown in Figure 15.9.

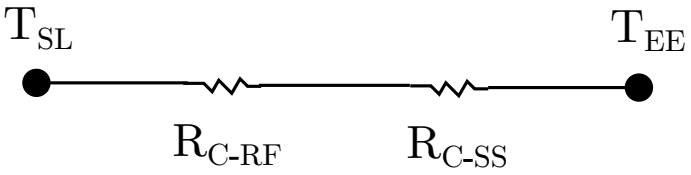

Figure 15.9: Circuit diagram for heat transfer from the slag layer to the external environment.

In the figure, T_{SL} and T_{EE} are the temperatures of slag and external environment respectively. The other variables are as described for heat transfer circuit described in Figure 15.8.

3. **Freeboard-alloy-external environment**. Again, Assumption A.9 simplifies the heat transfer circuit diagram for this path to that shown in Figure 15.10.

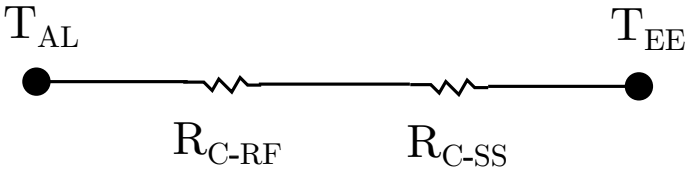

Figure 15.10: Circuit diagram for heat transfer from the alloy bath to the external environment.

In the figure, T_{AL} is the temperature of the alloy, which is assumed equal to the inner surface temperature of the refractory material. The other variables are as described for heat transfer circuit described in Figure 15.8.

Chapter 16

Implementation

The ESS steelmaking process model is implemented as a steady state mass and energy balance calculation, with decarburisation kinetics calculations included in the slag-alloy section. This chapter describes implementation of the formulation in Chapter 15 in software.

16.1 Software

The software used to develop the model is EMSIM, which is a web-based model development platform created and owned by Ex Mente Pty Ltd. EMSIM is capable of mass and energy balance calculations for steady-state models. Custom calculations written in Python programming language can be included in certain components of EMSIM. This allows for development of models that are specific to a given study. For this reason, the software was selected to develop the ESS steelmaking process model. EMSIM also simplifies the process of calculating mass and energy balances, which allows a model developer to focus on developing a sound model and adjustment of parameters.

16.1.1 Descriptions of Components in EMSIM

The EMSIM components used in the ESS steelmaking process model are described as follows:

Material input node - This is a container that carries information about material inputs during simulation. It emulates a feed material of the actual furnace such as iron ore in a steelmaking furnace. It is represented in EMSIM by a blue rectangle with an outward pointing arrow, with a lower case letter "i" in the rectangle..
Material output node - This is a container used to capture information about material outputs of a model during a simulation. It emulates a product material of the actual furnace such as alloy in a tapping ladle of a steelmaking operation. It is represented in EMSIM by a blue rectangle with an outward pointing arrow, with a lower case letter "o" in the rectangle.
Material Stream - This is a component used to emulate material flow in a system, such as the flow of gas from the tuyeres to reactive zones of a blast furnace. It is represented in EMSIM by a blue arrow, which is drawn from one material node to another.
Material Fraction Splitter - This component can be used to separate a material stream to more than one separate stream either by mass fraction, phase, phase fraction or by phase constituent. An example of it's equivalent in an actual system, is the separation of iron alloy from ferrous slag after reduction of iron oxide has occurred. It is represented in EMSIM by a blue circle, with an upper case letter "X" in the centre of the circle.
Isothermal Equilibrium Calculation Node - This node calculates a thermodynamic equilibrium for a given material input stream and target temperature. Energy changes from the node's calculation are also given with results. The node emulates a reaction zone in a system, such as the slag-alloy

interface of a smelting operation. It is represented in EMSIM by a blue rectangle with upper case letters "TEQ" in the centre.
Isenthalpic Equilibrium Calculation Node - This node calculates a thermodynamic equilibrium for a given material input stream and target enthalpy change. The resultant temperature of the system is given as a result after simulation is complete. It is represented in EMSIM by a blue rectangle with upper case letters "HEQ" in the centre.
Energy Balance Node - All elements for which an energy balance calculation is required, are placed inside an energy balance node. Energy inputs and outputs are connected directly to the energy balance node. It is represented in EMSIM by a red rectangle.
Energy input node - This component carries information about energy inputs to a system. It represents an energy source of an actual system, such as electrical energy input in an electric arc furnace. It is represented in EMSIM by a red rectangle with an outward pointing red arrow and a lower case "i" in the centre of the rectangle.
Energy deficit node - This is similar to the energy excess node, with the exception that information about an energy deficit is captured after simulation. It is used for purposes of analysis and has no equivalent in an actual system. It's representation is similar to the energy input node, except it has a lower case "d" instead of "i" in the middle of the rectangle.
Energy output node - This component carries information about energy outputs or sinks of a system. An example of its representation in an actual system is heat losses of a furnace. It is represented in EMSIM by a red rectangle with an outward pointing red arrow and a lower case "o" in the centre of the rectangle.
Energy Excess Node - This is a node used to capture information if an excess of energy is calculated in the energy balance. It has no equivalent in an actual system, and is used mainly for analytical purposes. It is represented in EMSIM like the energy output node, except it has a lower case letter "x" instead of "o" in the centre of the rectangle.
Energy Stream - This represents a flow path of energy from one location to another. It is used to join two energy components where there is flow between them. It is represented in EMSIM by a blue arrow leading from the energy source to the destination.

A mass balance is calculated using information contained in material input and output nodes. An energy balance is also calculated around isothermal equilibrium calculation nodes, from which the change in enthalpy is obtained.

16.1.2 EMSIM Model Flowsheet

Figure 16.1 shows the EMSIM version of the ESS steelmaking process model flow sheet that was developed in Chapter 11.1 . In the remainder of this section, implementation of chemical and physical reactions are described first, followed by descriptions of material and energy flow in the model.

16.2 Implementation of Chemical and Physical Reactions

Chemical and physical reactions of the ESS steelmaking furnace are represented as thermodynamic equilibrium calculations in this model. For the case of decarburisation kinetics, custom calculations were included in components that are described in Section 16.2.6.8. Implementation of reactions in key sections of the model are described further in the remainder of this section.

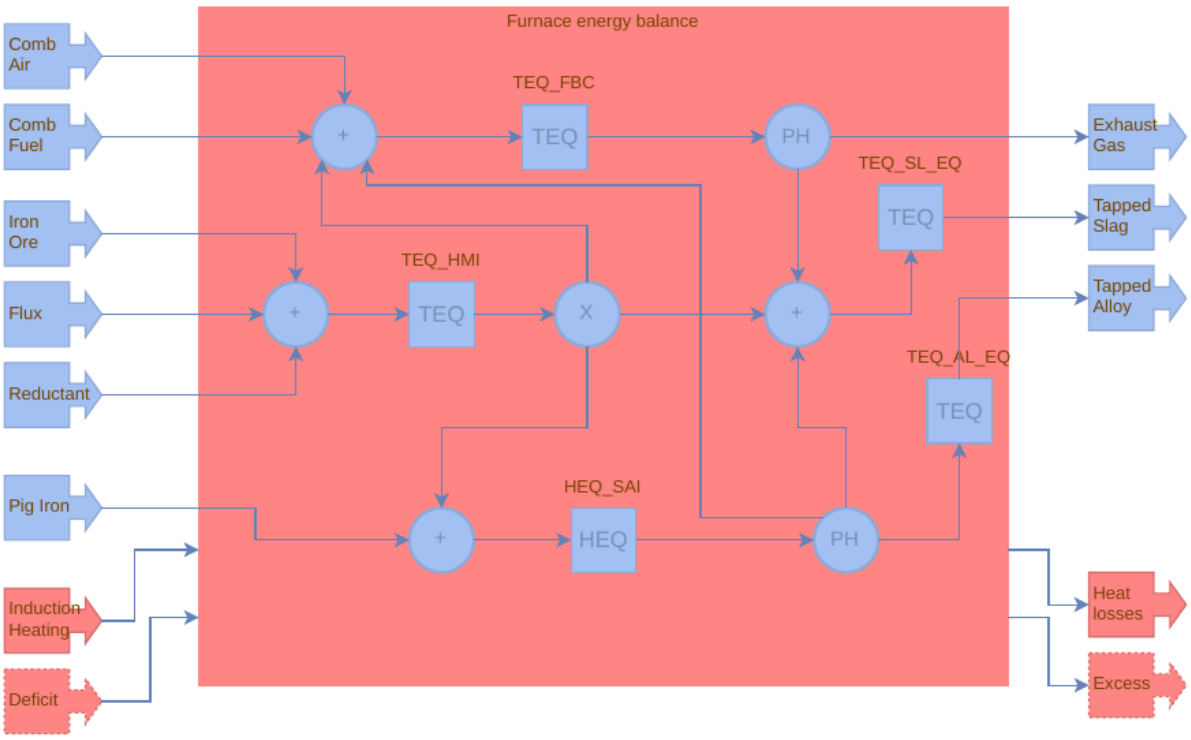

Figure 16.1: ESS steelmaking process model flow diagram froom EMSIM software.

16.2.1 Heap Surface Reactions Implementation

Node name:	Heap Melting Interface
Node codename:	TEQ_HMI
Node type:	Isothermal equilibrium calculation node
Purpose:	To simulate drying, partial reduction and melting reactions on the heap surface.
Reasoning:	The liquidus temperature of material on the surface is pre-determined and then used as the target temperature for the isothermal equilibrium calculation node. The node calculates the energy change, which represents enthalpy of reaction. This is a required result from the model and so this type of node was selected to represent the region.

16.2.2 Slag-alloy Interface Reactions Implementation

Node name:	Slag-alloy Interface
Node codename:	HEQ_SAI
Node type:	Isenthalpic equilibrium calculation node
Purpose:	To simulate reactions that occur as a result of contact between the slag and alloy baths.
Reasoning:	An Isenthalpic equilibrium calculation node makes for a better representation of the region in that temperature changes of alloy and slag due to iron-oxide reduction and carbon oxidation reactions can be monitored using the node. Thin layers of slag and alloy at the boundary between the two liquids is assumed adiabatic (Assumption A.10) in that heat is not transferred anywhere else besides the slag and alloy in these sections. Therefore, a target enthalpy change of 0 kWh can be set for the isenthalpic equilibrium calculation node.

16.2.3 Freeboard Combustion Reactions Implementation

Node name:	Freeboard Combustion Zone
Node codename:	TEQ_FCZ
Node type:	Isothermal equilibrium calculation node
Purpose:	To simulate freeboard combustion calculations.
Reasoning:	Using an isothermal equilibrium node allows for calculation of energy change due to reaction to be investigated. It also allows investigations of the influence of freeboard temperature on the energy of the furnace.

16.2.4 Slag Temperature Recalculation

Node name:	Slag Temperature Recalculation
Node codename:	TEQ_SL_EQ
Node type:	Isothermal equilibrium calculation node
Purpose:	To calculate energy required to obtain a completely molten slag after slag-alloy interface reactions.
Reasoning:	By using an isenthalpic equilibrium calculation node, some solid phases will be observed in the slag if the resulting temperature calculated in HEQ_SAI is lower than the slag's liquidus temperature. One of the aims of the furnace model is to determine energy consumptions for steady-state operation. In this regard, if the aforementioned scenario occurs, an isothermal equilibrium calculation for the product slag from TEQ_SAI is done where the target temperature is done at 5 °C above its liquidus. The energy balance is then calculated with a completely molten product slag, which gives a more accurate representation of successful steady-state operation in the ESS steelmaking process.

16.2.5 Alloy Temperature Recalculation

Node name:	Alloy Temperature Recalculation
Node codename:	TEQ_AL_EQ
Node type:	Isothermal equilibrium calculation node
Purpose:	To calculate energy required to obtain a completely molten alloy after slag-alloy interface reactions.
Reasoning:	As was described for TEQ_SL_EQ, this node is used to assist with calculating an energy balance with a completely molten alloy product.

16.2.6 Material Flow

Descriptions of material input, stream separator and combiners in EMSIM are provided in this section.

16.2.6.1 Combustion Air Input

Node Name:	Combustion Air
Node Codename:	m_in_C_air
Node type:	Material input node
Purpose:	Represents oxygen-containing gas fed into the furnace for combustion reactions in the freeboard.

16.2.6.2 Pulverised Coal Input

Name:	Combustion Fuel
Node Codename:	m_in_C_fuel
Node type:	Material input node
Node Purpose:	Represents fuel in the form of pulverised coal that is fed through burners thus supplying energy to the ESS steelmaking furnace.

16.2.6.3 Iron Ore Input

Node Name:	Iron Ore
Codename:	m_in_pig_iron
Node type:	Material input node
Purpose:	Represents solid iron ore that is fed into the furnace through feed ports installed on the roof close to the cold wall.

16.2.6.4 Flux Input

Node Name:	Flux
Codename:	m_in_flux
Node type:	Material input node
Purpose:	Represents solid burnt lime used for fluxing slag in the furnace, which is fed through feed ports installed in the roof.

16.2.6.5 Reductant Input

Node Name:	Reductant
Codename:	m_in_reductant
Node type:	Material input node
Purpose:	Represents solid coal fed to the furnace through feed ports installed in the roof. The primary purpose of the coal is to assist with pre-reduction of iron ore on the raw material heap surface.

16.2.6.6 Gas Input for Heap Melting Calculation

Node Name:	Heap Melting Gas
Codename:	m_in_heap_gas
Node type:	Material input node
Purpose:	The solver that does thermodynamic equilibrium calculations for solid material inputs only in EMSIM takes a long time. To solve this, a small amount of gas is added to allow more degrees of freedom for the solver and reduce simulation time. This has no equivalent in the actual furnace and is only a solution that improves calculation efficiency of the model.

16.2.6.7 Pig Iron Input

Node Name:	Pig Iron
Codename:	m_in_pig_iron
Node type:	Material input node
Purpose:	This represents pig iron that is fed to the alloy bath of the ESS steelmaking furnace.

16.2.6.8 Heap Melting Product Separator

Node Name:	HMP Separator
Codename:	m_sep_HMP
Node type:	Material fraction splitter node
Purpose:	This node splits the product of heap melting calculations into three streams. The first stream is gas, which is directed to freeboard combustion calculations. The second stream is referred to as "active slag" which is directed to slag-alloy reaction calculations. The final stream is referred to as "inactive slag" which is directed to slag bath equilibrium calculations. The method by which active and inactive slag are separated is discussed in Section 15.5.3.

16.2.6.9 Slag-alloy Interface Product Separator

Node Name:	SAI Separator
Codename:	m_sep_SAI
Node type:	Material fraction splitter node
Purpose:	This node separates the product of slag-alloy interface calculations into three separate streams of slag, gas and alloy respectively.

16.2.6.10 Freeboard Product Separator

Node Name:	FBCP separator
Codename:	m_sep_FBCP
Node type:	Material fraction splitter node
Purpose:	In the event that too much reductant is used in, or condensed-phases are calculated by the freeboard combustion calculation, this node removes the condensed phases and directs them to the slag equilibrium calculations. This represents the gas particles returning to the slag layer from recirculating spent freeboard gas.

16.2.6.11 Heap Melting Interface Input Combiner

Node Name:	HMI combiner
Codename:	m_comb_HMI
Node type:	Material combiner node
Purpose:	Thermodynamic equilibrium calculation nodes can only take one input and produce a result to one output stream. For this reason, solid material feed and the heap gas input are combined to one stream before adding to the equilibrium calculation. Using a material combiner node does not calculate equilibrium. Temperature recalculation is possible, but this feature is turned of for this combiner node.

16.2.6.12 Slag-alloy Interface Input Combiner

Node Name:	SAI combiner
Codename:	m_comb_SAI
Node type:	Material combiner node
Purpose:	Pig iron and active slag are combined using this node before adding these materials to the slag-alloy interface equilibrium calculation. Temperature recalculation is also deactivated in this combiner node.

16.2.6.13 Slag Product Combiner

Node Name:	SP combiner
Codename:	m_comb_SP
Node type:	Material combiner node
Purpose:	This node combines slag from the slag-alloy interface calculation, inactive-slag from the heap surface and any condensed phases from the freeboard combustion calculations. The combined stream is then directed to slag equilibrium calculations. Temperature recalculation is also deactivated in this combiner node.

16.2.6.14 Alloy Product Combiner

Node Name:	AP combiner
Codename:	m_comb_AP
Node type:	Material combiner node
Purpose:	This node combines alloy from the slag-alloy interface calculation and any alloy phases from slag equilibrium calculations before adding these to alloy equilibrium calculations. The combined stream is then directed to slag equilibrium calculations. Temperature recalculation is also deactivated in this combiner node.

16.2.6.15 Final Alloy Product

Node Name:	Alloy
Codename:	m_out_alloy
Node type:	Material output node
Purpose:	This represents alloy that is tapped from the furnace before it is refined using ladle metallurgy.

16.2.6.16 Final Slag Product

Node Name:	Slag
Codename:	m_out_slag
Node type:	Material output node
Purpose:	This represents slag that is tapped immediately from the furnace.

16.2.6.17 Final Exhaust Gas Product

Node Name:	Exhaust Gas
Codename:	m_out_exhaust_gas
Node type:	Material output node
Purpose:	This represents exhaust gas extracted from the furnace before it is sent to scrubbers and heat exchangers.

16.2.7 Energy Flow

16.2.7.1 Energy Balance Node

Node name	ESS Energy Balance
Node codename	e_bal_ESS
Node type	Energy balance calculation node
Purpose	This calculates an energy balance for the nodes contained within it. It is also a representation of boundaries for the furnace system studied in this research.

16.2.7.2 Induction Heating Input

Node name	Induction Heat
Node codename	e_in_ind_H
Node type	Energy input node
Purpose	This represents heat added to alloy in induction heating chambers, and subsequently to the alloy bath.

16.2.7.3 Deficit Heat Input

Node name	Deficit
Node codename	e_in_deficit
Node type	Energy deficit input node
Purpose	To produce the desired products at their respective temperatures, this node will capture the amount of energy required (deficit), if there is a lack thereof. This has no equivalent in the actual furnace, but is rather a tool used in EMSIM for energy balance calculations.

16.2.7.4 Excess Heat Output

Node name	Excess
Node codename	e_out_excess
Node type	Energy excess output node
Purpose	In contrast to the deficit node, this node will capture the result if there is an excess of energy supplied to the system. This also is used by the energy balance calculation node in EMSIM and has no equivalent in the actual furnace.

16.2.7.5 Heat Losses

Node name	H Losses
Node codename	e_out_losses
Node type	Energy output node
Purpose	This node calculates potential energy losses from the furnace, using the methods described in Section 15.7.3.

Part V

Process Simulation and Results

Chapter 17

Simulation Design

This chapter describes design of simulations made with the ESS steelmaking model.

17.1 Simulation Objectives

The simulations were designed to achieve the objectives in Section 2.2, by obtaining and using results specified in Section 10.5.1. These are broken down to more specific objectives as follows.

1. Determine the feed recipe required to produce a sufficient amount of molten slag with the most FeO content.
2. Determine the ideal heap surface melting temperature with the feed recipe found in item 1 of this list.
3. Determine the ideal heap surface melting rate that can decarburise 10 t of pig iron from 4.0 to 0.25 wt%C per hour.
4. Determine the rate of combustion air feed required for complete combustion in the freeboard.
5. Investigate the effect of combustion air feed temperature on the energy requirements of the furnace.
6. Determine the rate at which combustion fuel (pulverised coal) must be added to the furnace to supplement any energy deficit observed.
7. Estimate energy consumption or production at reaction interfaces of the furnace.

17.2 Monitored Variables

Dependent variables of the model that are monitored to provide answers for objectives stated in Section 17.1 are as follows.

1. Mass and composition of tapped alloy.
2. Phase composition of the product formed in heap reactions.
3. Phase composition of the product formed in slag-alloy interface reactions.
4. Mass and composition of the active component in the heap reaction product.
5. Mass transfer rates calculated by the decarburisation kinetics sub-model
6. Furnace energy balance (deficit or excess).
7. Heat production or consumption in reaction interface equilibrium calculations.
8. Heat losses from the furnace.

The results are stored in files that can be accessed by a tool developed in Python for plotting figures against independent variables.

17.3 Simulation Experiment Plans

This section describes the set up of simulation experiments designed to achieve the objectives stated in Section 17.1. All parameters except for the stated manipulated variable, are set to their default values for each experiment which are shown in Appendix

17.3.1 Experiment 1: Raw Material Feed Recipe

Purpose: To determine the solid raw material feed recipe that will give maximum molten slag with the highest iron(II)oxide (FeO) and least metallic phase concentrations, at the heap's active surface.

Manipulated variable: Ore, flux and reductant fractions in the heap material.

Manipulation ranges: Ore fraction = 0.1 to 0.9
Ore to Flux ratio = 1:9 up to 9:1
Reductant fraction = 1 - (Ore fraction + Flux fraction)

Measured variables: Mass and composition of molten material from heap melting that will participate in slag-alloy interface reactions (active slag).

Other adjustments: The melting rate of heap material was set to $10\,\mathrm{t\,h^{-1}}$ for this simulation. This was an arbitrary value selected, because the experiment's required result is dependent on thermochemistry and not melting rate at the heap.

17.3.2 Experiment 2: Minimum Heap Surface Temperature

Purpose: To determine the minimum heap surface temperature that will drive melting and pre-reduction reactions.

Manipulated variable: Heap Surface Temperature.

Manipulation ranges: 900.0 to 1500.0 °C

Measured variables: Mass and composition of molten material from heap surface reaction.

Other adjustments: The melting rate of heap material was set to $10\,\mathrm{t\,h^{-1}}$ for this simulation. Feed recipe was kept at the optimum values obtained in the experiment described in Section 17.3.1.

17.3.3 Experiment 3: Heap Surface Melting Rate

Purpose: To determine the heap surface melting rate required to give maximum decarburisation.

Manipulated variable: Heap melting rate.

Manipulation range: 1.0 to 1000.0 $\mathrm{kg\,h^{-1}}$

Measured variables:
1. Mass molten material produced in heap reactions (active slag).
2. Energy consumption at the heap melting interface.
2. Mass and composition of tapped alloy.

17.3.4 Experiment 4: Combustion Air and fuel Requirements

Purpose: To determine feed rate and input temperature of combustion air and fuel that is required to have sufficient energy in the furnace.

Manipulated variable:
1. Combustion air feed rate.
2. Combustion air temperature.
2. Combustion fuel feed rate.

Manipulation range: Combustion air feed rate: 0.0 to 800.0 $\mathrm{kg\,h^{-1}}$.
Combustion air temperature: 0.0 to 800.0 °C .
Combustion fuel feed rate: 0.0 to 800.0 $\mathrm{kg\,h^{-1}}$.

Measured variables:
1. Energy deficit node result.
2. Energy excess node result.
4. Energy release from freeboard combustion.
9. Energy losses from the furnace.

Chapter 18

Simulation Results

18.1 Experiment 1: Raw Material Feed Recipe

From first experiment's results, it was determined that for the Sishen iron ore assay used, an ore to flux ratio of 0.8 is required which translates to 200 kg flux per tonne of ore to achieve 100 % slag liquefaction in heap melting reactions as shown in Figure 18.1.

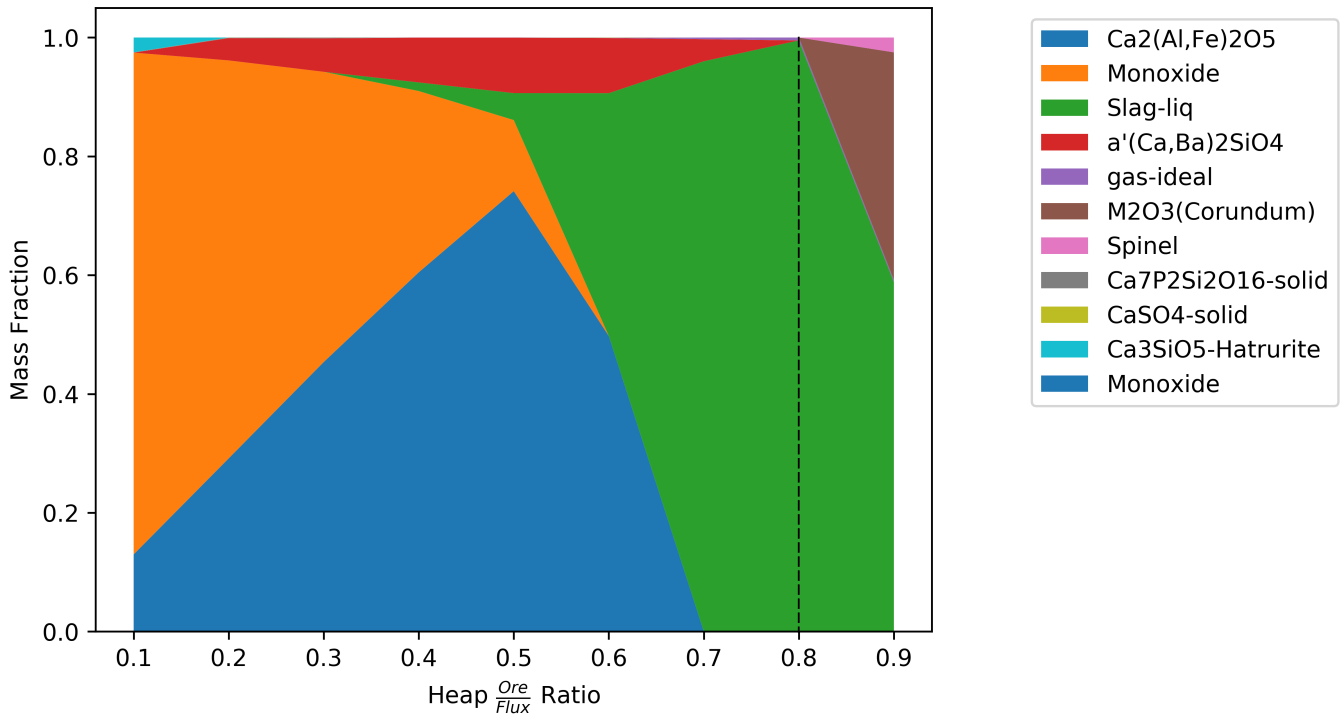

Figure 18.1: Composition of heap melting interface product as a function of Ore:Flux ratio.

A sub-experiment was then done to determine the influence of heap temperature on the melting product composition with the 4:1 ore to flux ratio. Figure 18.2 shows the result of a sub-experiment, where the composition of molten product from the heap is plotted against temperature of the heap surface, from which it was observed that the minimum required surface temperature for melting was 1345.0 °C. This was set as the surface temperature for the succeeding sub-experiment, where the reductant input required to produce the highest FeO content was investigated.

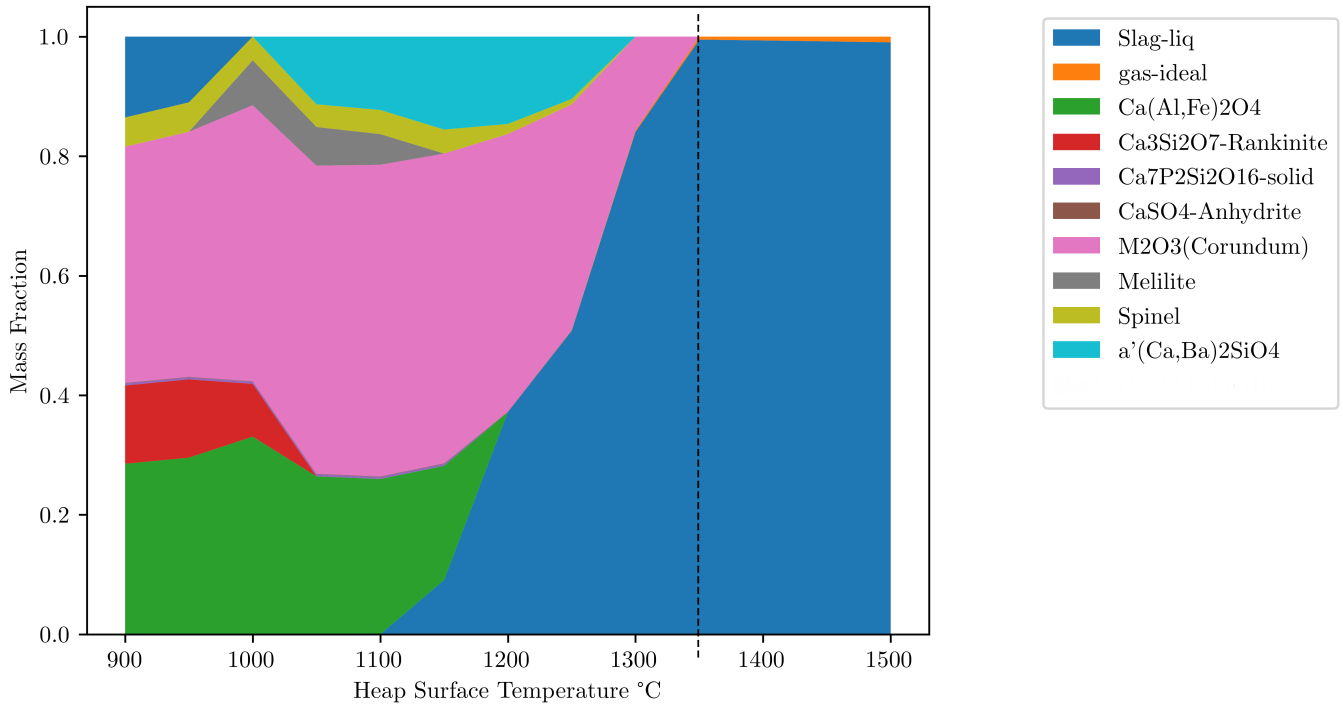

Figure 18.2: Heap reaction product composition as a function temperature on the heap surface.

The highest FeO concentration in the molten heap product was observed at an ore:reductant ratio of approximately 0.8 which translates to 57.9 kg per tonne of ore. The required ore:reductant ratio to achieve the highest amount of molten product was at 0.98, which is 19.5 kg reductant per tonne of ore. The highest FeO concentration in the molten product was observed at an ore:reductant ratio of 0.95 which is 57.9 kg per tonne of ore). In the first iteration shown in Figure 18.3, the ore:reductant ratio was not to exceed 0.8 if metallisation in the heap is to be avoided. Higher reductant input resulted in the formation of solid iron alloy and beyond a ratio of 0.7, liquid alloy was observed, which was a result of increased carbon in the system lowering the liquids temperature of solid alloy.

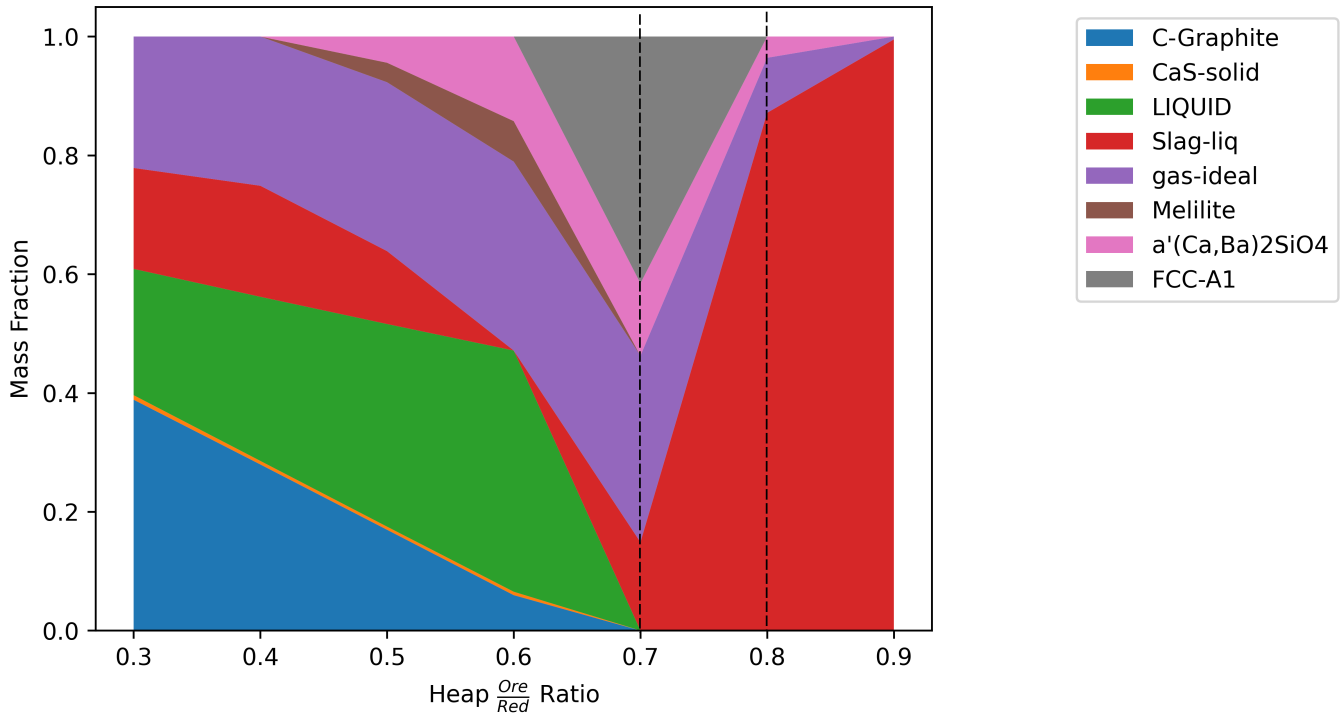

Figure 18.3: Heap reaction product composition as a function ore to reductant ratio on the heap surface.

18.2 Experiment 2: Minimum Heap Surface Temperature

With results from the experiment in Section 18.1, a second scan for the lowest temperature for complete melting was done and the minimum value was observed at 1360.0 °C. The phase composition of molten heap product versus temperature for the range from 1350.0 to 1365.0 °C is shown in Figure 18.4.

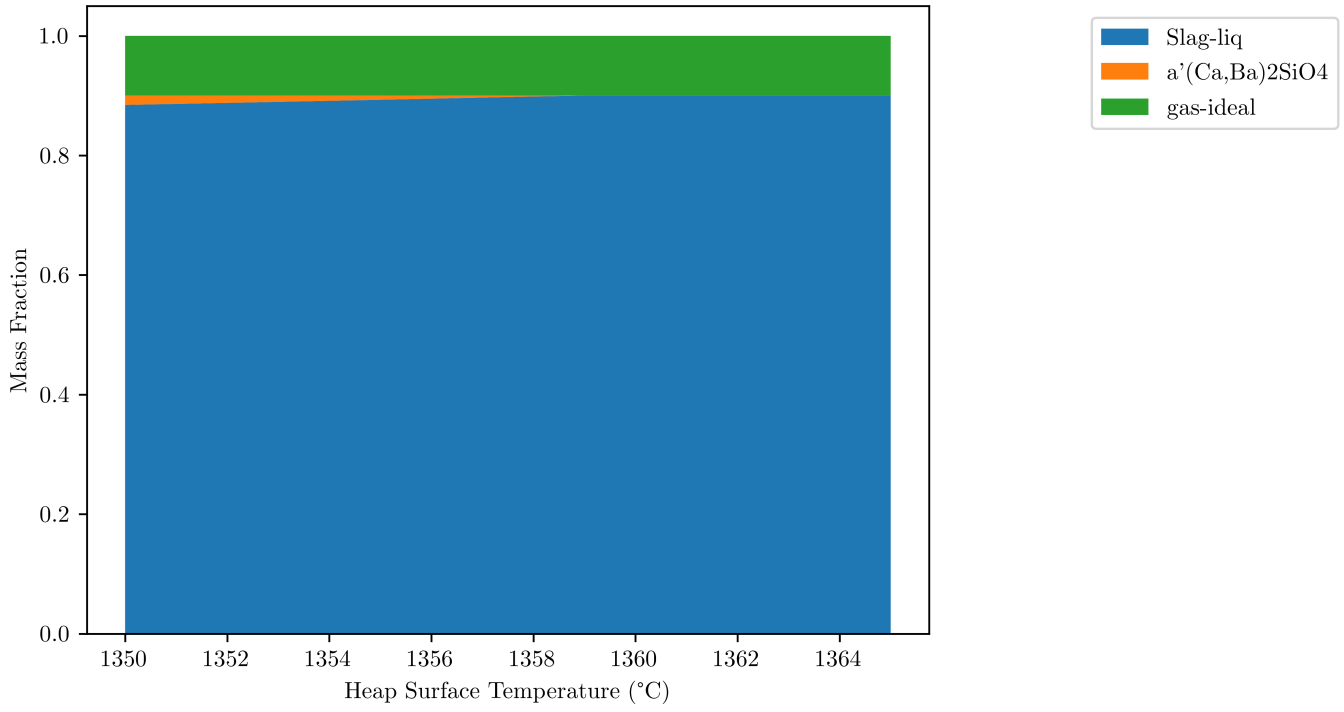

Figure 18.4: Reaction product phase composition as a function temperature on the heap surface.

18.3 Experiment 3: Heap Surface Melting Rate

The highest decarburisation rate was observed at a heap melting rate of approximately 654 kg h^{-1}. In terms of surface depth consumption the value is 1.7 cm h^{-1}, which implies very slow melting. At this melting rate, the predicted carbon composition of tapped alloy was 3.23 wt%C and the limiting rate was approximately 434 kg h^{-1}, which was of carbon in the alloy. Oxygen mass transfer rate in iron was calculated to be 986 kg h^{-1} and for iron-oxide in slag 3420 kg h^{-1}. Figure 18.5 shows the carbon concentration of tapped alloy, plotted as a function of the heap surface melting rate. The rate-limiting step below this value was mass transport of FeO in slag, and above, was carbon mass transport in the alloy. Energy consumption

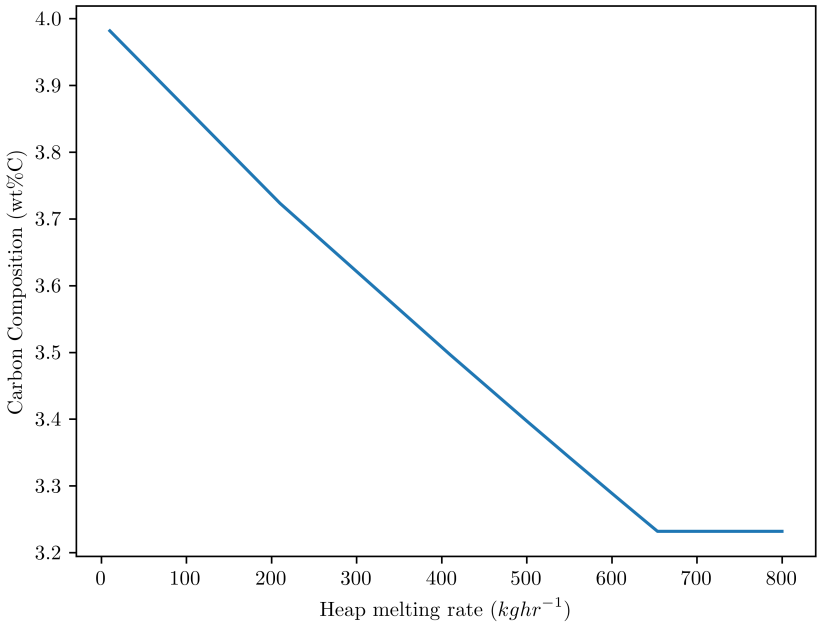

Figure 18.5: Tapped alloy carbon concentration as a function of heap surface melting rate.

at this heap melting rate and surface temperature was observed to be 332 kWh, which translates to a required heat flux of 46 kW m^{-2}. This is 26 % of the proposed 180 kW m^{-2}, and 38 % of the observed 120 kW m^{-2} capability of the ESS furnace.

18.4 Experiment 4: Combustion Air and Fuel Feed

In the first experiment, calculated heat losses from the furnace were approximately 130 kW lowest energy deficit observed 62.1 kW, where 495 kg h^{-1} of combustion air was fed to the furnace at 25 °C. Figure 18.6 shows the energy deficit as a function of combustion air input rate. With this calculated optimum input rate, the temperature yielded a zero energy balance at 457 °C. Combustion fuel was not required in the simulations since, in the aforementioned conditions, reaction of combustion air with carbon monoxide from reactions in the heap and slag-alloy interface would supply sufficient energy under steady state operation. This was due to the model's freeboard, slag and alloy bath temperatures being fixed to required values. For a more accurate prediction of combustion fuel requirements, a comprehensive heat transfer model would have to be incorporated, which was not possible with the version of EMSIM used. The energy balance from this investigation does however suggest that the process can be maintained at required temperatures with minimal additions of combustion fuel.

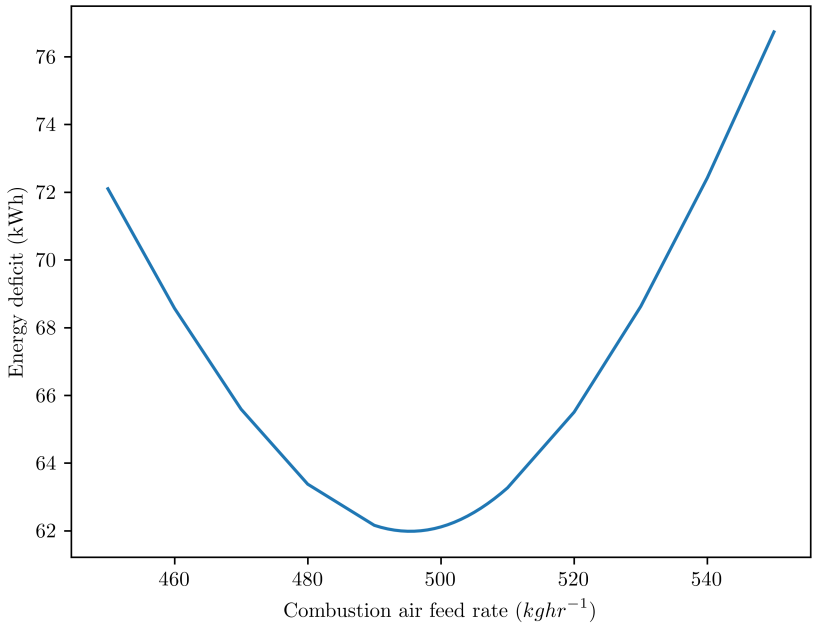

Figure 18.6: Energy balance of the ESS furnace model as a function of combustion air feed rate.

Chapter 19

Discussion

From simulation experiment results, it is likely that the ESS furnace will not be capable of producing alloy with less than 0.25 wt%C in one hour. Phenomena dictating decarburisation kinetics, particularly that of carbon mass transfer in the molten bath, will not happen fast enough to produce the required production specification. Considering methods by which the model predicts these results however, an actual ESS furnace may show better performance than is what predicted by model results.

Decarburisation rates were limited by iron-oxide mass transfer in slag for heap melting rates of up to 654 kg h^{-1} and beyond this, carbon mass transfer became the limiting rate factor. This is because carbon mass transfer was formulated using mass transfer, with the assumption that concentration in both the bath and gas-alloy reaction interfaces would remain constant. With this, carbon mass transfer was always at a constant value. Even if more melting occurred at the heap surface to provide more FeO, carbon mass transport would limit the overall reaction rate. The ESS furnace could therefore have different performance from what the model predicts.

The effects of bubbling on decarburisation rates was included in calculations of mass transfer coefficients. Mass transfer coefficients are not only dependent on bubbling and diffusivity, but also the area over which diffusion is occurring and the concentration of phases across boundary layers where they are produced or consumed. The slag-alloy surface area in the model was simplified to a planar region, which will definitely not be the case for the actual furnace. The area will be larger due to constant movement of carbon monoxide bubbles across the interface. Mass transfer rates would therefore be higher, and a lower carbon concentration could be achieved in the tapped alloy within an hour.

From a modelling perspective, there is a need to further understand decarburisation in the ESS process, particularly from the perspective provided in literature about the involvement of surfaces in reactions. Gas formation in a liquid requires high energy input in order to overcome nucleation forces, which are an obstruction to decarburisation reaction rates. This is the reason why oxygen-steelmaking processes (e.g Bessemer AOD process) have higher decarburisation rates than bath-steelmaking processes (e.g Basic open hearth furnace). High velocity gas jets disturb molten iron baths so much that nucleation of gas bubbles within the molten iron is occurs more easily, as was observed in experiments by several authors in published literature. From another point of view, nucleation of gas may prove problematic for the ESS furnace in the induction heating channels. Gas formation here would result in a break of the secondary circuit formed by the molten iron circulating through channels. If the circuit is broken for long enough, the alloy will cool down and ultimately solidify. This will block off the source of reheated alloy to the slag-alloy interface, which will reduce circulation in the bath. Mass transfer rates will be reduced, and ultimately, decarburisation rates will be lower than what has been observed in this model.

Greater consideration is required in terms of refractory materials than what was formulated in this work. While oxygen steelmaking refractory materials are generally designed to withstand physical and chemical attacks from melts with high turbulence, bath steelmaking relies greatly on their design for nucleation of gas bubbles. If no nucleation can occur, the bath will most likely stand still, with no decarburisation occurring.

Considering that parameters in the model were underestimated in most of the model phenomena, the furnace may perform better than predicted. This may be an advantage or disadvantage in terms of process control. While better performance would acknowledge feasibility, it may also bring challenges of its own, which were not studied in this research work. With the information obtained from this research, there are phenomena that require studies in greater detail, such as a multi-physics model, which will most likely give more information with regards to steady state operation.

Part VI

Closure

Chapter 20

Closure

20.1 Conclusions

Computer-based modelling work was used to investigate steelmaking capabilities of the ESS furnace. It was uncovered that sub-reactions occur at different locations of the furnace that affect rates in the process. There is still more to be understood about the furnace to successfully quantify steady state behaviour using a modelling approach, but from investigations in this research work, it is predicted that the ESS furnace will not be capable of decarburising pig iron to less than 0.25 wt%C, due to the limiting rate of carbon mass transfer in molten iron solutions, based on available mathematical descriptions of the process.

20.2 Recommendations

Other zones in the furnace were not fully analysed from simulations in this research. It is recommended that a more comprehensive approach be used to understand geometry and mass transfer phenomena that will dictate steady state performance and allow for a successful steelmaking process.

In this research, radiation was not investigated to great detail. Some simplifications and assumptions were made to account for this. Instead of assuming sufficient energy to melt material as required, incorporating a radiation model would give a better understanding of energy consumption in the furnace. There is also opportunity to further improve understanding of the furnace by investigating the following.

1. Electromagnetic induction in the heating channels and their effect on furnace operation.
2. Influence of phenomena in finite regions of the furnace in multi-physics modelling.

Other aspects which may influence steady state behaviour of the furnace may not have been identified within the scope of this research. These will most likely be revealed in future investigations if research on the process is continued.

20.3 Summary

A mass and energy balance model, that included decarburisation kinetics was developed and used to calculate whether it would be possible to make steel from molten pig iron, given known capabilities of the furnace. Phenomena that would have an influence on steelmaking performance during steady-state operation, were analysed from a metallurgical perspective. The studies revealed that the furnace may not be capable of achieving set targets, although more work is required to better understand the nature of the ESS process and its metallurgical phenomena. Aspects such as radiation in the freeboard, electromagnetic heating and finite region analyses are required to quantify with greater confidence, the potential performance of the ESS steelmaking furnace.

References

Agarwal, D.P. and D.R. Gaskell (1975). "The self-diffusion of iron in Fe_2SiO_4 and $CaFeSiO_4$ melts". In: *Metall. Mater. Trans. B* 6.2, pp. 263–267.

Ashman, S. (Dec. 2016). "The crises in steel and mining and what they mean for the South African economy". In: *Amandla!* 49.50. URL: http://aidc.org.za/crises-steel-mining-mean-south-african-economy/.

Atkins, P. and J. de Paula (2010). *Atkins' Physical Chemistry*. 9th. Oxford University Press. ISBN: 9780199543373.

Attah-Kyei, D. et al. (Oct. 2018). "Printed circuit board leach residue as a reductant for pyrometallurgical operation." In: *Wastecon 2018*.

Basu, S (June 15, 2007). "Studies on dephosphorisation in steelmaking". PhD thesis. Royal Institute of Technology.

Benavidez, E.R. et al. (2015). "Thermal and mechanical properties of commercial MgO-C bricks". In: *Materia* 20.3, pp. 571–579.

Bishop, H. L. et al. (1956). "Equilibria of Sulfur and Oxygen Between Liquid Iron and Open Hearth-Type Slags". In: *JOM* 8.7, pp. 862–868. ISSN: 1543-1851. DOI: 10.1007/BF03377783.

Booth, W.C., G.G. Colomb, and J.M. Williams (2009). *The Craft of Research, Third Edition*. Chicago Guides to Writing, Editing, and Publishing. University of Chicago Press. ISBN: 9780226062648. URL: https://books.google.co.za/books?id=Y31pUtkwb2oC.

Brockenbrough, R. L. (1999). *Structural Steel Designer's Handbook*. Ed. by Roger L. Brockenbrough and Frederick S. Merritt. 3rd. McGraw-Hill, Inc.

Carniglia, S. C. and G. L. Barna (1992). *Handbook of Industrial Refractories Technology: Principles, types, properties, and applications*. Ed. by Rointan F. Bunshah, Gary E. McGuire, and Stephen M. Rossnagel. Noyes Publications.

Darken, L.S. (1964). "Kinetics of Metallurgical processes." In: *Basic Open Hearth Steelmaking*. Ed. by G. Derge. 3rd. American Institute of Mining, Metallurgical and Petroleum Engineers. Chap. 15, pp. 588–639.

Derge, G (1964). *Basic Open Hearth Steelmaking*. Ed. by Physical Chemistry of Steelmaking Committee. 3rd ed. The American Institute of Mining, Metallurgical, and Petroleum Engineers.

Dolan, M.D. and R.F. Johnston (2004). "Multicomponent diffusion in slags". In: *Metall. Mater. Trans. B* 35, pp. 675–684.

DTI-RSA (June 12, 2018). "Status of the South African Steel Industry". In: *Presentation to the Portfolio Committee on trade and industry* (Johannesburg, South Africa, June 12, 2018). The Department of Trade and Industry (RSA). URL: https://www.thedti.gov.za/parliament/2018/SA_Steel.pdf (visited on 10/18/2019).

EncyclopediaBrittanica (June 2017). *Joule's law*. English. Encyclopædia Britannica, inc. URL: https://www.britannica.com/science/Joules-law.

Eriksson, G. (Nov. 20, 1974). "Thermodynamic Studies of High Temperature Equilibria". In: *Chemica Scripta* 8.7, pp. 100–103.

— (1975). "Quantitative Equilibrium Calculations In Multiphase Systems At High Temperatures, With Special Reference To The Roasting Of Chalcopyrite $(CuFeS)_2$". PhD thesis. Department of Inorganic Chemistry, University of Umea.

Eriksson, G. and K. Hack (May 10, 1983). "Calculation Of Phase Equilibria In Multicomponent Alloy Systems Using A Specially Adapted Version Of The Program 'Solgasmix'". In: *CALPHAD* 8.1, pp. 15–24. DOI: 10.1016/0364-5916(84)90025-7.

Eriksson, G. and E. Rosen (1972). "An Equilibrium Model For Examining The Chemistry Of High Temperature Processes". In: *Transactions of the Royal Institute of Technology Stockholm* 34.

Fourie, L. J. and L. J. Erasmus (2015). "ESS Smelting Technology Enabling FeNi Smelting from Limonite". In: *The Fourteenth International Ferroalloys Congress*.

Fourie, L.J. and L.J Erasmus (2016). Private communication.

— (2017). "ESS Smeting Technology". In: *The Journal of The Minerals, Metals and Materials Society* 69 (2).

Fruehan, R.J. (1998). *The Making Shaping and Treating of Steel: SteelmSteel and Refining Volume*. Ed. by R.J. Fruehan. 11th. ISBN: 978-0-930767-02-0. AIST. Chap. 1 Overview of Steelmaking Processes and Their Development.

Fruehan, R.J. and P.C. Pistorius (2014). "Treatise on process metallurgy: Process Phenomena". In: ed. by S. Seetharaman. Vol. 2. Elsevier. Chap. 2, Metallurgical Process Phenomena, pp. 141–239.

Geyer, H (Nov. 3, 2011). "Biobenefication of Sishen Hematite Iron Ore, using bacterial cultures to remove potassium (Muscovite) and phosphorous (Apatite)". MA thesis. University of Pretoria.

Goldstein, Robert (2014). "Magnetic Flux Controllers in Induction Heating and Melting". In: *ASM Handbook* 4C, pp. 634–645.

Hack, K. and M. Van Ende (2014). "Treatise on process metallurgy: Process Phenomena". In: ed. by S. Seetharaman. Vol. 2. 8. Elsevier. Chap. 5.4, Process Modelling.

Hamadeh, Hamzeh, Olivier Mirgaux, and Fabrice Patisson (2018). "Detailed Modeling of the Direct Reduction of Iron Ore in a Shaft Furnace." eng. In: *Materials (Basel, Switzerland)* 11 (10).

Keller, H. and K. Schwerdtfeger (1986). "Measurement of tracer diffusivities of Ca^{45} and Fe^{59} in silica saturated FeO-CaO-SiO_2 melts with the Porous Frit Technique". In: *Metall. Mater. Trans. B* 17.3, pp. 497–501.

Larsen, B.M. (1956). "A new look at the nature of the open-hearth process". In: *NOHC Special report series*.

Mills, K.C. and B.J. Keene (1987). "Physical properties of BOS slags". In: *Int. Mater. Rev.* 32.1-2, pp. 1–120.

Min, D.J. and R.J. Fruehan (1992). "Rate of reduction of FeO in slag by Fe-C drops". In: *Metall. Mater. Trans. B* 23B, pp. 29–37.

Montiea, Bruce (July 2015). *South African steel industry faces global oversupply*. EN. URL: http://www.engineeringnews.co.za/article/south-african-steel-industry-faces-global-oversupply-2015-07-10.

Mori, K. and K. Suzuki (1968). "Diffusion in Iron Oxide Melts". In: *Tetsu-to-Hagane* 54.12, pp. 1199–1203.

South African Primary Steel Industry (2014). South African Iron and Steel Institute. Cape Town: OECD/South Africa Workshop on Steelmaking Raw Materials.

O'Flaherty, Paul (Sept. 2015). *The hard reality about SA steel industry*. English. ArcelorMittal South Africa. URL: https://www.iol.co.za/business-report/opinion/the-hard-reality-about-sa-steel-industry-1918730.

Ono, Y. (1977). "Diffusion in liquid iron and it's alloys". In: *Tetsu to Hagane* 63.8, pp. 1350–1361.

Ottojunker (2018). *Channel-type induction furnaces for melting*. Last accessed: 31-08-2018. OTTO JUNKER GmbH. URL: https://www.otto-junker.com/cache/c231534abaa6bb1c56d4949a517c47e3.jpeg.

Paul, A., B. Deo, and N. Sathyamurty (1994). "Kinetic model for reduction of iron oxide in molten slags by iron-carbon melt". In: *Steel Research* 65.10, pp. 415–419.

Pauw, Ockert Gerbrandt (1989). "Dynamic simulations of pyrometallurgical processes involving fast reactions at phase boundaries". PhD thesis. University of Pretoria.

Philbrook, W.O. (1961). "Process Kinetics of Basic Oxygen Steelmaking". In: *AIME National Open Hearth Steel Conference*.

Philbrook, W.O. et al. (1951). *Basic Open Hearth Steelmaking*. Ed. by W.O. Philbrook et al. 2nd. The American Institute of Mining and Metallurgical Engineers. Chap. One.

Poirier, D.R and G.H Geiger (1994). *Transport Phenomena in Materials Processing*. The Minerals, Metals & Materials Society. ISBN: 0-87339-272-8.

Posch, V. et al. (2002). *Desulphurization of liquid steel with refining top slags*. Tech. rep. EUR 20474. B-1049 Brussels, Belgium: European Commission.

Powell, R.T., C.Y. Ho, and P.E. Liley (Aug. 1966). *Thermal conductivity of selected Materials*. Tech. rep. National Bureau of Standards.

Rao, Y. K. (1985). *Stoichiometry and thermodynamics of metallurgical processes*. Cambridge University Press. ISBN: 0521258561.

Robertson, D.G.C. and B.B. Staples (1974). "Model studies on mass transfer across a metal-slag interface stirred by bubbles". In: *Process Engineering of Pyrometallurgy - Proceedings of a Joint Meeting of the Institution of Mining and Metallurgy and the Institution of Chemical Engineers*. Ed. by Jones M.J. The Institution of Mining and Metallurgy, pp. 51–59.

Sayad-Yaghoubi, Y., S. Sun, and S. Jahanshahi (1997). "The effect of iron-oxide on the chemical diffusivity of oxygen in slags". In: *Molten slags, fluxes and salts*, pp. 839–844.

Schane, Philip Jr. and U Willard Talor (1959). "Open Hearth Steelmaking Process". Pat. 610,001.

Sugita, Kyoshi (July 2008). *Historical Overview of Refractory Technology in the Steel Industry*. Technical Report 98. Japan: Nippon Steel.

Taylor, CR and John Chipman (Jan. 2, 1942). "Equilibria of Liquid Iron and Simple Basic and Acid Slags in a rotating induction Furnace". In: *Transactions of The American Institute of Mining, Metallurgical and Petroleum Engineers* 313.

Vert, Tom (Apr. 2016). *Refractory selection in steelmaking*. Ed. by Tom Vert. 4th. Wiley Publishing Co. DOI: http://doi.10.1002/9781119219873.

Win, Thant Zin (2015). "An Analytical Study of Cooling Pond System for Coreless Induction Furnace". Presentation. Last accessed: 31-Aug-2018.

Woolley, D.E. (1998). "Electrochemically Enhanced Reduction of Iron Oxide from Slag". PhD thesis. Massachusets Institute of Technology.

Woolley, D.E. and U.B. Pal (1999a). "Experimental evidence for electrochemical nature of the reaction between iron oxide in calcia-silica-alumina slag and carbon in liquid iron". In: *Metallurgical and Materials Transactions B: Process Metallurgy and Materials Processing Science* 30, pp. 877–889.

— (1999b). "Rate of reduction of ferric and ferrous oxide from calcia-silica-alumina slag by carbon in liquid iron". In: *The Iron and Steel Institute of Japan* 39.2, pp. 103–112.

— (2002). "Enhancing rate of slag-metal reactions involving carbon in liquid iron". In: *Ironmaking and Steelmaking* 29.2, pp. 125–132.

Yue, Q., C. B. Zhang, and X. H. Pei (2017). "Magnetohydrodynamic flows and heat transfer in a twin-channel induction heating tundish". In: *Ironmaking & Steelmaking* 44.3, pp. 227–236. DOI: 10.1080/03019233.2016.1209919.

Zietsman, J., W. Pretorius, and A. Steyn (Feb. 2018). "Evaluating pre-treatment and smelting options with EMSIM to improve production efficiency". In: *INFACON XV: International Ferro-Alloys Congress*.

Zietsman, J.H. (Apr. 30, 2004). "Interactions Between Freeze Lining and Slag Bath in Ilmenite Smelting". PhD thesis. University of Pretoria.

Appendix A

Fixed Parameter Default Values

Default values of fixed parameters are given in Table A.1. The "Calculated value" column includes values that were given an initial value in EMSIM (a requirement of the modelling suite), and were then recalculated based on their relationship to known default values. As an example, the heat losses from the furnace are initially unknown and therefore set to zero. Once alloy and slag bath dimensions, contact surfaces, and therefore thermal resistances are calculated, the heat loss values could then be determined. Where the default value is different from that calculated, the parameter was defined by a custom calculation, whose result was stored for debugging purposes.

Table A.1: Parameters used in the ESS steelmaking mass and energy balance model.

Name	Default Value	Calculated Value	Units
Temperatures and Pressure			
Alloy Meniscus Pressure	1.0	103129.4	atm
Furnace Floor Pressure	1.0	103143.09	atm
Standard Pressure	1.0	1.0	atm
Alloy Tapping Temperature	1550.0	1550.0	°C
Combustion Air Feed Temperature	700.0	700.0	°C
Freeboard Combustion Temperature	1900.0	1900.0	°C
Heap Surface Melting Temperature	1000.0	1000.0	°C
Pig Iron Feed Temperature	1550.0	1550.0	°C
Slag-alloy Interface Temperature	1500.0	1500.0	°C
Slag Tapping Temperature	1600.0	1600.0	°C
Ambient Conditions			
Pressure	1.0	1.0	atm
Temperature	25.0	25.0	°C
Energy Parameters			
Induction Heating Input	200.0	200.0	kW
Total Heat Losses	0.0	0.0	kW
Zone 1 Heat Losses	0.0	903464.65	kW
Zone 2 Heat Losses	0.0	62378.71	kW
Zone 3 Heat Losses	0.0	1676.74	kW
Zone 4 Heat Losses	0.0	3592.02	kW
Zone 5 Heat Losses	0.0	14197.05	kW
Zone 6 Heat Losses	0.0	0.0	kW
Zone 7 Heat Losses	0.0	25949.06	kW
Thermal Resistance of Zone 1 Firebrick	1e+99	0.0	K/kW

Continued on next page.

Table A.1 continued.

Name	Default value	Calculated value	Units
Thermal Resistance of Zone 1 Magnesite	1e+99	0.00202	K/kW
Thermal Resistance of Zone 1 Steel Shell	1e+99	5.334	K/kW
Total Thermal Resistance of Zone 1	1e+99	0.002075	K/kW
Thermal Resistance of Zone 2 Firebrick	1e+99	0.0283	K/kW
Thermal Resistance of Zone 2 Magnesite	1e+99	0.001625	K/kW
Thermal Resistance of Zone 2 Steel Shell	1e+99	0.0001	K/kW
Total Thermal Resistance of Zone 2	1e+99	0.030	K/kW
Thermal Resistance of Zone 3 Firebrick	1e+99	0.8854	K/kW
Thermal Resistance of Zone 3 Magnesite	1e+99	0.0508	K/kW
Thermal Resistance of Zone 3 Steel Shell	1e+99	0.003125	K/kW
Total Thermal Resistance of Zone 3	1e+99	0.93932	K/kW
Thermal Resistance of Zone 4 Firebrick	1e+99	0.40	K/kW
Thermal Resistance of Zone 4 Magnesite	1e+99	0.023	K/kW
Thermal Resistance of Zone 4 Steel Shell	1e+99	0.001412	K/kW
Total Thermal Resistance of Zone 4	1e+99	0.42455	K/kW
Thermal Resistance of Zone 5 Firebrick	1e+99	0.10417	K/kW
Thermal Resistance of Zone 5 Magnesite	1e+99	0.003125	K/kW
Thermal Resistance of Zone 5 Steel Shell	1e+99	0.000125	K/kW
Total Thermal Resistance of Zone 5	1e+99	0.10742	K/kW
Thermal Resistance of Zone 6 Firebrick	1e+99	0.0	K/kW
Thermal Resistance of Zone 6 Magnesite	1e+99	0.0	K/kW
Thermal Resistance of Zone 6 Steel Shell	1e+99	0.0	K/kW
Total Thermal Resistance of Zone 6	1e+99	1e+99	K/kW
Thermal Resistance of Zone 7 Firebrick	1e+99	0.06944	K/kW
Thermal Resistance of Zone 7 Magnesite	1e+99	0.002604	K/kW
Thermal Resistance of Zone 7 Steel Shell	1e+99	0.000208	K/kW
Total Thermal Resistance of Zone 7	1e+99	0.072257	K/kW
Furnace Geometry			
Area of Alloy Bath Meniscus	8.0	8.0	m^2
Area Refractory Zone 1: Radius 1	18.55	18.546	m^2
Area Refractory Zone 1: Radius 2	20.42	18.746	m^2
Area Refractory Zone 2	10.0	10.0	m^2
Area Refractory Zone 3	0.32	0.32	m^2
Area Refractory Zone 4	0.708	0.708	m^2
Area Refractory Zone 5	8.06	8.0	m^2
Area Refractory Zone 6	13.2	13.2	m^2
Area Refractory Zone 7	4.8	4.8	m^2
Alloy Bath Height	0.177	0.177	m
Cold Wall Firebrick Thickness	0.2	0.2	m
Cold Wall Magnesia Thickness	0.1	0.1	m
Floor Fireclay depth	0.5	0.5	m
Floor Magnesia depth	0.2	0.2	m
Hot wall firebrick Thickness	0.17	0.17	m
Hot Wall Refractory Magnesia Thickness	0.13	0.13	m
Roof Magnesia Thickness	0.3	0.3	m
Slag Bath Height	0.08	0.08	m

Continued on next page.

Table A.1 continued.

Name	Default value	Calculated value	Units
Exposed Cold Wall Height	1.2	1.2	m
Exposed Hot Wall Height	2.5	2.5	m
Furnace Floor Actual Width	4.015	2.3094	m
Furnace Length	4.0	4.0	m
Furnace Width	4.0	4.0	m
Heap Melting Interface Width	1.8	1.8	m
Roof Arc Radius	4.6365	4.6365	m
Slag-alloy Interface Width	1.8	1.8	m
Slag Meniscus Width	2.0	2.0	m
Steel Shell Thickness	0.05	0.05	m
Specific gas constant of air	287.058	287.058	$J\,kg^{-1}\,K^{-1}$
Alloy bath volume	1.43	0.708	m^3
Freeboard volume	46.0	0.64	m^3
Slag bath volume	1.43	0.64	m^3
Combustion air input density	1.1839	3.5797e-06	$kg\,m^{-3}$
Molten Slag density	2300.0	2300.0	$kg\,m^{-3}$
Furnace floor angle	5.0	5.0	degrees
Heap angle of repose	30.0	30.0	degrees
Heap Melting Interface Reactions			
Heap Melting Rate	10000.0	10000.0	$kg\,h^{-1}$
Material Flow Rates			
CO Bubble Flow Rate Through Alloy	0.0	4.295	m^3s^{-1}
Combustion Air Volume Input Rate	0.0	0.0	m^3h^{-1}
Combustion Fuel Input Rate	0.0	0.0	$kg\,h^{-1}$
Pig Iron Input Rate	0.0	0.0	$kg\,h^{-1}$
Combustion Air Mass Input rate	0.0	0.0	$kg\,h^{-1}$
Material Properties			
Oxygen supersaturation in steelmaking baths	0.26	0.26	wt/% O
Thermal Conductivity of Firebrick	0.6	0.6	$W\,m^{-1}\,K$
Thermal Conductivity of Magnesia Brick	8.0	8.0	$W\,m^{-1}\,K$
Thermal Conductivity of A36 Steel	50.0	50.0	$W\,m^{-1}\,K$
Actual active Fe2O3 in slag	0.0		$kg\,m^{-3}$
Molten Pig Iron density	7000.0	7874.032	$kg\,m^{-3}$
Total Available Fe2O3 in the slag	0.0	0.0	$kg\,m^{-3}$
Total Available FeO in the slag	0.0	0.0	$kg\,m^{-3}$
Actual Oxygen Concentration in the Bath	0.0	184.29	$kg\,m^{-3}$
Oxygen equilibrium saturation in iron	0.0		$kg\,m^{-3}$
Oxygen concentration in steelmaking bath	0.0	1.30478	wt/% O
Oxygen concentration in steelmaking baths	0.0	0.22856	wt/% O
Solid Raw Material Recipe			
Flux Recipe Fraction	0.16	0.2	
Iron Ore Recipe Fraction	0.8	0.8	
Reductant Recipe Fraction	0.0	0.0	
Slag-alloy Interface Reactions			
Mass Transfer Proportionality Constant for Deep Alloy Baths	12000.0	12000.0	m^{-1}

Continued on next page.

Table A.1 continued.

Name	Default value	Calculated value	Units
Mass Transfer Proportionality Constant for Shallow Alloy Baths	8000.0	8000.0	m^{-1}
Mass Transfer Proportionality Constant for Deep Slag Baths	5000.0	5000.0	m^{-1}
Mass Transfer Proportionality Constant for Shallow Slag Baths	4000.0	4000.0	m^{-1}
Diffusivity of Carbon in Molten Iron	0.0	2.07e-08	$m^2 s^{-1}$
Diffusivity of Fe (III) in slag	0.0	4.474e-08	$m^2 s^{-1}$
Diffusivity of Oxygen in Molten Iron	0.0	1.2738e-08	$m^2 s^{-1}$
Carbon Diffusion Constant in Molten Iron	5.2e-07	5.2e-07	$m^2 s^{-1}$
Iron Diffusion Constant in Slags	1e-07	1e-07	$m^2 s^{-1}$
Oxygen Diffusion Constant in Molten Iron	3.2e-07	3.2e-07	$m^2 s^{-1}$
Carbon Diffusion Activation Energy in Molten Iron	50208.0	50208.0	$J mol^{-1}$
Iron Diffusion Activation Energy in Slags	10700.0	10700.0	$J mol^{-1}$
Oxygen Diffusion Activation Energy in Molten Iron	50208.0	50208.0	$J mol^{-1}$
Active Slag Fraction	0.0	0.0598	
Mass transfer coefficient of carbon in molten iron alloy	5e-05	0.5423	$m s^{-1}$
Mass transfer coefficient of iron in slag	2.5e-06	0.5882	$kg h^{-1}$
Mass transfer coefficient of oxygen in molten iron alloy	5e-05	0.4254	$m s^{-1}$
Mass transfer rate of carbon in molten iron alloy	5e-05	433.81	$kg h^{-1}$
Mass Transfer Rate of Iron Oxide in Slag	0.0	52645.3	$kg h^{-1}$
Mass transfer rate of oxygen in molten iron alloy	0.0	964.21	$kg h^{-1}$
Mass transfer rate of Rate-limiting Step	0.0	433.81	$kg h^{-1}$

Continued on next page.

Appendix B

Summary of Parameters and Variables

This section is a summary of parameters and variables used in the model in tabular form (Table B.1). References to a parameters definition and formulation in this document are also provided in Table B.1.

Table B.1: Summary of parameters used in the ESS steelmaking process model.

Parameter/ Variable	Symbol	Type	Description	Ref.
Process Materials:				
Pig Iron feed		Fixed	Pig iron fed to the ESS process	15.2.1
Iron ore		Fixed	Iron ore fed to the ESS process	15.2.2
Flux		Fixed	Flux fed to the ESS process	15.2.3
Reductant		Fixed	Reductant fed to the ESS process	15.2.4
Combustion Fuel		Fixed	Combustion fuel fed to the ESS process	15.2.4
Combustion air		Fixed	Combustion air fed to the ESS process	15.2.5
Refractory material		Fixed	Refractory materials used in the ESS furnace	15.2.6
Furnace Geometry:				
Alloy bath:				
Meniscus Area	A_{AB-m}	Fixed	Area of alloy bath top surface in contact with slag.	15.3.1
Refractory contact area	A_{AB-RF}	Fixed	Area of surface where there is contact between the alloy bath and refractory material.	15.3.1
Maximum depth	$d_{AB,max}$	Fixed	Maximum depth of the alloy bath during steady operation.	15.3.1
Average depth	$d_{AB,avg}$	Fixed	Maximum depth of the alloy bath during steady operation.	15.3.1
Slag layer:				

Continued on next page

Table B.1 – continued from previous page

Parameter	Symbol	Type	Description	Ref.
Refractory contact area	A_{SL-RF}	Fixed	Area of surface where there is contact between the slag layer and refractory material.	15.3.2
Maximum depth	d_{SL}	Fixed	Maximum depth of the slag layer during steady operation.	15.3.2
Raw material heap:				
Surface Area	A_{RMH}	Fixed	Area of the raw material heap's top surface which is exposed to radiation from the freeboard.	15.3.3
Melted depth	d_{RMH}	Calculated	depth to which melting occurs in the raw material heap's active region.	15.3.3
Refractory lining:				
Alloy contact thickness	d_{RL-AB}	Fixed	Thickness of refractory material in the region whose surface is in contact with the alloy bath.	15.3.5
Slag contact thickness	d_{RL-SL}	Fixed	Thickness of refractory material in the region whose surface is in contact with the slag layer.	15.3.5
Roof thickness	$d_{RL-roof}$	Fixed	Thickness of refractory material in the roof arc.	15.3.5
Hot wall thickness	d_{RL-hot}	Fixed	Thickness of refractory material in the regions whose surfaces are exposed to radiation from hot freeboard gas.	15.3.5
Hot surface Area	A_{RL-hot}	Fixed	Area of refractory material exposed to radiation from hot gas in the freeboard.	15.3.5
Steel shell:				
Thickness	d_{SS}	Fixed	Thickness of the steel shell enclosing the ESS furnace	15.3.5
Fluid and Particulate Flow:				
Pig iron feed rate	$\dot{m}_{pi}$	Fixed	The rate at which pig iron is fed into the furnace during steady state operation.	15.4
Iron ore feed rate	$\dot{m}_{pi}$	Fixed	The rate at which iron ore is fed into the furnace during steady state operation.	15.4

Continued on next page

Table B.1 – continued from previous page

Parameter	Symbol	Type	Description	Ref.
Flux feed rate	$\dot{m}_{pi}$	Fixed	The rate at which flux is fed into the furnace during steady state operation.	15.4
Reductant feed rate	$\dot{m}_{pi}$	Fixed	The rate at which reductant is fed into the furnace during steady state operation.	15.4
Combustion fuel feed rate	$\dot{m}_{pi}$	Fixed	The rate at which combustion fuel is fed into the furnace during steady state operation.	15.4
Combustion air feed rate	$\dot{m}_{pi}$	Fixed	The rate at which combustion air is fed into the furnace during steady state operation.	15.4
Gas bubble flow	$\dot{m}_{GB}$	Calculated	Flow rate of gas bubbles through the alloy and slag bath during steady state operation.	15.4.1
Tapped alloy flow rate	$\dot{m}_{TA}$	Calculated	Flow rate at which steel is tapped from the furnace during steady state operation.	15.4
Tapped slag flow rate	$\dot{m}_{TS}$	Calculated	Flow rate at which slag is tapped from exits the furnace during steady state operation.	15.4
Off gas flow rate	$\dot{m}_{OG}$	Calculated	Flow rate at which gas exits the furnace during steady state operation.	15.4
Energy Flow:				
Alloy bath heat loss	$\dot{H}_{AB-EE}$	Calculated	Rate at which heat is transferred from the alloy bath, through the refractory lining and steel shell to the external environment.	15.7.3
Slag layer heat loss	$\dot{H}_{SL-EE}$	Calculated	Rate at which heat is transferred from the slag layer, through the refractory lining and steel shell to the external environment.	15.7.3
Freeboard heat loss	$\dot{H}_{FB-EE}$	Calculated	Rate at which heat is transferred from hot freeboard gas, through the refractory lining and steel shell, to the external environment.	15.7.3

Glossary

absolute temperature (T) The Kelvin (K) scale of thermodynamic temperature whose lowest value is zero. 11, 13, 14, 15, 130

boundary The edge of a system or universe. 130

condensed Compactly, or highly concentrated in a small volume. 13
constituent A chemical building block of a material phase.. 81

diathermic system A system whose boundary allows flow of heat. 130

endothermic Requires absorption of heat (q) to occur spontaneously. 13
energy (E) A number defining the capacity for a system to do work (w). 12, 130, 131
enthalpy (H) A state function that accounts for heat (q) contained by matter at a given temperature (β). 12
entropy (S) A state function defining the. 12
exothermic Results in the release of heat (q) when occuring spontaneously. 13

heat capacity ($C_{\text{conditions}}$) A property denoting the amount of energy required to raise the absolute temperature (T) of a system by 1.0 K. The subscript "conditions" may be "P" or "V" denoting that the system has either constant pressure (P) or volume (V) respectively.. 12
heat (q) A form of energy (E) that is transferred between a diathermic system and its surroundings, if the two are not at thermal equilibrium. 11, 130

interface A region where two streams of unidentical properties combine, resulting in some type of chemical or physical reaction.. 81
internal energy (U) A state function defining the total energy (E) contained by a system. 11, 12
isenthalpic A condition in which an isolated system does not change its energy content over a course of events.. 81
isolated system A system whose boundary does not allow exchange of any kind with the surroundings. 11, 12
isothermal A condition in which an isolated system remains a constant temperature over a course of events.. 81

observer A person or device that measures a property of a system without effecting changes to its state. 131
open system A system whose boundary allows exchange of matter with the surroundings. 12

pressure (P) . 130

state The condition of matter under specific kinetic conditions. 130, 131
state function A property that is defined by the current state of a system, that is independent of the method used to reach the current state. 130
stream The path followed by a specific amount of material or energy from one physical space to another.. 81

surroundings The region of the universe that excludes the system, where an observer is usually situated. 12, 81, 130, 131

system A specific region of the universe that is of interest to an observer. 81, 130, 131

temperature (β) An intensive physical property by which the average thermal energy state of atoms or molecules in a system can be quantified. It can also be described as the thermal equilibrium distribution of atoms or molecules in a system given a number of available thermal energy states. 130, 131

thermal equilibrium The condition where two systems have identical temperature (β)s. 11, 130, 131

thermochemical system A system whose chemical state changes as a result of changes its thermal state. 13

thermodynamic temperature A temperature (β) scale devised for convenience of communication. The four types are Kelvin (K), Celsius (°C), Rankine (°R) and Fahrenheit (°F) scales. 130

thermodynamics The study of energy and its relationship to work, equilibrium states and variables of systems of interest. 11, 131

universe The total physical space available for interrogation by an observer. 130, 131

volume (V) The physical 3-dimensional space within the boundaries of a system or universe. 130

work (w) A number defining motion done against an opposing force. In thermodynamics, it is more suitable to state that it is the transfer of energy (E) with the surroundings that results in, or is a result of, the uniform motion of a system's atoms or molecules. 11, 130

Appendix C

Declaration on Plagiarism

DECLARATION ON PLAGIARISM
UNIVERSITY OF PRETORIA
Faculty of Engineering, the Built Environment and Information Technology
Department of Materials Science and Metallurgical Engineering

The University places great emphasis upon integrity and ethical conduct in the preparation of all written work submitted for academic evaluation. While academic staff teach you about systems of referring and how to avoid plagiarism, you too have a responsibility in this regard. If you are at any stage uncertain as to what is required, you should speak to your lecturer before any written work is submitted.

You are guilty of plagiarism if you copy something from a book, article or website without acknowledging the source and pass it off as your own. In effect you are stealing something that belongs to someone else. This is not only the case when you copy work word-by-word (verbatim), but also when you submit someone else's work in a slightly altered form (paraphrase) or use a line of argument without acknowledging it. You are not allowed to use another student's past written work. You are also not allowed to let anybody copy your work with the intention of passing it off as his/her work.

Students who commit plagiarism will lose all credits obtained in the plagiarised work. The matter may also be referred to the Disciplinary Committee (Students) for a ruling. Plagiarism is regarded as a serious contravention of the University's rules and can lead to expulsion from the University.

The declaration which follows must be appended to all written work submitted within the department. No written work will be accepted unless the declaration has been completed and attached.

I (full names) Thabisani Nigel Phuthi

Student number 29205337

Topic of work Steelmaking with the ESS Furnace: A model-based analysis

Declaration
1. I understand what plagiarism is and am aware of the University's policy in this regard.
2. I declare that this report is my own original work. Where other people's work has been used (from

a printed source, internet or any other source), this has been properly acknowledged and referenced in accordance with departmental requirements.
3. I have not used another student's past written work to hand in as my own.
4. I have not allowed, and will not allow, anyone to copy my work with the intention of passing it off as his or her own work.

Signature: